

# 博士論文

## **Development of highly reaction-selective electrocatalysts based on covalent organic frameworks modified with single platinum atoms**

(単一白金原子を担持した共有結合性有機構造体から成る  
高反応選択的電極触媒の開発)

**by Ryo Kamai**

釜井 亮

**Department of Advanced Interdisciplinary Studies  
Graduate School of Engineering  
The University of Tokyo**

**September 2016**



# Table of Contents

## Chapter 1.

<b>General Introduction</b> .....	<b>1</b>
1.1. Background and objective of this study.....	1
1.2. Single atom catalysis on electrochemistry.....	4
1.2.1. Overview.....	4
1.2.2. Complex-based molecular catalyst.....	6
1.2.3. Directly deposited single metal atom catalysts.....	8
1.3. Ordered porous organic materials.....	11
1.3.1. Overview.....	11
1.3.2. Covalent organic frameworks.....	12
1.4. Outline of this thesis.....	16
References.....	18

## Chapter 2.

<b>Platinum-modified covalent triazine frameworks hybridized with carbon nanoparticles as methanol-tolerant oxygen reduction electrocatalysts</b> .....	<b>23</b>
2.1. Introduction.....	24
2.2. Experimental details.....	25
2.2.1. Synthesis procedure of Pt-CTF/CP.....	25
2.2.2. Electrochemical characterization.....	25
2.2.3. Physical characterization.....	26
2.3. Results.....	26
2.3.1. Morphological characterization of Pt-CTF/CP.....	26
2.3.2. Electrochemical characterization of Pt-CTF/CP.....	29
2.3.3. X-ray characterization of Pt-CTF/CP.....	33
2.4. Discussion.....	40
2.5. Conclusions.....	42
References.....	43

### **Chapter 3.**

<b>Oxygen-tolerant single Pt-atom catalysts supported on a covalent triazine framework for the hydrogen oxidation reaction</b> .....	<b>49</b>
3.1. Introduction.....	50
3.2. Experimental details.....	51
3.2.1. Catalyst synthesis.....	51
3.2.2. Electrochemical characterizations.....	51
3.2.3. Physical characterizations.....	52
3.2.4. Membrane electrode assembly (MEA) preparation.....	52
3.2.5. Fuel cell testing.....	53
3.3. Results.....	53
3.3.1. Physical characterization of Pt-CTF/CP.....	53
3.3.2. Electrocatalytic HOR activity.....	58
3.3.3. Electrocatalytic HOR activity of 0.29 wt% Pt-CTF/CP.....	60
3.3.4. Electrocatalytic ORR activity.....	64
3.3.5. Evaluation of Pt-CTF/CP as a PEFC anode catalyst.....	66
3.4. Discussion.....	69
3.5. Conclusions.....	72
References.....	80

### **Chapter 4.**

<b>Selective electrochemical reduction of nitrogen oxides by covalent triazine frameworks modified with single Pt atoms</b> .....	<b>87</b>
4.1. Introduction.....	88
4.2. Experimental details.....	91
4.2.1. Catalyst synthesis.....	91
4.2.2. Electrochemical measurements.....	91
4.3. Results.....	92
4.3.1. Characterizations.....	92
4.3.2. Electrochemical characteristics for nitrate reduction.....	94
4.3.3. Electrochemical characteristics for nitrite reduction.....	97
4.4. Discussion.....	99
4.5. Conclusions.....	101
References.....	102

**Chapter 5.**

**Conclusions and Perspectives**.....106

5.1. Conclusions.....106

5.2. Future Perspectives.....110

References.....113

**List of Publications**.....116

**Acknowledgements**.....118



# Chapter 1.

## General introduction

### 1.1. Background and objective of this study

Along with the expansion of world's population and progress of the industrialization, rapid increase in energy consumption is predicted in 21<sup>st</sup> century. To solve the energy problem, scientists need to be addressed more aggressively in order to realize a sustainable society. Losses in energy utilization by using heat from combustion of fossil fuels are very large, for example, more than 60 % in case of the thermal power generation plant [1]. Since the electrochemical reaction performs direct conversion between electrical energy and chemical energy, the energy use with electrochemical reactions can be possible to reduce the energy loss along with the thermal process. Thus, the energy utilization through the electrochemical reaction is important in achieving low carbon society because it is capable of high energy utilization efficiency. The key factor in the energy conversion efficiency of the electrochemical reactions is an electrocatalyst which is a dominant factor of electrode overpotential, and their three elements required for the actual use are activity, selectivity and durability.

The electrocatalyst whose active center is a single metal atom is expected to show reaction selectivity because there is no possibility to take the adsorption structure across the multiple metal atoms on the basis of its single adsorption site nature. In addition to this, a single metal atom electrocatalyst is expected to have a specific activity and high metal atom utilization efficiency derived from the characteristics of 1) large interaction with support material [2,3], 2) large interaction with ligands [4] and 3) no neighboring metal atoms. Such specificity is highly attractive from the point of view of the functional improvement of the electrocatalyst. In fact, the research on the

electrocatalyst carrying a single metal atom has become an active field [5-10]. However, in general, there is a problem that single metal atoms carried on the electrode substrate are easy to aggregate because of their high surface energy (Fig. 1.1) or easy to drop off [8,9,11,12]. Therefore, the development of the electrocatalyst material which carries high concentration of single atom with high stability is strongly desired.

Covalent triazine frameworks (CTFs), one class of regular porous polymer, are the leading candidate material to achieve a stable carrying of a high density of single metal atoms because it contains high concentration of nitrogen atoms having a lone pair that can be a coordination environment of the metal atoms in its pore [13,14]. On the other hand, since the conductivity of CTFs are extremely low, there had been no report for utilizing them as an electrocatalyst.

Based on this background, in the present study, the author focused on CTFs as a support material of single metal atoms. Firstly, the author tackled to synthesize a novel CTF-based conductive material carrying an atomically dispersed metal atom for use as an electrocatalyst. To achieve this, he polymerized a monomer of CTF in the presence of conductive carbon nanoparticle in order to make hybrid material of CTF and carbon nanoparticles.

The purpose of this study is to clarify the specificity of a single atom electrocatalyst by applying synthesized CTF-based material to the electrochemical systems, and to find out useful reaction systems. Especially, the author focused on platinum as a target metal which is the most widely commercialized catalyst material to electrochemical devices such as polymer electrolyte fuel cells and electrolyzers. More specifically, the author focused attention on the high reaction selectivity expected on a single metal atom, and tackled to the realization of 1) selective oxygen reduction reaction in the presence of methanol, 2) selective hydrogen oxidation reaction in the presence of oxygen and 3) selective reduction reactions on nitrogen oxides.

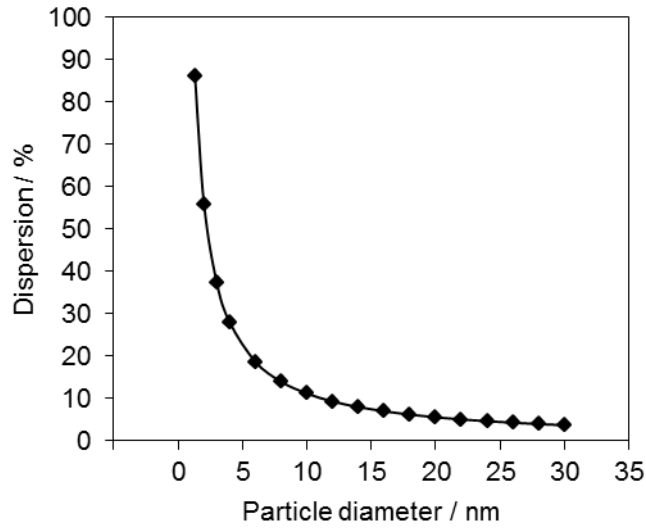


**Fig. 1.1 | Relationships between surface exposure ratio of Pt atoms (dispersion,  $D_{Pt}^{\dagger}$ ) and particle diameter.** (See Note 1.1 for elicitation method.)

**Note 1.1 |  $\dagger$ Estimation method of the  $D_{Pt}$ .**

The surface exposure ratio of the Pt atom of a particle ( $D_{Pt}$ ) was estimated by using uniform sphere model. In this model, the entire surface was assumed to have following proportions of low index planes: (111):(100):(110) = 1:1:1, i.e. the area of one Pt atom would be  $8.07 \text{ \AA}^2$ . The

$D_{Pt}$  is given by

$$D_{Pt} = n_s / n_a = S / n_a a_m$$

where  $n_s$  is the number of atoms at the surface of a particle of surface area  $S$ ,  $n_a$  is the number of atoms of mass  $m_a$  which are in a particle of mass  $m$ , and  $a_m$  is the area occupied by a surface atom.

Since  $n_a = m / m_a$  and  $m_a = \mu / N_A$ , and  $S = 6m / \rho d_n$ ,  $D_{Pt}$  is given by

$$D_{Pt} = 6\mu N_A a_m \rho d_n$$

where  $N_A$  is Avogadro's constant,  $\mu$  is the relative atomic mass,  $\rho$  is the density, and  $d_n$  is the diameter of a particle.

## 1.2. Single atom catalysis on electrochemistry

### 1.2.1. Overview

As a strategy for improving the selectivity and the number of active site of the catalytic reaction, it has been clarified that the reduction of the size of the metal particle is effective approach [15-17]. Such specific reactivity had been reported to be shown by reducing the particle size of noble metal from nano to subnano [16,17]. In a catalytic reaction, interaction of the reactants with the metal active center is one of the most important elements as a point of view of the activity and selectivity. One of the dominant factors for determining the interaction of the reactant with the metal active center is the coordination number of active site. The smaller coordination number sites use fewer electrons and orbitals for coupling, i.e., the larger electrons and orbitals are capable of binding to the reactant. Further, these sites have less steric hindrance. Calle-Vallejo *et al.* revealed that there is a linear relationship between the coordination number of the focused site and interaction of small molecules by the calculation based on density functional theory (DFT) [18,19] (Fig. 1.2). They used the coordination number weighted by coordination number of neighbor atoms ( $\overline{CN}$ ) as a parameter. They also confirmed these relationships experimentally by fabricating low coordination site on Pt particles and conducting oxygen reduction reaction (ORR). Hu *et al.* also confirmed the linear relationship between coordination number of catalytic active site and adsorption energy of oxygen by using Pd, and revealed the relationship with activity [20]. As shown in Fig. 1.1, when the particle size of the Pt is reduced, the surface exposure ratio of the Pt atoms (dispersion of Pt:  $D_{Pt}$ ) is increased, i.e., the coordination number is reduced. The ultimate form of reducing the particle size is a single atom state. Since all of the particles are present on the surface, the surface energy of the metal particle is extremely high in a single metal atom catalyst (Fig. 1.1). Thus, it can be expected that single atom catalysts show specific catalytic activity by strong

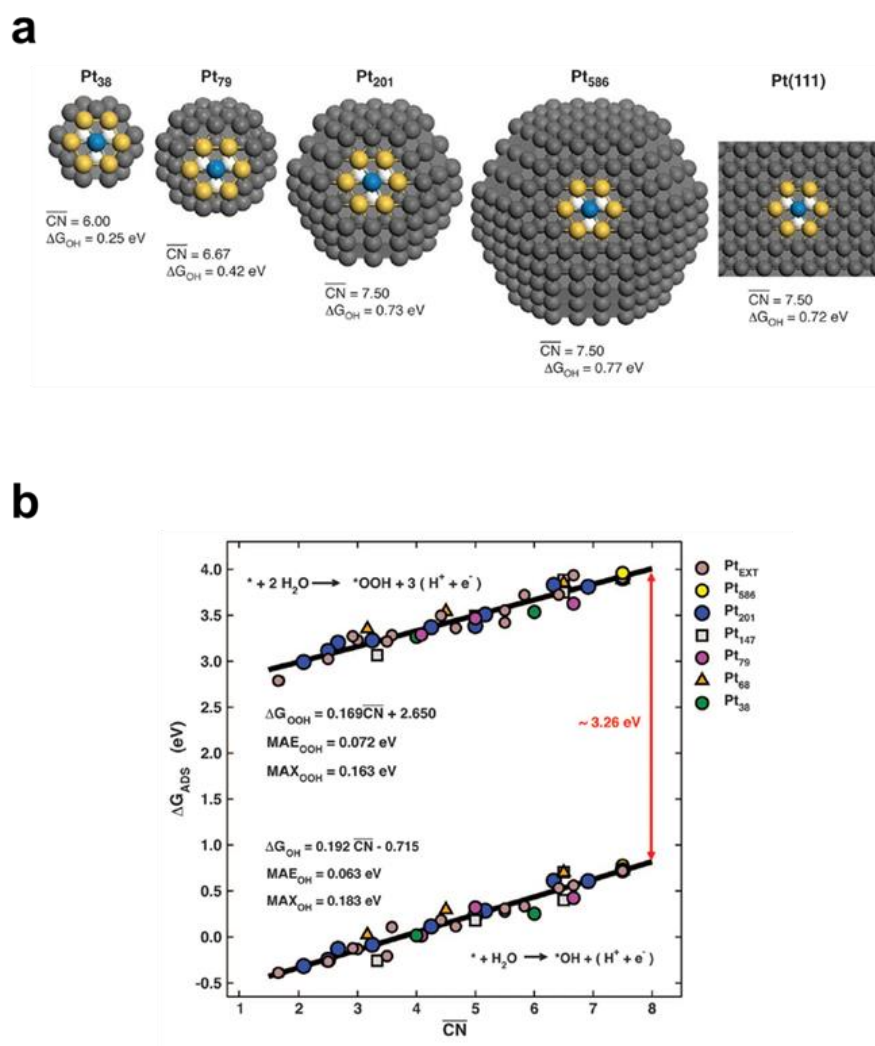


**Fig. 1.2 | Relationship between the coordination number and adsorption energies of oxygen species.** (a) Active sites which have coordination number (CN) of 9 on various sizes of Pt particles and Pt(111) plane. The value of  $\Delta G_{OH}$  changes significantly ( $\sim 0.5$  eV) in spite of same CN. (b) Relationship of  $\Delta G_{OH}$  and  $\Delta G_{OOH}$  versus the coordination number weighted by coordination number of neighbor atoms ( $\overline{CN}$ ). These relationships showed clear linearity with low distribution. Reproduced with permission for Ref. 20. Copyright © 2015, American Association for the Advancement of Science.

interaction between the reactants and single metal atom active centers.

However, as mentioned above, easy aggregation of single metal atoms becomes a problem generally because of their high surface energy [8,9,11,12]. In order to solve the strong tendency of aggregation, for example, 1) a method of carrying through the complex-forming material, 2) a method of carrying on a support material which strongly interacts with the metal atom, can be considered.

### 1.2.2. Complex-based molecular catalysts

A method of carrying through the complex-forming material stabilizes a single metal by a strong interaction with ligands. This stabilization can be explained by Ligand Field Stabilization Energy (LFSE) as follows. When the ligand coordinated to the metal ion, repulsive interaction due to the Coulomb force between the negative charge of the electrons and the ligands in the metal orbitals occurs. This interaction increases with closer the two negative charges spatially. Thus, the magnitude of this interaction is different from the direction of the lobes of the  $d$ -orbital of the metal. As a result, the energy level of the metal orbital is splitted about 1 ~ 3 eV depends on the coordination structure of the complex (for example, Fig. 1.3b) [21]. Pt(II), which has  $d8$  configuration, usually takes a square planar coordination structure. In case of square planar structure, LFSE can be represented as following Eq(1).

$$\text{LFSE} = (1.23k+0.23l-0.43m-0.51n)\Delta_0 \quad \text{Eq(1)}$$

where  $k$ ,  $l$ ,  $m$  and  $n$  are the number of electrons in  $dx^2-y^2$ ,  $d_{xy}$ ,  $dz^2$  and  $d_{xy}+d_{yz}$  orbitals, respectively.  $\Delta_0$  is the ligand field splitting parameter which depends on the type of ligands. Therefore, in general, the electron energy is stabilized when a strong interaction between the metal and the ligand occurs.

Application of the metal complex-based electrode to the electrochemical reaction was first reported by Lane *et al.* in 1973 [22]. They fabricated the electrode consists of Fe (III) complex with a salicylate ligand carried on the Pt metal substrate. In

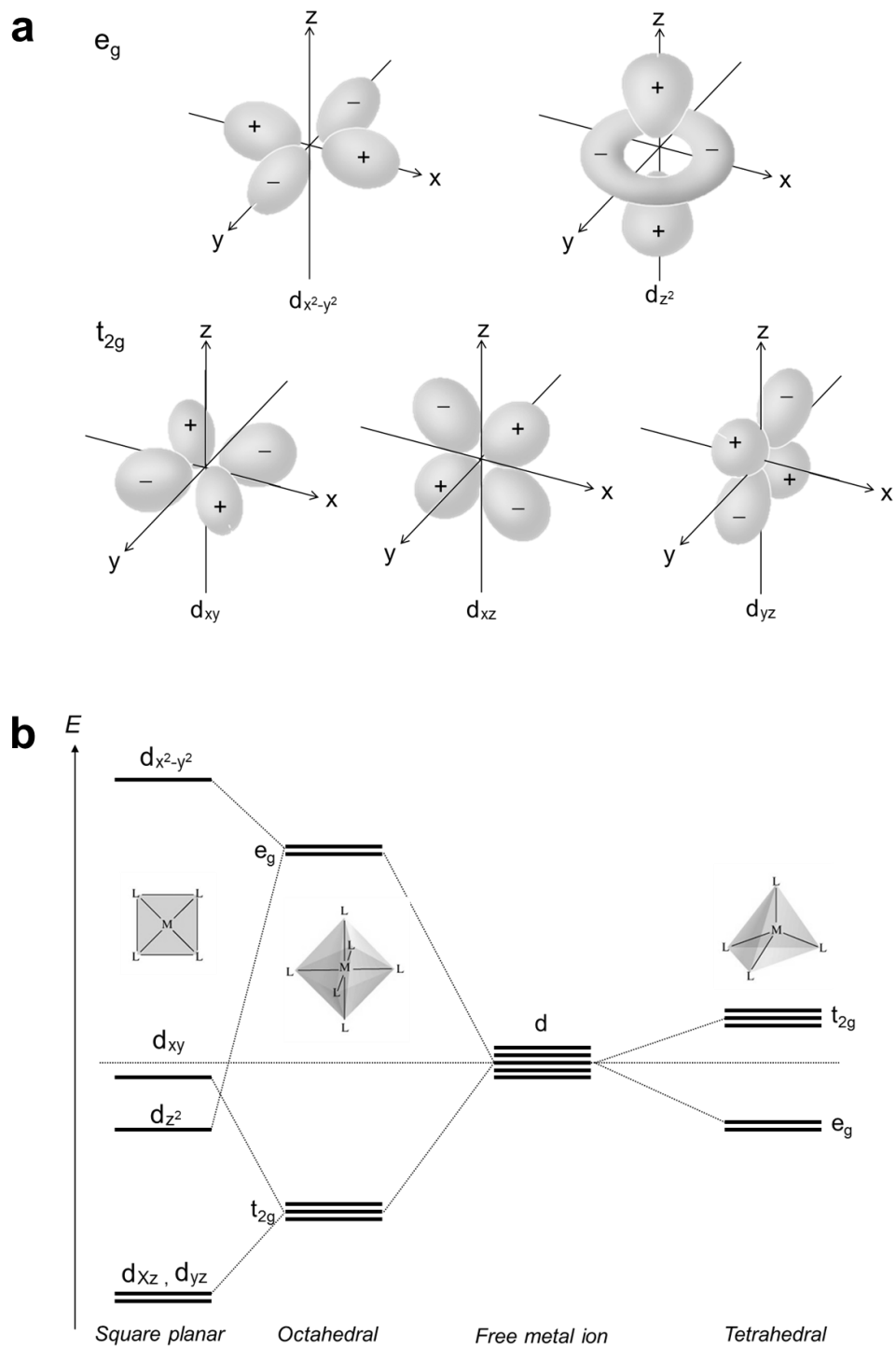


**Fig. 1.3 | Shapes and energy diagram of  $d$  orbitals of a metal atom.** (a) Shapes of the  $d$  orbitals, (b) splitting of  $d$  orbitals by each geometry of ligands.

their study, the ligand chemically adsorbed to Pt substrate through olefinic group, but the stability was significantly decreased with changing the electrode potential. After that, chemically modified electrode using carbon substrate was developed by Watkins et al. in 1975 [23]. They made carboxyl group on graphite surface by heating graphite in air at first, then bind amino acids via amide bond to this site. Whereas they modified carbon via amid bond, Brown *et al.* demonstrated that Fe (III) porphyrin compounds strongly adsorbed onto carbon substrate without covalent bond and these electrodes were able to apply directly to the electrochemical reaction systems [24]. Thereafter, electrocatalytic activities of the many types of electrode carrying a metal-complex having a porphyrin or phthalocyanine ring on carbon material have been reported so far. These metal-complex/carbons are often used as an electrocatalyst for the oxygen reduction reaction [25-29]. The biggest advantage of these catalysts carrying metal-complex is that it can be handled in an immobilized form as heterogeneous catalyst while it is possible to obtain a high catalytic activity by only a small amount of metal as a homogeneous catalyst [30]. However, there is a durability problem in these metal-complex/carbon material. Baranton *et al.* and Cheng *et al.* reported respectively that the catalytic ORR activity of the complex-based electrocatalysts which consist of phthalocyanine complex and conductive carbon particles significantly decreased only within 10 cycles [26,27]. This degradation of electrocatalytic activity was explained by desorption of metal complex, demetallation of the complex, and disruption of macrocycle due to the strong adsorption of the oxygen species [26,27]. Therefore, it is necessary for long time operation that 1) the ligands which function as a metal anchor are firmly immobilized on a carrier, and 2) metals are strongly interacted with ligands.

### **1.2.3. Directly deposited single metal atom catalysts**

A method of carrying a single metal atom directly to the substrate stabilizes a single metal through a strong interaction with substrate material. In this method, single

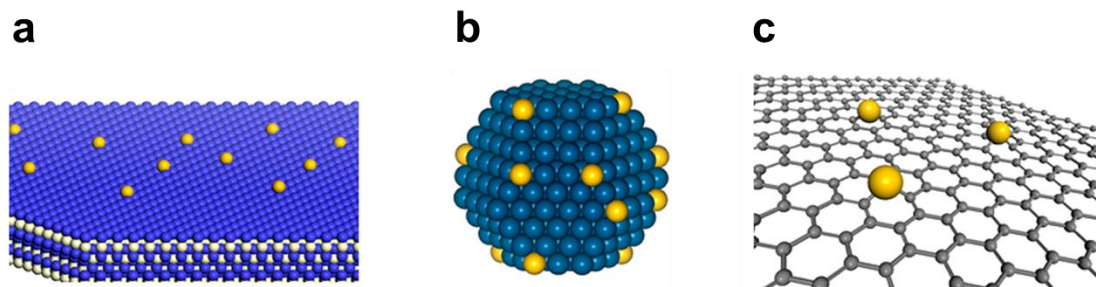


**Fig. 1.4 | Schematic illustrations of single metal atom catalysts.** Single metal atoms directly deposited on (a) metal oxides, (b) another kind of metal and (c) graphene. Reproduced with permission for Ref. 38. Copyright © 2013 American Chemical Society.

metal atoms are anchored to the substrate by chemical interaction. As such substrates, metal oxides (Fig. 1.4a), another kind of metal surface (Fig. 1.4b) and porous materials such as graphene (Fig. 1.4c) had been reported. For example, Qiao *et al.* deposited single Pt atoms on  $\text{FeO}_x$  substrate and applied this material to CO oxidation reaction [31]. Shi *et al.* applied this  $\text{Pt}_1/\text{FeO}_x$  to the counter electrode of dye sensitized solar cells and demonstrated that  $\text{Pt}_1/\text{FeO}_x/\text{FTO}$  effectively catalyzes the reduction reaction of triiodide ( $\text{I}_3^-$ ) to iodide ( $\text{I}^-$ ) [32]. Moses-DeBusk *et al.* also demonstrated that  $\text{Al}_2\text{O}_3$  is also able to use as a support of single Pt atoms and the resulting  $\text{Pt}_1/\text{Al}_2\text{O}_3$  exhibited significantly high CO oxidation activity [33]. As another type of oxide substrate, Wang *et al.* reported that  $\text{Co}_3\text{O}_4$  can serve as a support of single Rh atoms, and  $\text{Rh}_1/\text{Co}_3\text{O}_4$  acts as a selective catalyst for the reduction reaction from NO to  $\text{N}_2$  [34]. In these metal oxide substrates, surface defects were supposed to function as an anchoring site of single metal atoms [31]. Recently, Yang *et al.* reported that single Pt atom loaded on a titanium nitride substrate predominantly generates  $\text{H}_2\text{O}_2$  via the  $2e^-$  ORR pathway [35]. According to the DFT calculations, Pt atoms are likely to exist in an N-vacancy site on the TiN substrate. As an example using another metal as a carrier, Lucci *et al.*

demonstrated that single Pt sites were obtained by depositing approximately 1 at% of Pt on Cu metal surface using electron beam evaporation. The resulting Pt-Cu alloy catalyzes thermal H<sub>2</sub> activation via the bridge type adsorption between Pt atom and Cu atom [36]. Each atomically dispersed Pt atoms were confirmed to exist in the replaced site of the lattice structure of Cu. Further, Yan *et al.* successfully synthesized single Pd atom deposited graphene by atomic layer deposition technique [37]. They performed selective hydrogenation reaction of 1,3-butadiene under relatively low temperature. On the graphene layer, Pd single atoms were immobilized by interacting with oxygen functionalized group in the defect site of graphene. From the point of view of the electrocatalyst, only a few examples that utilizes single atom of platinum group metals had been reported [32,35], as described above.

The loading amounts of platinum group metals of the catalysts reported so far were summarized in Table 1.1. As shown in Table 1.1, a single atomic state had been achieved only in a very dilute concentration of 0.5 wt% or less in any of the catalyst. If these concentrations of metal atoms rise to a few percent or more, the cluster of metal forms inevitably [31,33-35,37]. This strong tendency of the aggregation is supposed to be due to relatively weak interaction between single metal atom and substrate compared to a complex. Therefore, in order to realize a single metal atom based electrocatalyst which has a practical concentration of metal for the use of electrochemical devices, it is necessary to apply a substrate which has a stronger interaction with metal atoms than the substrate shown in Table 1.1.

**Table 1.1 | Summary of the loading amount of platinum group metals.**

Metal	Substrate	Loading amount of metal	Reference
Pt	FeO <sub>x</sub>	0.17 wt%	[31]
Pt	Al <sub>2</sub> O <sub>3</sub>	0.18 wt%	[33]
Rh	Co <sub>3</sub> O <sub>4</sub>	0.18 wt%	[34]
Pt	TiN	0.35 wt%	[35]
Pd	Graphene	0.25 wt%	[37]

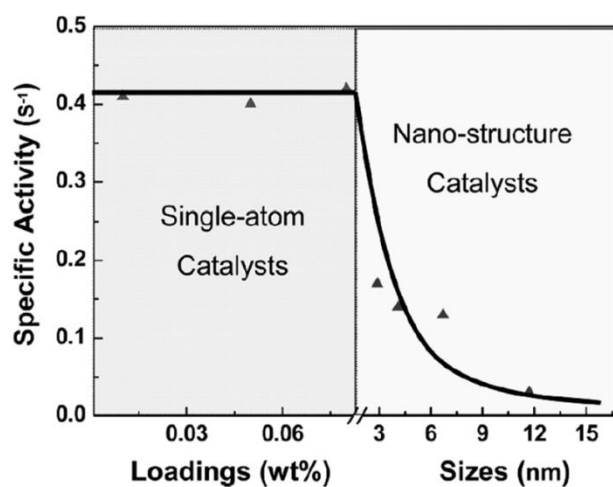


**Fig. 1.5 | Specific activity versus metal loadings and metal particle sizes.** Data was collected from Ref. 39. Reproduced with permission for Ref. 38. Copyright © 2013 American Chemical Society.

### 1.3. Ordered porous organic materials

#### 1.3.1. Overview

Porous materials represented by activated carbon and zeolites are widely used in various applications such as adsorption, occlusion, separation and catalyst; they are essential material to modern society. Use of a porous material began from the inorganic porous material that are exists in nature. In general, porous structure of the inorganic porous material is extremely complicated; it is difficult to obtain the porous structure as intended.

Under such circumstances, porous materials with a hybrid of organic-inorganic called metal organic frameworks (MOFs) were developed in 1990s [40-42]. During the synthesis process of MOFs, coordinative assembling between metal ions and rigid

organic ligands occurs to form building units, and subsequently form porous structure in a self-organized manner. Thus, MOFs are able to design a porous structure in a bottom-up way by choosing structures of metal ions and organic ligands. Although the MOFs have various advantages such as the freely controllable pores and high specific surface area, in general, stability in basic or acidic solutions is poor since metal ions and organic ligands form a structure by coordination bond [43]. For that reason, the use of MOFs as an electrocatalyst in such low or high pH electrolyte conditions is difficult.

As materials to overcome this problem, Côté *et al.* developed porous crystalline materials composed only of organic compounds, so called covalent organic frameworks (COFs), in 2005. They firstly synthesized two types of COFs which are polymerized via the dehydration of 1,4-benzenediboronic acid (COF-1) or 1,4-benzenediboronic acid and hexahydroxytri-phenylene together (COF-5) [44]. In contrast to the MOFs which are constituted by a coordination bonds, the COFs are composed only of covalent bonds. In addition, COFs are also different from supermoleculars which form porous structures through hydrogen bonds or van der Waals' force. Therefore, in general, many of the COFs are chemically and physically stable derived from the covalent bond.

Classifying various structures for each type of building unit and arranged from 1D to 3D structure were summarized in Fig. 1.6.

### **1.3.2. Covalent organic frameworks**

Covalent organic frameworks (COFs) are porous material having a repeating structure whose building unit is cross-linked by covalent bond and consists of only light element (H, B, C and O). As well as the MOFs, COFs are able to design porous structure flexibly by selecting the structure of the building unit (Fig. 1.7). Thereafter the first examples of COFs having boroxine bond were reported by Côté *et al.* [44], it had been synthesized a lot of types of COFs having a variety of bonding species such as boronic acid ester bond [54], imine bond [55], amide bond [56], imide bond [57],

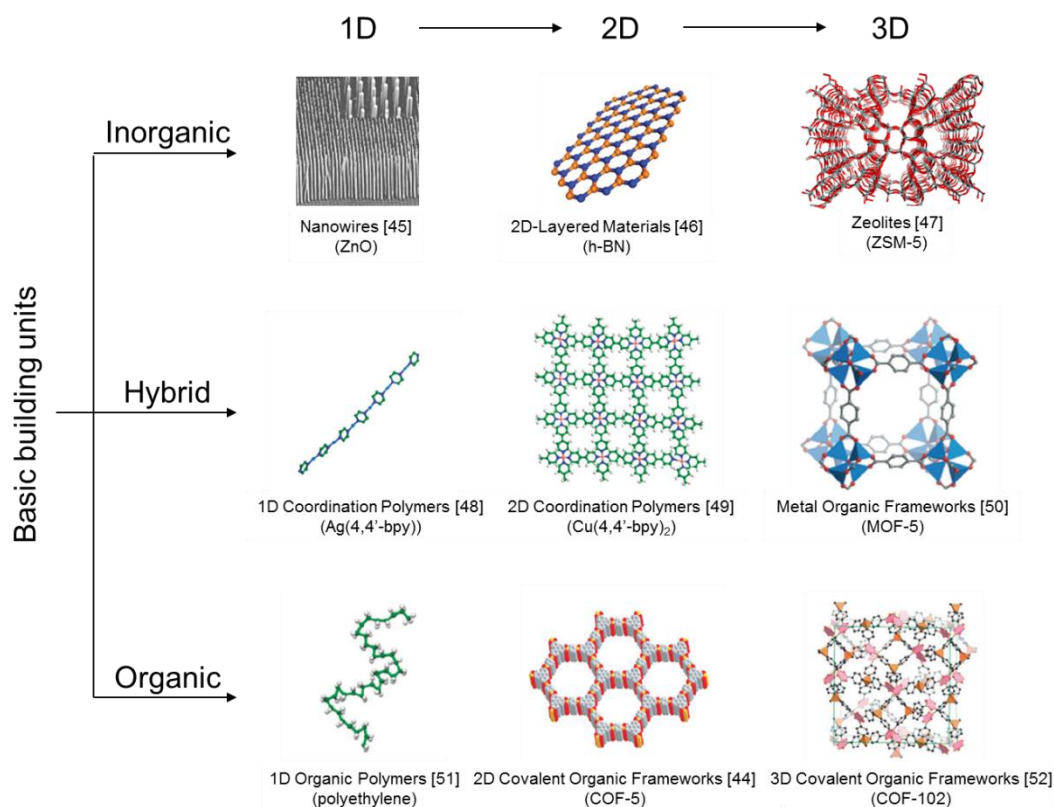


**Fig. 1.6 | Classification of various structures for each type of building unit.** Reproduced with permission for Ref. 53. Copyright © The Royal Society of Chemistry 2013.

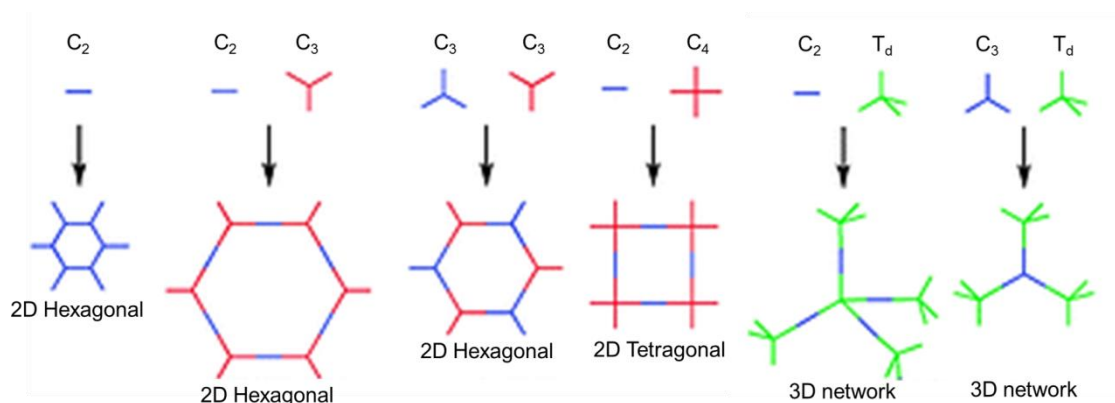
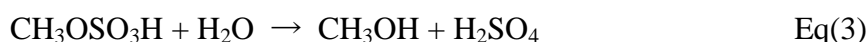


**Fig. 1.7 | Schematic illustration of reticular chemistry of COFs.** Reproduced with permission for Ref. 58. Copyright © The Royal Society of Chemistry 2012.

triazine bond [58], and so on. In general, the crystallinity of COFs correlates with reversibility of the reactions to form covalent bond between each building unit. While the crystallinity of COFs improves with higher reaction reversibility, the chemical stability decreases. Especially, the COFs composed of imide and triazine bond have low reversibility and high chemical stability. These imide and triazine-based COFs are stable even in the acidic and basic electrolyte.

Among a variety of COFs, those having a triazine structure in repeating unit are called covalent triazine frameworks (CTFs). CTFs were first reported by Kuhn *et al.* in 2008 [13]. They synthesized CTFs by polymerizing an aromatic compound having a plurality of cyano groups in molten-salt of zinc chloride. In this process, polymerization reaction proceeds through the formation of triazine ring by pericyclic reaction via the cyclic transition state composed of three cyano groups. In common with other COFs, various structures of CTFs are able to obtain by selecting the monomer. The examples of monomer group that can obtain CTFs are summarized in Fig. 1.8.

From the point of view of the catalyst, the characteristics of CTFs such as high specific surface area, high chemical and physical robustness, high design flexibility, and high density of nitrogen, are attractive. Since the nitrogen atoms among the CTFs possess lone pair, the nitrogen sites are suitable as a coordination environment of the single metal atoms. Actually, for example, Palkovits *et al.* reported that 2,6-dicyanopyridine (DCP)-based CTF can carry high concentration of Pt atoms of approximately C/N/Pt = 3.2/1/0.15 with high stability even in the strong acid condition [14]. They demonstrated that Pt modified CTF (Pt-CTF) selectively catalyze partial oxidation reaction of methane to methanol as following equation (Eq(5)).



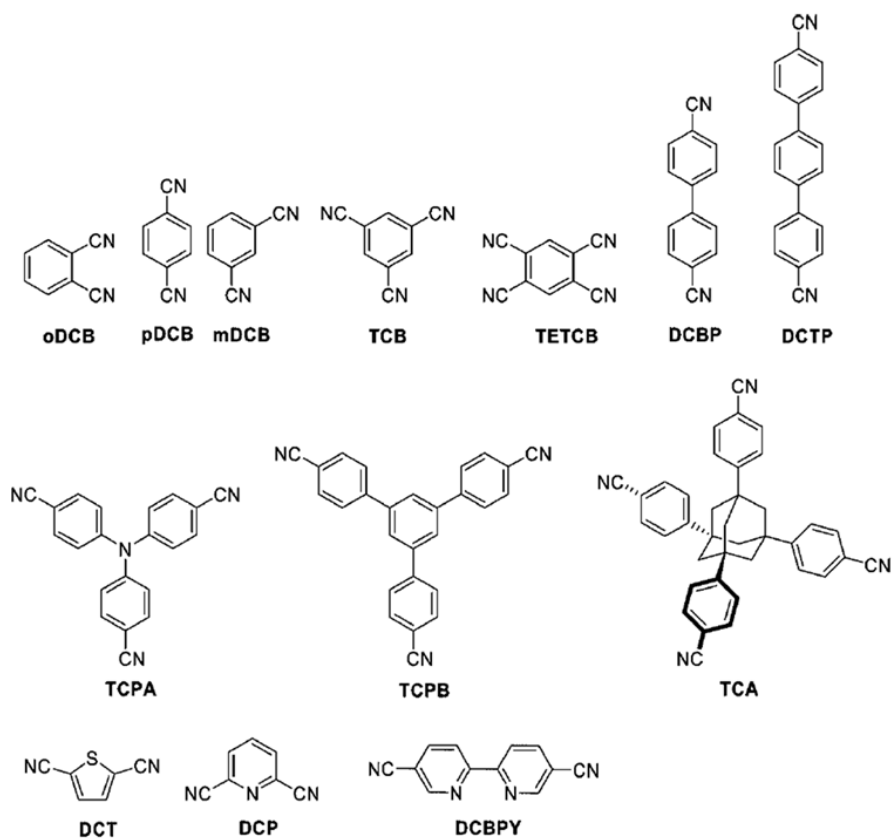


**Fig. 1.8 | Examples of monomers to produce CTFs.** Reproduced with permission for Ref. 59.

Copyright © 2008 American Chemical Society.

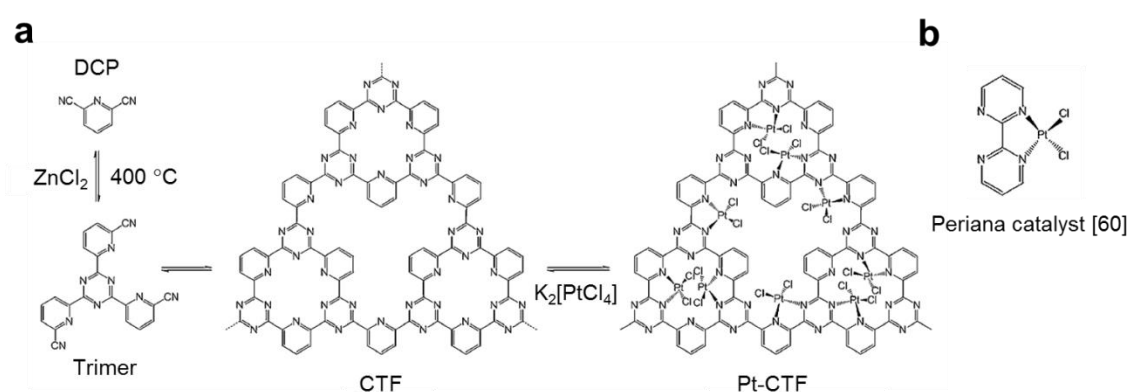


**Fig. 1.9 | Synthesis procedure of Pt-CTF.** (a) Trimerization in molten  $\text{ZnCl}_2$  and subsequent impregnation of Pt, (b) Pt-bipyrimidine molecular complex catalyst. Reproduced with permission for Ref. 14 © 2008 Wiley-VCH Verlag GmbH & Co. KGaA, Weinheim.

Interestingly, the turnover number, i.e. catalytic activity, of heterogeneous Pt-CTF showed comparable value to homogeneous Periana catalyst [60]. This indicates that the Pt atoms were effectively utilized for the catalytic cycles through atomically dispersed form. Bavykina *et al.* synthesized Ir-modified CTF which has 16 wt% of Ir by polymerizing the mixture of 2,6-dicyanobenzene (DCB) and 4,4'-biphenyldicarbonitrile (DCBP), and subsequent impregnation of Ir complex [61]. The resulting Ir-modified CTF catalyzed hydrogen evolution reaction in thermal process through  $\beta$ -elimination of formic acid at Ir site. Since the produced gas phase hydrogen limits the contact of reactant at active site, the diffusivities of both the reactant and the produced hydrogen are important for the catalytic activity. As the CTF synthesized from the mixture of DCB and DCBP had a preferred mesoporous structure, the diffusion of the reactant and the produced hydrogen were effectively proceeded, and then the catalytic reaction was facilitated.

As described above, CTFs are attractive as a catalyst platform since CTFs can carry single metal atoms at high concentration with high stability. However, CTFs show extremely low electrical conductivity derived from their closed conjugated structure. For this reason, the use of CTFs as an electrocatalyst had never been reported so far.

#### **1.4. Outline of this thesis**

Based on the background as mentioned above, in this study the author synthesis novel CTF-based electrocatalyst carrying atomically dispersed Pt, and put the focuses on to reveal the reaction selectivities on the single Pt atom and find out useful selective reaction systems. To achieve the purpose this thesis, following three reaction systems were adopted.

##### **1) Selective oxygen reduction reaction in the presence of methanol (chapter 2)**

In chapter 2, the author firstly synthesized the novel CTF-based catalyst with

single Pt atoms. Then, the synthesized catalyst was applied to the mixed system consists of methanol containing acidic solution and dissolved oxygen, and revealed the reaction selectivity in this system. Also, catalytic activities were confirmed in non-mixed system for each reactant, and clarified the mechanism of the reaction selectivity.

## **2) Selective hydrogen oxidation reaction in the presence of oxygen (chapter 3)**

In chapter 3, the author applied the synthesized catalyst to the hydrogen oxidation reaction (HOR) which is an anode reaction of polymer electrolyte fuel cells (PEFCs). Furthermore, the synthesized catalyst was applied to a PEFC by making a membrane electrode assembly (MEA), and evaluated the performance in a practical device. In actual environment, oxygen is inevitably mixed to the hydrogen fuel from the air during the stop of the PEFC, and entrained oxygen causes the corrosion of cathode carbon support. Therefore, oxygen tolerance is important to improve the durability of PEFCs. To evaluate the tolerance for oxygen, catalytic activities for HOR and oxygen reduction reaction (ORR) were compared.

## **3) Selective reduction reactions of nitrogen oxides (chapter 4)**

In chapter 4, the reaction selectivity between nitrate and nitrite on the synthesized catalyst were compared. Nitrate reduction reaction on Pt metal surface is known to proceed with co-adsorption structure of nitrate and hydrogen, on the other hand, the reduction reaction of NO derived from nitrite is known to proceed involving with aqueous proton. It was confirmed that the under-potentially-deposited hydrogen did not form on single Pt atoms. These hydrogen-free Pt sites are attractive for selective reactions. Then, by using hydrogen-free Pt sites, the roles of hydrogen in nitrogen oxide reduction reactions were clarified.

Throughout this thesis, in chapter 5, the author summarize the reaction tendency on single Pt atoms. Then, the concept of the mechanism of selective reaction on single metal atom catalyst was proposed.

## References

- [1] Regulagadda, P., Dincer, I. & Naterer, G. F. *Appl. Therm. Eng.* **30**, 970-976 (2010).
- [2] Yoon, B., Häkkinen, H., Landman, U., Wörz, A. S., Antonietti, J.-M., Abbet, S., Judai, K., Heiz, U. *Science* **307**, 403-407 (2005).
- [3] Campbell, C. T. *Nat. Chem.* **4**, 597-598 (2012).
- [4] Benjamin, M. M. & Leckie, J. O. *Environ. Sci. Technol.* **15**, 1050-1057 (1981).
- [5] Jirkovský, J. S., Panas, I., Ahlberg, E., Halasa, M., Romani, S. & Schiffrin, D. J. *J. Am. Chem. Soc.* **133**, 19432-19441 (2011).
- [6] Zhang, X., Guo, J., Guan, P., Liu, C., Huang, H., Xue, F., Dong, X., Pennycook, S. J. & Chisholm, M. F. *Nat. Commun.* **4**, 1924 (2013).
- [7] Yang, S. & Lee, H. *ACS Catal.* **3**, 437-443 (2013).
- [8] Shi, Y., Zhao, C., Wei, H., Guo, J., Liang, S., Wang, A., Zhang, T., Liu, J. & Ma, T. *Adv. Mater.* **26**, 8147-8153 (2014).
- [9] Yang, S., Kim, J., Tak, Y. J., Soon, A. & Lee, H. *Angew. Chem. Int. Ed.* **54**, 1-6 (2015).
- [10] Fei, H., Dong, J., Arellano-Jiménez, M. J., Ye, G., Kim, N. D., Samuel, E. L. G., Peng, Z., Zhu, Z., Qin, F., Bao, J., Yacaman, M. J., Ajayan, P. M., Dongliang, C. & Tour, J. M. *Nat. Commun.* **6**, 8668 (2015).
- [11] Qiao, B., Wang, A., Yang, X., Allard, L. F., Jiang, Z., Cui, Y., Liu, J., Li, J. & Zhang, T. *Nat. Chem.* **3** (2011) 634–641.
- [12] Wei, H., Liu, X., Wang, A., Zhang, L., Qiao, B., Yang, X., Huang, Y., Miao, S., Liu, J. & Zhang, T. *Nat. Commun.* **5** (2014) 5634.
- [13] Kuhn, P., Antonietti, M. & Thomas, A. *Angew. Chem. Int. Ed.* **47**, 3450–3453 (2008).
- [14] Palkovits, R., Antonietti, M., Kuhn, P., Thomas, A. & Schüth, F. Solid Catalysts for the Selective Low-Temperature Oxidation of Methane to Methanol. *Angew. Chem. Int. Ed.* **48**, 6909–6912 (2009).
- [15] Lu, Q., Rosen, J., Zhou, Y., Hutchings, G. S., Kimmel, Y. C., Chen, J. G. & Jiao, F. *Nat.*

- Commun.* **5**, 3242 (2014).
- [16] Shuai, D., Choe, J. K., Shapley, J. R. & Werth, C. J. *Environ. Sci. Technol.* **46**, 2847-2855 (2012).
- [17] Gao, D., Zhou, H., Wang, J., Miao, S., Yang, F., Wang, G., Wang, J. & Bao, X. *J. Am. Chem. Soc.* **137**, 4288-4291 (2015).
- [18] Hillier, I. H., Guest, M. F., Higginson, B. R. & Lloyd, D. R. *Mol. Phys.* **27**, 215-223 (1973).
- [19] Calle-Vallejo, F., Loffreda, D., Koper, M. T. M. & Sautet, P. *Nat. Chem.* **350**, 403-410 (2015).
- [20] Calle-Vallejo, F.; Tymoczko, J., Colic, V., Vu, Q. H., Pohl, M. D., Morgenstern, K., Loffreda, D., Sautet, P., Schuhmann, W. & Bandarenka, A. S. *Science* **350**, 185-189 (2015).
- [21] Hu, G., Nitze, F., Gracia-Espino, E., Ma, J., Barzegar, H. R., Sharifi, T., Jia, X., Shchukarev, A., Lu, L., Ma, C., Yang, G. & Wågberg, T. *Nat. Commun.* **5**, 5253 (2015).
- [22] Lane, R. F. & Hubbard, A. T. *J. Phys. Chem.* **77**, 1401-1410 (1973).
- [23] Watkins, B. F., Behling, J. R., Kariv, E. & Miller, L. L. *J. Am. Chem. Soc.* **97**, 3549-3550 (1975).
- [24] Brown, A. P., Koval, C. & Anson, F. C. *J. Electroanal. Chem.* **72**, 379-387 (1976).
- [25] Yamazaki, S., Yamada, Y., Ioroi, T., Fujiwara, N., Siroma, Z., Yasuda, K. & Miyazaki, Y. *J. Electroanal. Chem.* **576**, 253-259 (2005).
- [26] Baranton, S., Coutanceau, C., Roux, C., Hahn, F. & Léger, J.-M. *J. Electroanal. Chem.* **577**, 223-234 (2005).
- [27] Chen, R., Li, H., Chu, D. & Wang, G. *J. Phys. Chem. C* **113**, 20689-20697 (2009).
- [28] Zhang, W., Shaikh, A. U., Tsui, E. Y. & Swager, T. M. *Chem. Mater.* **21**, 3234-3241 (2009).
- [29] Morozan, A., Campidelli, S., Filoramo, A., Jusselme, B. & Palacin, S. *Carbon* **49**, 4839-4847 (2011).
- [30] Michalska, Z. M. & Webster, D. E. *Platinum Metals Rev.* **18**, 65-73 (1974).
- [31] Qiao, B., Wang, A., Yang, X., Allard, L. F., Jiang, Z., Cui, Y., Liu, J., Li, J. & Zhang, T. *Nat. Chem.* **3**, 634-641 (2011).

- [32] Shi, Y., Zhao, C., Wei, H., Guo, J., Liang, S., Wang, A., Zhang, T., Liu, J. & Ma, T. *Adv. Mater.* **26**, 8147-8153 (2014).
- [33] Moses-DeBusk, M., Yoon, M., Allard, L. F., Mullins, D. R., Wu, Z., Yang, X., Veith, G., Stocks, G. M. & Narula, C. K. *J. Am. Chem. Soc.* **135**, 12634-12645 (2013).
- [34] Wang, L., Zhang, S., Zhu, Y., Patlolla, A., Shan, J., Yoshida, H., Takeda, S., Frenkel, A. I. & Tao, F. F. *ACS Catal.* **3**, 1011-1019 (2013).
- [35] Yang, S., Kim, J., Tak, Y. J., Soon, A. & Lee, H. *Angew. Chem. Int. Ed.* **55**, 2058–2062 (2016).
- [36] Lucci, F. R., Marcinkowski, M. D., Lawton, T. J. & Sykes, E. C. H. *J. Phys. Chem. C* **119**, 24351-24357 (2015).
- [37] Yan, H., Cheng, H., Yi, H., Lin, Y., Yao, T., Wang, C., Li, J., Wei, S. & Lu, J. *J. Am. Chem. Soc.* **137**, 10484-10487 (2015).
- [38] Yang, X.-F., Wang, A., Qiao, B., Li, J., Liu, J. & Zhang, T. *Acc. Chem. Res.* **46**, 1740-1748 (2013).
- [39] Zhang, X., Shi, H. & Xu, B. Q. *Angew. Chem., Int. Ed.* **44**, 7132–7135 (2005).
- [40] Yaghi, O. M., Li, G. & Li, H. *Nature* **378**, 703-706 (1995).
- [41] Müller, A., Reuter, H. & Dillinger, S. *Angew. Chem. Int. Ed. Engl.* **34**, 2311-2327 (1995).
- [42] Janiak, C. *Angew. Chem. Int. Ed. Engl.* **36**, 1431-1434 (1997).
- [43] Huang, L., Wang, H., Chen, J., Wang, Z., Sun, J., Zhao, D. & Yan, Y. *Microporous Mesoporous Mater.* **58**, 105-114 (2003).
- [44] Côté, A. P., Benin, A. I., Ockwig, N. W., O’Keeffe, M., Matzger, J. & Yaghi, Y. *Science* **310**, 1166-1170 (2005).
- [45] Wang, N., Cai, Y. & Zhang, R. Q. *Mater. Sci. Eng., R* **60**, 1-51 (2008).
- [46] Pacilé, D., Meyer, J. C., Girit, C. Ö. & Zettl, A. *Appl. Phys. Lett.* **92**, 133107 (2008).
- [47] Davis, M. E. *Nature* **417**, 813-821 (2002).
- [48] Blake, A. J., Champness, N. R., Crew, M. & Parsons, S. *New J. Chem.* **23**, 13-15 (1999).
- [49] Cervera, B., Sanz, J. L., Ibáñez, M. J., Vila, G., LLoret, F., Julve, M., Ruiz, R. Ottenwaelder, X., Aukauloo, A., Poussereau, S., Journaux, Y. & Muñoz M. C. *J. Chem.*

- Soc., Dalton Trans.* **5**, 781-790 (1998).
- [50] Cervera, B., Sanz, J. L., Ibáñez, M. J., Vila, G., Lloret, F., Julve, M., Ruiz, R., Ottenwaelder, X., Aukauloo, A., Poussereau, S., Journaux, Y. and Muñoz, M. C. *J. Chem. Soc., Dalton Trans.* **5**, 781-790 (1998).
- [51] Richards, R. B. *J. Appl. Chem.* **1**, 370-376 (1951).
- [52] El-Kaderi, H. M., Hunt, J. R., Mendoza-Cortés, J. L., Côté, A. P., Taylor, R. E., O’Keeffe, M. & Yaghi, O. M. *Science* **316**, 268-272 (2007).
- [53] Ding, S.-Y. & Wang, W. *Chem. Soc. Rev.* **42**, 548—568 (2013).
- [54] Feng, X., Chen, L., Dong, Y. & Jiang, D. *Chem. Commun.* **47**, 1979–1981 (2011).
- [55] Uribe-Romo, F. J., Hunt, J. R., Furukawa, H., Klöck, C., O’Keeffe, M. & Yaghi, O. M. *J. Am. Chem. Soc.* **131**, 4570–4571 (2009).
- [56] Weber, J., Antonietti, M. & Thomas, *Macromolecules* **41**, 2880–2885 (2008).
- [57] Fang, Q., Zhuang, Z., Gu, S., Kaspar, R. B., Zheng, J., Wang, J., Qiu, S. & Yan, Y. *Nat. Commun.* **5**, 4503 (2014).
- [58] Feng, X., Ding, X. & Jiang, D. *Chem. Soc. Rev.* **41**, 6010–6022 (2012).
- [59] Kuhn, P., Thomas, A. & Antonietti, M. *Macromolecules* **42**, 319–326 (2009).
- [60] Periana, R. A., Taube, D. J., Gamble, S., Taube, H., Satoh, T. & Fujii, H. *Science* **280**, 560-564 (1998).
- [61] Bavykina, A. V., Goesten, M. G., Kapteijn, F., Makkee, M. & Gascon, J. *ChemSusChem* **8**, 809 – 812 (2015).



## Chapter 2.

### Platinum-modified covalent triazine frameworks hybridized with carbon nanoparticles as methanol-tolerant oxygen reduction electrocatalysts

Covalent triazine frameworks (CTFs), which are crosslinked porous polymers with two-dimensional molecular structures, are promising materials for heterogeneous catalysts. However, the application of the frameworks as electrocatalysts has not been achieved to date because of their poor electrical conductivity. In this chapter, the author attempted to synthesize a novel hybrid material composed of CTF and conductive carbon nanoparticles as a catalyst for electrochemical reactions. After that, he clarified the difference of the reactivities between single Pt atoms carried on synthesized hybrid material and commercial Pt/C catalyst using methanol/oxygen system.

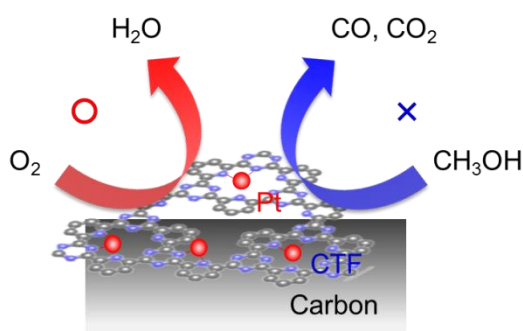


**Figure | Schematic illustration of the selective reaction between hydrogen oxidation reaction and oxygen reduction reaction on single Pt atom modified CTF.**

## 2.1. Introduction

Covalent organic frameworks (COFs) have attracted a keen attention as novel catalyst platforms [1–6] because of their unique physicochemical properties, including their nano-porous structure, mechanical robustness and high design flexibility. For example, Ding *et al.* reported that a palladium-modified imine-linked COF catalyzed Suzuki–Miyaura coupling reactions with a high stability and an easy recyclability [7]. Chan-Thaw *et al.* deposited palladium nanoparticles on covalent triazine frameworks (CTFs) and demonstrated that this material was an effective catalyst for liquid-phase glycerol oxidation [8]. Another interesting example of a COF-based catalyst is platinum modified CTF (Pt-CTF) developed by Palkovits *et al.* [9,10], which has been known to function as a heterogeneous (solid) catalyst for partial oxidation of methane ( $\text{CH}_4$ ) to methyl bisulfate ( $\text{CH}_3\text{OSO}_3\text{H}$ ) in  $\text{H}_2\text{SO}_4$  using oleum as an oxidant. The Pt-CTF was developed by being inspired by Pt-bipyrimidine complex, known as a Periana catalyst, which could catalyze the same partial oxidation reaction [11,12]. Thus, the work carried out by Palkovits *et al.* is important in that they developed the concept of molecular complex catalysts to the robust heterogeneous Pt-CTF materials.

Pt-CTFs are attractive also as heterogeneous electrocatalysts, since molecular Pt complexes with a single metal center is known to exhibit reaction selectivity in some homogeneous redox reactions, such as alkane oxidation [13,14] and carbon dioxide reduction reactions [15]. Considering that molecular complex-based electrocatalysts are generally unstable, it is expected that Pt-CTFs can serve as electrocatalysts with both unique selectivity and high robustness. However, CTF-based materials have not previously been applied as electrocatalysts because of their poor electrical conductivity [16]. In the present work, the author demonstrates a solution to this problem by synthesizing a hybrid material consisting of Pt-CTF and conductive carbon nanoparticles (CPs). The hybridized material (Pt-CTF/CP) exhibits electrocatalytic

activity for oxygen reduction reaction (ORR) in acidic solution with a high methanol tolerance, which is a very attractive property for direct methanol fuel cells (DMFCs) as the methanol crossover effect is one of the issues to be addressed [17–21]. To the best of our knowledge, this is the first demonstration of the potential for CTF-based materials to serve as electrocatalysts.

## **2.2. Experimental details**

### **2.2.1. Synthesis procedure of Pt-CTF/CP**

CTF/CP was synthesized by polymerization of 2,6-dicyanopyridine in a molten salt of zinc chloride ( $\text{ZnCl}_2$ ). Specifically, 1.363 g  $\text{ZnCl}_2$  (Wako), 0.129 g 2,6-dicyanopyridine (Sigma) and 0.129 g Ketjen Black EC600JD were mixed in a globe box. The mixture was placed in a Pyrex glass tube and the tube was sealed, evacuated, heated and kept at a terminal temperature of 400 °C for 21 h. The resulting powder was washed with 0.1 M HCl, water, tetrahydrofolate and acetonitrile, and dried in vacuo. Pt atoms were modified by impregnation in 160 mM  $\text{K}_2[\text{PtCl}_4]$  (Wako) aqueous solution at 60 °C for 4 h before being washed with water and acetone.

### **2.2.2. Electrochemical characterization**

Electrochemical activity for ORR was evaluated using a rotating disk electrode. Working electrodes were first prepared by dispersing 5mg of powder samples in 175 ml ethanol and 47.5 ml Nafion solution (5 wt% solution in a mixture of lower aliphatic alcohols and water, Aldrich). A 7-ml aliquot of ink was dropped on a glassy carbon electrode ( $0.196 \text{ cm}^{-2}$ ). The catalyst loading was controlled at  $0.8 \text{ mg cm}^{-2}$ . A Pt wire and Ag/AgCl (saturated KCl) were used as the counter and reference electrodes, respectively. Commercial 20 wt% Pt/C and Pt-Vulcan XC-72 were purchased from Tanaka Kikinzoku and Fuel Cell Earth, respectively. The electrical conductivity of the

catalysts was measured with a resistivity meter (Mitsubishi Chemical, Loresta GP). The working electrode was rotated with a rotation speed of 1,500 r.p.m.

### 2.2.3. Physical characterization

X-ray photoelectron spectra (Axis Ultra, Kratos Analytical Co.) were taken with monochromated Al  $K\alpha$  X-rays at  $h\nu = 1,486.6$  eV. For detailed chemical analysis, backgrounds of core-level spectra were subtracted using the Shirley method. N-1s spectra were fitted with Voigt (70% Gaussian and 30% Lorentzian) functions. Hard X-ray absorption measurements (XAFS) were performed at the hard X-ray beam line BL01B01 at SPring-8, Japan and by using R-XAS Looper (Rigaku). Transmission-yield spectra were acquired using a double-crystal Si (111) monochromator. The morphological structures were characterized using TEM with an EDX detector (ARM-200F, JEOL) and SEM (SU-8000, Hitachi). The nitrogen adsorption-desorption isotherm at 77 K was obtained by a BET (NOVA-4200e, Quantachrome).

## 2.3. Results

### 2.3.1. Morphological characterization of Pt-CTF/CP

Pt-CTF/CP was synthesized by modifying the standard synthesis protocol of Pt-CTF [9,10,22,23]. Briefly, CTFs were obtained by in situ polymerization of 2,6-dicyanopyridine in molten  $ZnCl_2$  containing CPs (the weight ratio of 2,6-dicyanopyridine to CP was 1: 1), after which the CTF/CP was impregnated with a platinum chloride salt to obtain Pt-CTF/CP. Scanning electron microscopic (SEM) inspection reveals that the particles of Pt-CTF/CP (20–200 nm, Fig. 2.1a) are much smaller than that of Pt-CTF polymerized without CPs (1–5  $\mu$ m, Fig. 2.1b), suggesting that CTF is well mixed with CPs during the in situ polymerization. Then, the author conducted high-resolution transmission electron microscopy (HR-TEM, Fig. 2.2a) and

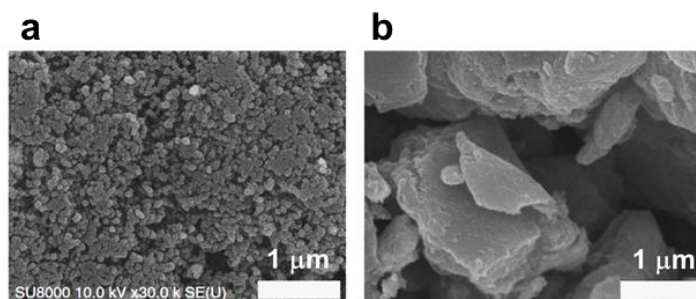


**Fig. 2.1 | Representative SEM images.** (a) Pt-CTF/CP and (b) Pt-CTF.

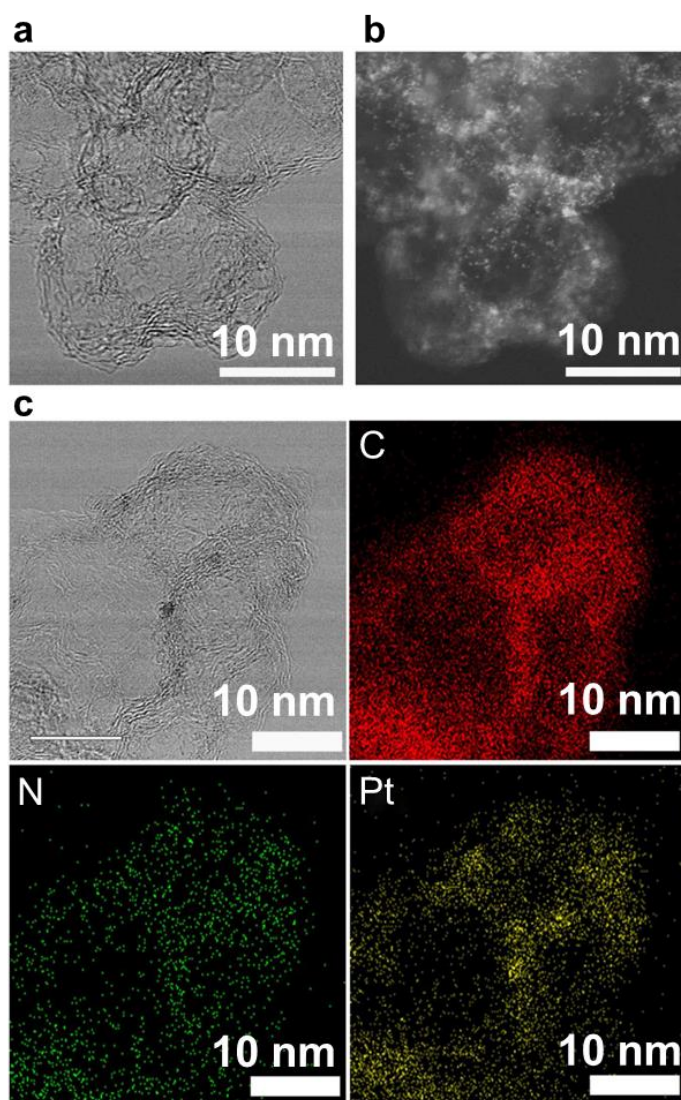


**Fig. 2.2 | Transmission electron microscopic images of Pt-CTF/CP.** (a) A representative HR-TEM image of Pt-CTF/CP and (b) the corresponding HAADF-STEM image. (c) Another HR-TEM image of Pt-CTF/CP and the corresponding EDX mappings for C, N and Pt atoms.

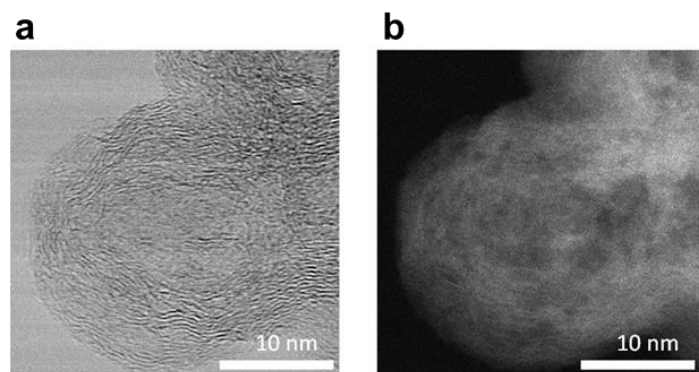


**Fig. 2.3 | Transmission electron microscopic images of CP (without Pt-CTF).** (a) HR-TEM image and (b) the corresponding HAADF-STEM image.

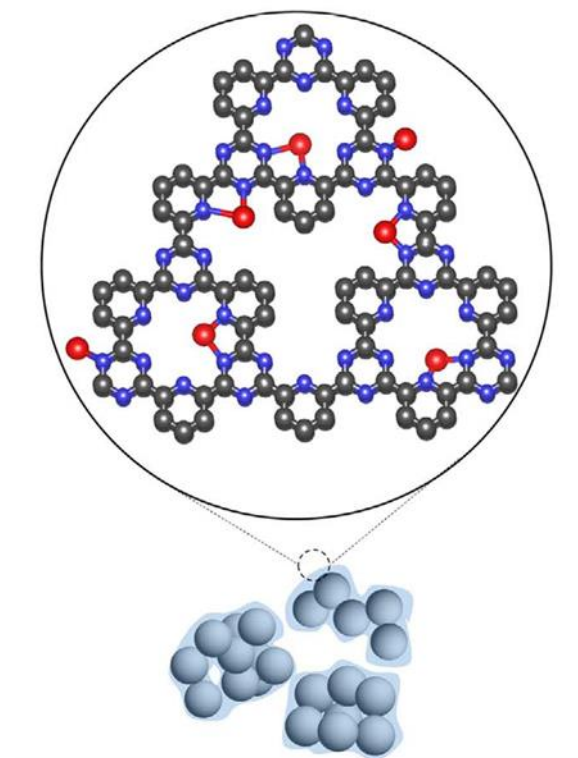


**Fig. 2.4 | Schematic illustration of Pt-CTF/CP.** Blue: N, red: Pt and black: C, Chlorine atoms are not shown for clarity.

the corresponding high-angle annular dark-field scanning transmission electron microscopy (HAADF-STEM, Fig. 2.2b), the latter of which is a powerful tool for discerning individual heavy atoms [24–26]. It was confirmed that the bright spots corresponding to Pt atoms (the sizes < 0.5 nm) were uniformly dispersed and almost no Pt nanoparticles (the sizes > 1 nm) were observed (Fig. 2.2b). Such bright spots could not be observed on the CPs (without Pt-CTF) as shown in Fig. 2.3. Figure 2.2c exhibits another HR-TEM image and the corresponding elemental maps (carbon, nitrogen and platinum) obtained by energy dispersive X-ray (EDX) technique. Notably, the EDX maps revealed that Pt and N atoms are localized at the edges of CPs, strongly suggesting that CPs (or the aggregates) are covered with Pt-CTF as schematically shown in Fig. 2.4.

Next, the nitrogen adsorption–desorption isotherms were obtained to analyze the pore structure of Pt-CTF/CP (Fig. 2.5). Type IV isotherm and H<sub>2</sub> hysteresis loop were observed, suggesting that porous structures existed in the synthesized Pt-CTF/CP [27,28]. The pore-size distribution calculated based on nonlocal density functional theory was shown in the inset of Fig. 2.5. Although CP (Ketjen Black) is known to exhibit a peak at 3.6–3.7nm (refs 29,30), the synthesized Pt-CTF/CP exhibited peaks at 1.4 and 5.3 nm. The total pore volume and the BET surface area were estimated to be 0.79 cm<sup>3</sup> g<sup>-1</sup> and 555 m<sup>2</sup> g<sup>-1</sup>, respectively.

### **2.3.2. Electrochemical characterizations of Pt-CTF/CP**

Figure 2.6 shows current density (*j*) versus potential (*U*) curves for Pt-CTF/CP obtained in an oxygen-saturated 0.5 M H<sub>2</sub>SO<sub>4</sub> solution. Although the ORR activity of Pt-CTF (without CP) was very low (blue curve), the ORR current increased significantly upon hybridization of Pt-CTF with CPs (red curve). This enhancement in ORR activity can be explained on the basis that both the electric conductivity and the electrochemically active surface area of the material were increased by the hybridization

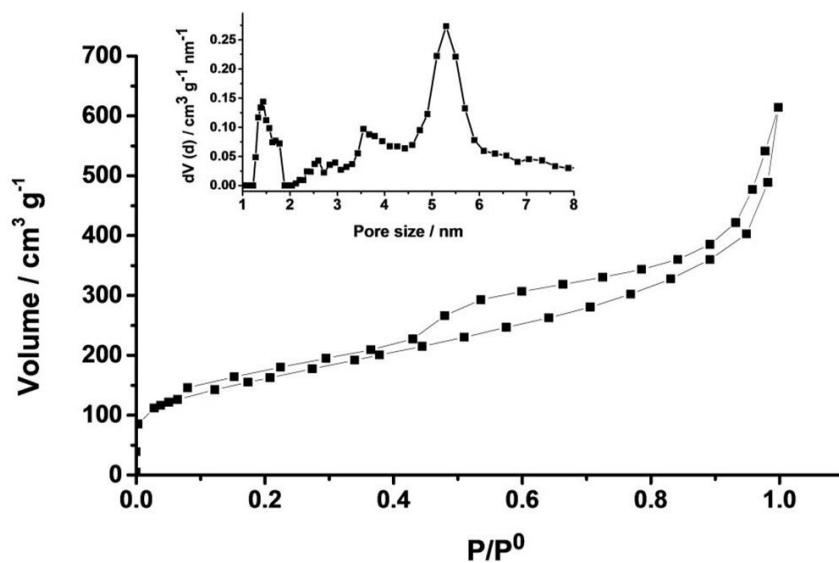


**Fig. 2.5 | Nitrogen adsorption-desorption isotherms for Pt-CTF/CP.** The inset shows the size distribution calculated based on nonlocal density functional theory (NL-DFT).

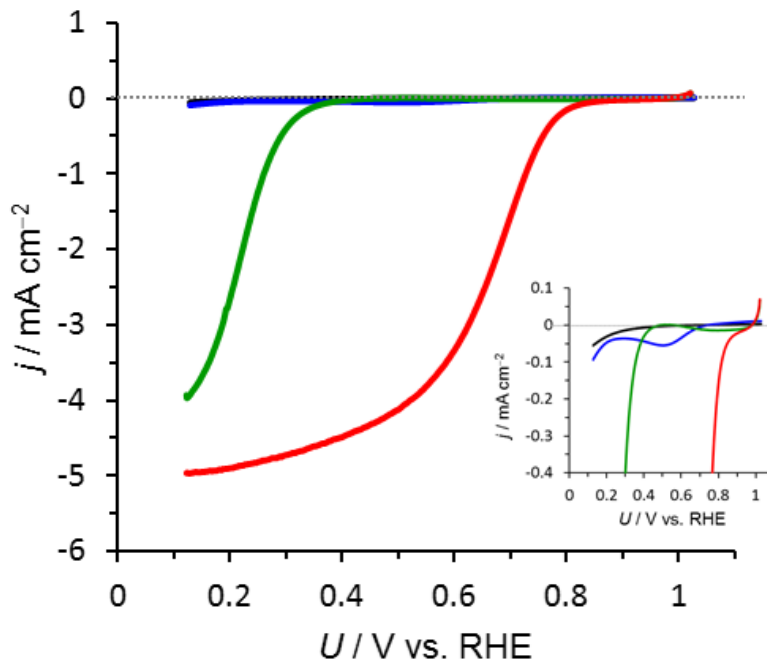


**Fig. 2.6 | ORR electrocatalytic activities.**  $j$  versus  $U$  curves for CTF (black), CTF/CP (green), Pt-CTF (blue) and Pt-CTF/CP (red) in 0.5 M H<sub>2</sub>SO<sub>4</sub> saturated with dissolved oxygen, obtained at a scan rate of 10 mV s<sup>-1</sup>. Rotation rate 1,500 r.p.m. (Inset) Magnified curves.

with CPs (Fig. 2.1a,b and Table 2.1). In contrast, when the CTFs (without Pt) were hybridized with CPs (green curve), the ORR onset potential was much negative than that of Pt-CTF/CP, indicating that the Pt atoms in Pt-CTF/CP are an active centre for ORR. To the best of our knowledge, this is the first demonstration of the application of a CTF-based material as an electrocatalyst.

Next, to investigate the methanol tolerance of Pt-CTF/CP, the author intentionally added methanol to a 0.5 M  $\text{H}_2\text{SO}_4$  solution in the presence of oxygen. Cyclic voltammograms obtained in the presence of methanol are shown in Fig. 2.7. In case of a commercial 20 wt% Pt/C, the oxidation peak of methanol can be clearly observed at around +600 mV versus RHE (Fig. 2.7b). After the addition of 1 M methanol, the onset potential of the cathodic current shifted  $\sim 200$  mV in the negative direction, reaching 580 mV versus RHE. In contrast, surprisingly, the overlap of the methanol oxidation current with that of the ORR was almost negligible for Pt-CTF/CP

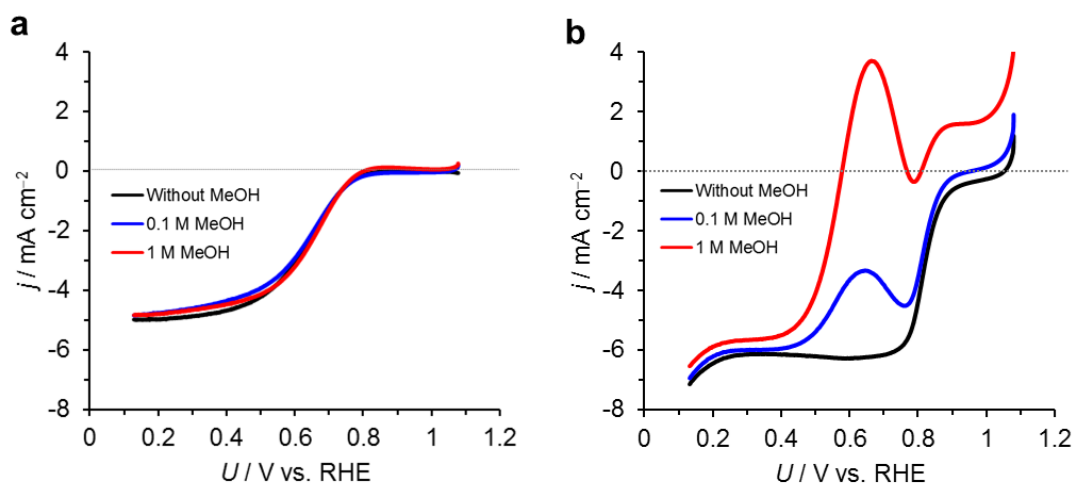


**Fig. 2.7 | Methanol oxidation activity of Pt-CTF/CP and Pt/C.**  $j$  versus  $U$  curves for (a) Pt-CTF/CP and (b) 20 wt% Pt/C in 0.5M  $\text{H}_2\text{SO}_4$  in the absence of oxygen. Methanol concentration: (black) 0M, (blue) 0.1M and (red) 1.0 M.

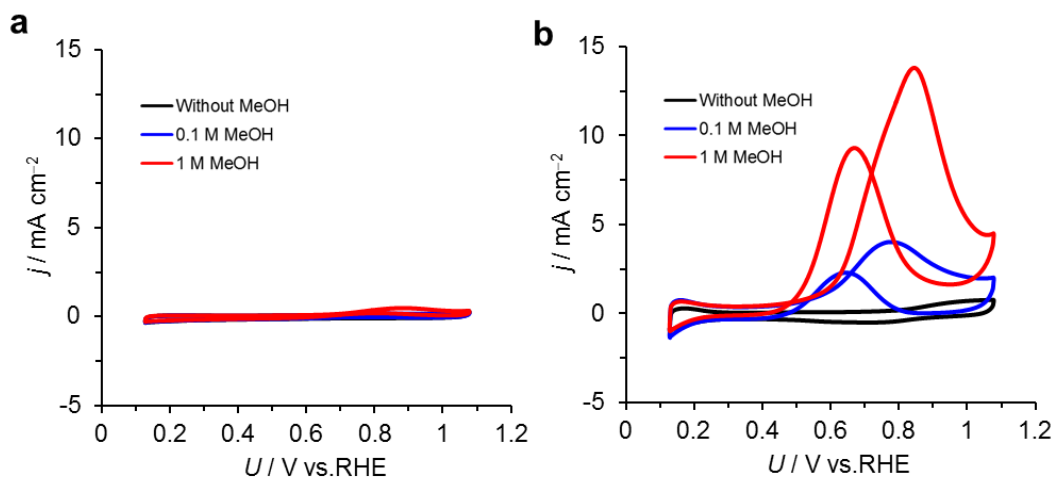


**Fig. 2.8 | Methanol oxidation activity of Pt-CTF/CP and Pt/C.**  $j$  versus  $U$  curves for (a) Pt-CTF/CP and (b) 20 wt% Pt/C in 0.5 M H<sub>2</sub>SO<sub>4</sub> in the absence of oxygen. Methanol concentration: (black) 0 M, (blue) 0.1 M and (red) 1.0 M.

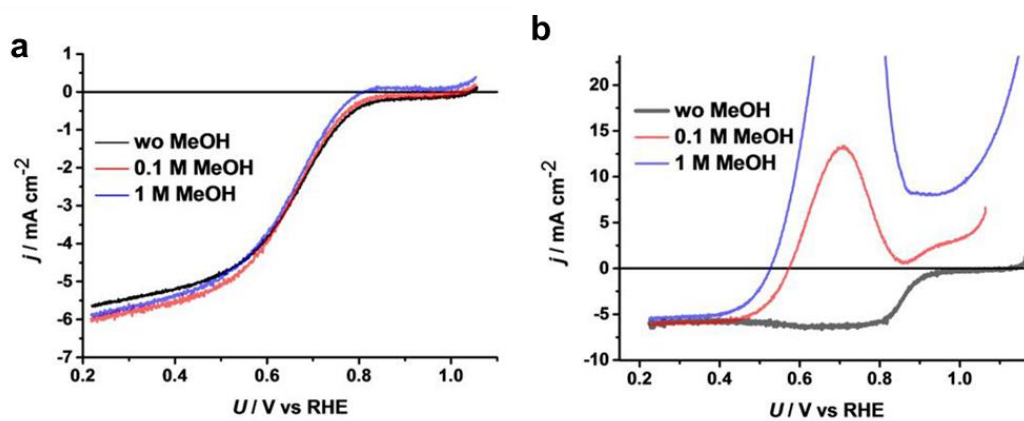


**Fig. 2.9 | ORR electrocatalytic activities in 0.5 M HClO<sub>4</sub>.**  $j$  versus  $U$  curves for (a) Pt-CTF/CP and (b) 20 wt% Pt-Vulcan XC-72 with saturated dissolved oxygen. Methanol concentration: (black) 0 M, 0.1 M (black)

even in the presence of 1 M methanol. To directly compare the methanol oxidation activity of Pt-CTF/CP and 20 wt% Pt/C, the author obtained cyclic voltammograms in H<sub>2</sub>SO<sub>4</sub> solution containing methanol in the absence of dissolved oxygen (Fig. 2.8). The peak currents for methanol oxidation with Pt-CTF/CP (Fig. 2.8a) were ~1/40 compared with those with Pt/C (Fig. 2.8b). The author confirmed that methanol oxidation is inactive even in 0.5 M HClO<sub>4</sub> as shown in Fig. 2.9, which excludes the possibility that the methanol tolerance originated from the suppression of methanol oxidation by strongly adsorbed sulfate/bisulfate [31,32]. Thus, the above results clearly showed that Pt-CTF/CP exhibits little activity with regard to methanol oxidation.

### 2.3.3. X-ray characterizations of Pt-CTF/CP

Characterizations of Pt-CTF/CP were conducted using various X-ray techniques to obtain information on the molecular mechanism of the methanol tolerance. The surface concentration of each element was determined by an X-ray photoelectron spectroscopy (XPS), and the results are summarized in Table 2.1. Peaks assignable to Pt and N were confirmed, and the Pt/N elemental ratio did not show a clear dependence on

<b>Table 2.1   XPS-elemental analyses.</b>					
<b>Catalyst</b>	<b>C content (at%)</b>	<b>N content (at%)</b>	<b>Pt content (at%)</b>	<b>Cl content (at%)</b>	<b>Pt/N</b>
CTF	81	17	—	2.6	—
Pt-CTF	76	15	3.0	5.5	0.20
Pt-CTF/CP	91	5.6	1.0	2.3	0.18

CP, carbon nanoparticle; CTF, covalent triazine framework; Pt-CTF, platinum-modified CTF; XPS, X-ray photoelectron spectroscopy.  
The composition ratios are estimated from the XPS results.

the amount of CP (the right column of Table 2.1), implying that the structures of Pt-CTFs are essentially identical even by hybridizing with CPs. In addition, the surface concentration of C, which was calculated with XPS, became higher with the increasing ratio of CP. Taking into account that the CP aggregates are uniformly covered by Pt-CTFs (Fig. 2.1), these results indicated that the thickness of Pt-CTFs is less than the escape depth of photoelectrons (ca.  $\sim 3$  nm) as schematically shown in Fig. 2.4, which enabled the Pt-CTF to possess electronic conduction with the CPs.

The details of the electronic structures of Pt-CTFs were investigated by taking XPS and X-ray absorption near-edge structures (XANES; Figs 2.10–2.13). The Pt-4f<sub>7/2</sub> peaks were located at 72.5 eV for Pt-CTF/CP and 72.2 eV for Pt-CTF (Fig.2.10). These binding energies were over 1 eV higher than those for metal Pt (70.9 eV), revealing that the valence state of Pt was Pt(II) [33,34]. In addition, XANES of Pt L<sub>3</sub> edge shown in Fig. 2.11 exhibited that the white-line intensities at 11,562 eV for Pt-CTF (1.45) and

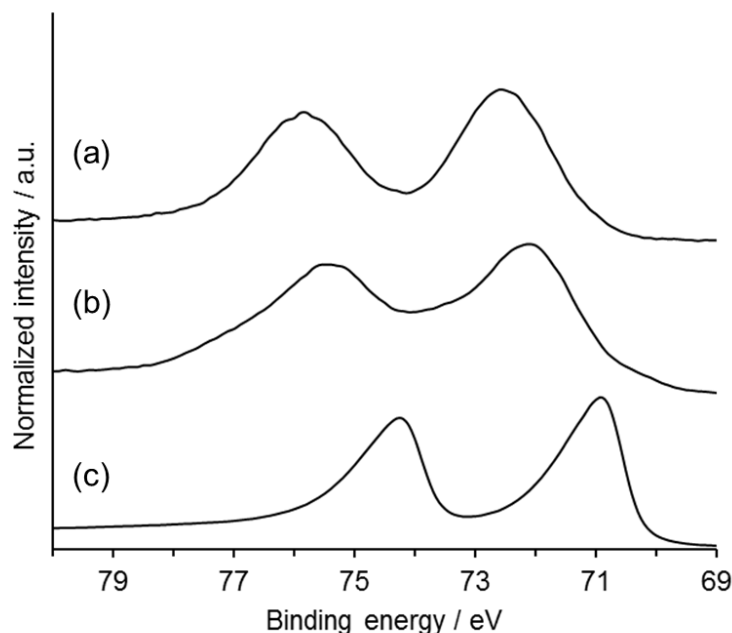


**Fig. 2.10 | Pt-4f XPS spectra.** (a) Pt-CTF/CP, (b) Pt-CTF and (c) Pt metal.

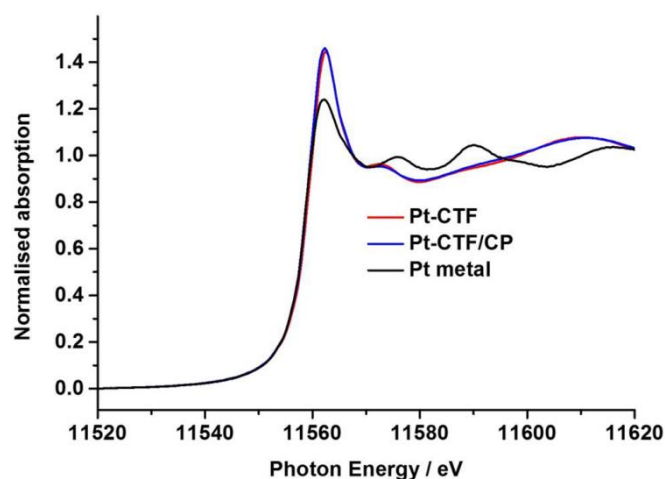


Fig. 2.11 | Pt  $L_3$  XANES spectra for Pt-CTF, Pt-CTF/CP and Pt metal.

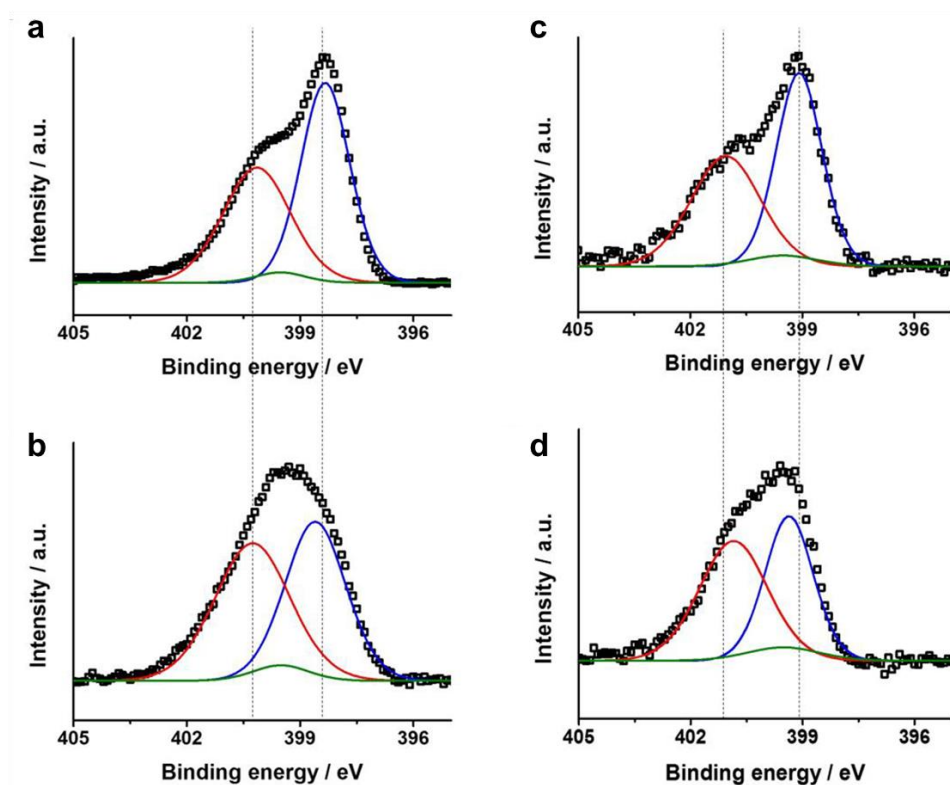


Fig. 2.12 | N-1s XPS spectra. (a) CTF, (b) Pt-CTF, (c) CTF/CP and (d) Pt-CTF/CP. Black dots, measured data; lines, deconvoluted curves (blue:  $C_2NH$ , red:  $C_3N$ , green: cyano group). Note that the peak positions were not identical upon adding CP as CTF is not conductive and easily to be charged by X-ray irradiation.

**Table 2.2 | Binding energies and relative ratios of the four nitrogen compounds derived from decomposed N-1s XPS spectra.**

**a) CTF**

	<b>Binding energy / eV</b>	<b>Relative ratio / %</b>
C <sub>2</sub> NH	398.4	61.5
C <sub>3</sub> N	400.1	35.3
C≡N	399.5	3.2

**b) Pt-CTF**

	<b>Binding energy / eV</b>	<b>Relative ratio / %</b>
C <sub>2</sub> NH	398.4	61.5
C <sub>3</sub> N	400.1	35.3
C≡N	399.5	3.2

**c) CTF/CP**

	<b>Binding energy / eV</b>	<b>Relative ratio / %</b>
C <sub>2</sub> NH	398.4	61.5
C <sub>3</sub> N	400.1	35.3
C≡N	399.5	3.2

**d) Pt-CTF/CP**

	<b>Binding energy / eV</b>	<b>Relative ratio / %</b>
C <sub>2</sub> NH	398.4	61.5
C <sub>3</sub> N	400.1	35.3
C≡N	399.5	3.2

Pt-CTF/CP (1.46) are higher than those for metal Pt (1.24), indicating that Pt atoms existed as oxidized forms in both Pt-CTF and Pt-CTF/CP [35]. Thus, the Pt-4f XPS and the XANES results also show that there was no formation of Pt aggregates (metal Pt) on Pt-CTFs. Next, the author focused on the N-1s XPS spectrum (Fig. 2.12 and Table 2.2). The N-1s peak at 399.2 eV observed for the 2,6-dicyanopyridine (that is, the catalyst monomer, Fig. 2.13) was not observed for the Pt-CTF/CP, indicating that the cyclical trimerization of cyano reaction groups efficiently proceeded. The N-1s peak of Pt-CTF/CP could be deconvoluted into C<sub>2</sub>NH (398–399 eV) and C<sub>3</sub>N (400–401 eV) [4]. The peak assigned to C<sub>2</sub>NH was shifted to the higher-energy side upon Pt loading on both CTF and CTF/CP, indicating that the electron density of the N atoms became lower in the presence of Pt atoms. The decrease in the electron density of the N atoms can be explained by considering the formation of Pt-N coordination bonds (this point will be argued later). All the features described above were confirmed even for Pt-CTF (that is, without CPs), indicating that the hybridization with CPs did not influence on the electronic properties of N atoms in Pt-CTFs.

Next, the author conducted extended X-ray absorption fine structure (EXAFS) analyses of Pt *L*<sub>3</sub> edge to obtain information on the molecular structure of Pt-CTF/CP. Fourier transformations of *k*<sup>3</sup>-weighted EXAFS oscillations for Pt-CTF/CPs, Pt-CTFs, commercial Pt(bpy)Cl<sub>2</sub> (bpy: 2,20-bipyridine), PtO<sub>2</sub>, K<sub>2</sub>[PtCl<sub>4</sub>] and Pt metal are shown in Fig. 2.14. The peak corresponding to a Pt–Pt bond at 2.6 Å was not observed at all for Pt-CTF/CPs. Instead, two peaks at *R* = 1.5 and 1.9 Å assignable to Pt–N and Pt–Cl bonds, respectively, were clearly observed, indicating that Pt exists in the form of a single atom as illustrated in Fig. 2.4. The ratio of the Pt–N peak to the Pt–Cl peak for Pt-CTFs corresponded to that for Pt(bpy)Cl<sub>2</sub> (model PtN<sub>2</sub>Cl<sub>2</sub> complex), implying that Pt atoms mainly existed as PtN<sub>2</sub>Cl<sub>2</sub>. It should be noted here that there was no clear difference in the EXAFS spectra between Pt-CTF/CP and Pt-CTF, indicating that the molecular structure of Pt-CTF is maintained upon the hybridization with CPs.

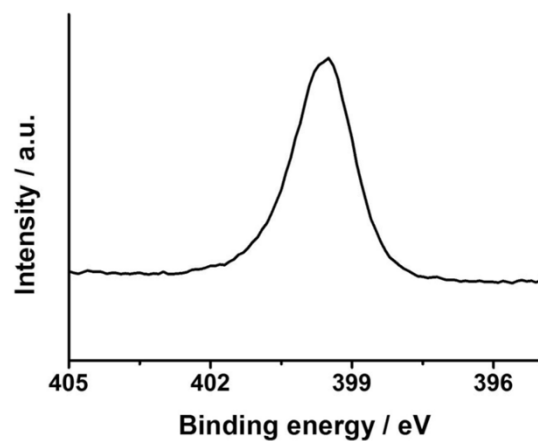


**Fig. 2.13** | N-1s XPS spectra for 2,6-dicyanopyridine.

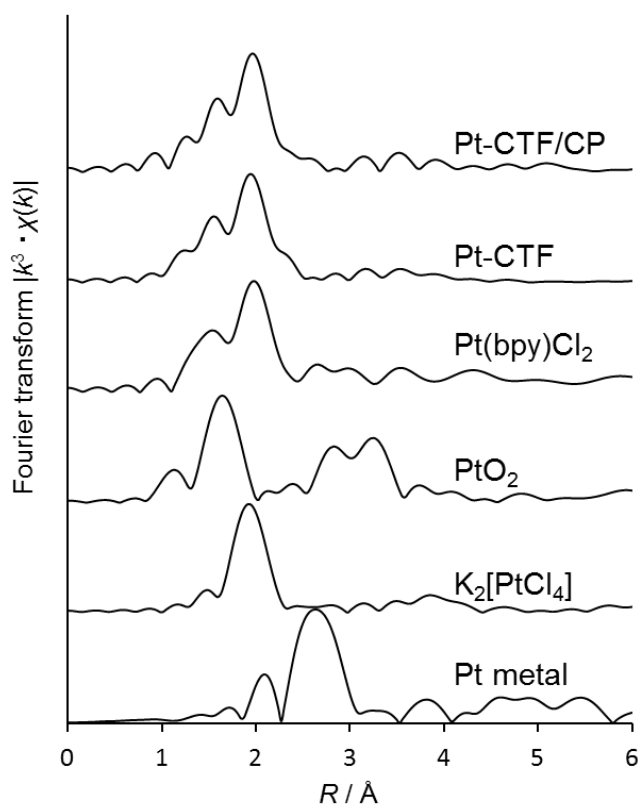


**Fig. 2.14** | EXAFS analyses.  $k^3$ -weighted Fourier transform spectra of EXAFS of Pt  $L_3$  edge for Pt-CTF/CP and Pt-CTF. The spectra of Pt(bpy)Cl<sub>2</sub>, PtO<sub>2</sub>, K<sub>2</sub>[PtCl<sub>4</sub>] and Pt metal are also shown as reference.

Table 2.3   Electrical resistances of Pt-CTF, Pt-CTF/CP and Pt/C.	
Catalyst	Resistance ( $\Omega$ cm)
Pt-CTF	$> 10^6$
Pt-CTF/CP	14
20 wt% Pt/C	3.8

Electrical resistances were measured with a resistivity meter using four probe method. Each catalyst powder was pelleted by press molding in 3.5 ton/cm<sup>2</sup>.

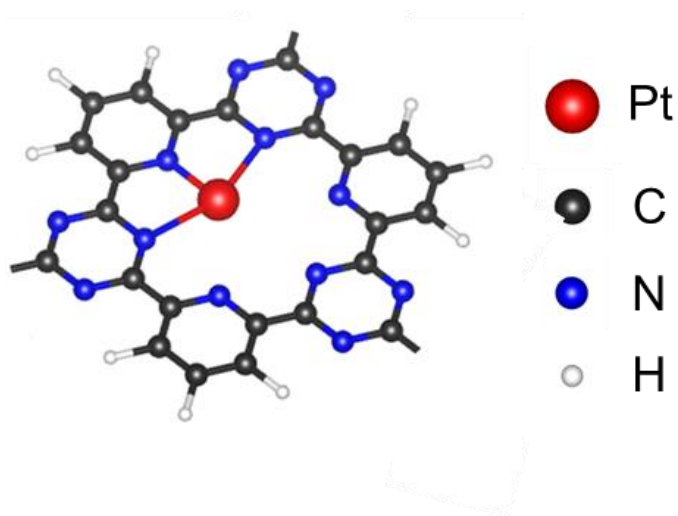


**Fig. 2.15 | Estimated Pt coordination structure at a pore site of CTF optimized by density functional theory (DFT) calculations. The calculation was carried out by Open MX.**

## 2.4. Discussion

Let us consider here about the molecular mechanism of the methanol-tolerant ORR electrocatalytic activity of Pt-CTF/CP. First, the author consider about the ORR on a single Pt site. An oxygen molecule is known to adsorb on a single Pt atom through either the Griffiths model (side-on adsorption) or the Pauling model (end-on adsorption) [36]. After the adsorption,  $\pi$  donation from the oxygen  $2\pi$  orbitals to the unoccupied Pt  $5d$  orbitals, and the  $\pi$  back donation from occupied Pt  $5d$  orbitals to the oxygen  $2\pi^*$  orbitals could simultaneously occur, resulting in the O–O bond activation [36,37]. In fact, Nakamura *et al.* [38] revealed using  $^{18}\text{O}$  isotopic infrared study that a single Pt atom and an oxygen molecule exchanged electrons, forming Pt–O<sub>2</sub> adduct through the side-on adsorption. Li *et al.* [39] also demonstrated by using first principles calculations that the O–O bond was activated on single Pt site via the  $\pi$  back donation through the end-on adsorption, resulting in the weakening of the O–O bond. These reported lines of work suggested that electrocatalytic ORR could proceed even on a single Pt atom.

On the contrary, a number of researchers have suggested that at least two Pt atoms are needed to oxidize methanol [40–46]. It is well known that methanol can be oxidized via a dual-path mechanism on Pt, that is, the carbon monoxide (CO) pathway and the non-CO pathway [44,45,47]. Cuesta [45,48] revealed by using cyanide-modified Pt electrode that dehydrogenation reaction of methanol to CO, a critical step of the CO pathway, required at least three contiguous Pt sites. As for the non-CO pathway, Osawa and colleagues [44] proposed a molecular mechanism based on the results obtained from in situ infrared (IR) absorption spectroscopy. They suggested that adsorbed oxygenated species (that is, O<sub>ad</sub> or OH<sub>ad</sub>) on the Pt site next to the methanol adsorption site are needed for first dehydrogenation of the O–H bond in methanol. This molecular mechanism was further supported by Kuzume *et al.* [49] again by in situ IR absorption spectroscopy. The previous lines of work have thus revealed that at least two adjacent Pt sites are required for methanol oxidation regardless

of whether the reaction proceeds via the CO or the non-CO pathways. Actually, to the best of our knowledge, there have been no reports of methanol oxidation on a single Pt-atom site. Considering these literatures, the methanol tolerance of Pt-CTF is reasonably explained because the EXAFS results demonstrated that the Pt atoms in Pt-CTF were isolated.

## 2.5. Conclusions

In this chapter, the author successfully synthesized Pt-CTF hybridized with CP, preserving its electronic and molecular structure, which exhibited ORR activity in acidic solutions with a high methanol tolerance. The methanol tolerance of the Pt-CTF/CP indicates that the methanol-crossover effect can be ignored. This property allows a considerable increase in the concentration of methanol in DMFC; consequently, the energy density of DMFC is expected to increase because of the use of Pt-CTF/CP. Another interesting aspect of this work is that it is the first demonstration of electrocatalytic function in CTF-based materials. This was achieved by hybridizing non-conductive CTFs with conductive CPs. The author anticipates that this methodology could be applied generally to other CTFs with unique catalytic properties.

## References

- [1] Côté, A. P., Benin, A. I., Ockwig, N. W., O’Keeffe, M., Matzger, A. J. & Yaghi, O. M. Porous, crystalline, covalent organic frameworks. *Science* **310**, 1166–1170 (2005).
- [2] Chan-Thaw, C. E., Villa, A., Prati, L. & Thomas, A. Triazine-based polymers as nanostructured supports for the liquid-phase oxidation of alcohols. *Chem. Eur. J.* **17**, 1052–1057 (2011).
- [3] Ding, S.-Y. & Wang, W. Covalent organic frameworks (COFs): from design to applications. *Chem. Soc. Rev.* **42**, 548–568 (2013).
- [4] Chan-Thaw, C. E., Villa, A., Veith, G. M., Kailasam, K., Adamczyk, L. A., Unocic, R. R., Prati, L. & Thomas, A. Influence of periodic nitrogen functionality on the selective oxidation of alcohols. *Chem. Asian J.* **7**, 387–393 (2012).
- [5] Feng, X., Ding, X. & Jiang, D. Covalent organic frameworks. *Chem. Soc. Rev.* **41**, 6010–6022 (2012).
- [6] Pachfule, P., Kandambeth, S., Diaz, D. D. & Banerjee, R. Highly stable covalent organic framework-Au nanoparticles hybrids for enhanced activity for nitrophenol reduction. *Chem. Commun.* **50**, 3169–3172 (2014).
- [7] Ding, S.-Y., Gao, J., Wang, Q., Zhang, Y., Song, W.-G., Su, C.-Y. & Wang, W. Construction of covalent organic framework for catalysis: Pd/COF-LZU1 in Suzuki-Miyaura coupling reaction. *J. Am. Chem. Soc.* **133**, 19816–19822 (2011).
- [8] Chan-Thaw, C. E., Villa, A., Katekomol, P., Su, D., Thomas, A. & Prati, L. Covalent triazine framework as catalytic support for liquid phase reaction. *Nano Lett.* **10**, 537–541 (2010).
- [9] Palkovits, R., Antonietti, M., Kuhn, P., Thomas, A. & Schueth, F. Solid catalysts for the selective low-temperature oxidation of methane to methanol. *Angew. Chem. Int. Ed.* **48**, 6909–6912 (2009).
- [10] Palkovits, R., Malotki, C., Baumgarten, M., Müllen, K., Baltes, C., Antonietti, M., Kuhn, P., Weber, J., Thomas, A. & Schüth, F. Development of molecular and solid catalysts for the

- direct lowtemperature oxidation of methane to methanol. *ChemSusChem* **3**, 277–282 (2010).
- [11] Periana, R. A., Taube, D. J., Gamble, S., Taube, H., Satoh, T. & Fujii, H. Platinum catalysts for the high-yield oxidation of methane to a methanol derivative. *Science* **280**, 560–564 (1998).
- [12] Kua, J., Xu, X., Periana, R. A. & Goddard, W. A. Stability and thermodynamics of the PtCl<sub>2</sub> type catalyst for activating methane to methanol: a computational study. *Organometallics* **21**, 511–525 (2002).
- [13] Shilov, A. E. & Shul'pin, G. B. Activation of C-H bonds by metal complexes. *Chem. Rev.* **97**, 2879–2932 (1997).
- [14] Stahl, S. S., Labinger, J. A. & Bercaw, J. E. Homogeneous oxidation of alkanes by electrophilic late transition metals. *Angew. Chem. Int. Ed.* **37**, 2181–2192 (1998).
- [15] Mitton, S. J. & Turculet, L. Mild reduction of carbon dioxide to methane with tertiary silanes catalyzed by platinum and palladium silyl pincer complexes. *Chem. Eur. J.* **18**, 15258–15262 (2012).
- [16] Guo, J., Xu, Y., Jin, S., Chen, L., Kaji, T., Honsho, Y., Addicoat, M. A., Kim, J., Saeki, A., Ihee, H., Seki, S., Irle, S., Hiramoto, M., Gao, J. & Jiang, D. Conjugated organic framework with three-dimensionally ordered stable structure and delocalized p clouds. *Nat. Commun.* **4**, 2736 (2013).
- [17] Krewer, U., Vidakovic-Koch, T. & Rihko-Struckmann, L. Electrochemical oxidation of carbon-containing fuels and their dynamics in low-temperature fuel cells. *ChemPhysChem* **12**, 2518–2544 (2011).
- [18] Argyropoulos, P., Scott, K. & Taama, W. M. The effect of operating conditions on the dynamic response of the direct methanol fuel cell. *Electrochim. Acta* **45**, 1983–1998 (2000).
- [19] Daems, N., Sheng, X., Vankelecom, I. F. J. & Pescarmona, P. P. Metal-free doped carbon materials as electrocatalysts for the oxygen reduction reaction. *J. Mater. Chem. A* **2**, 4085–

4110 (2014).

- [20] Gewirth, A. A. & Thorum, M. S. Electroreduction of dioxygen for fuel-cell applications: materials and challenges. *Inorg. Chem.* **49**, 3557–3566 (2010).
- [21] Brownson, D. A. C., Kampouris, D. K. & Banks, C. E. An overview of graphene in energy production and storage applications. *J. Power Sources* **196**, 4873–4885 (2011).
- [22] Kuhn, P., Thomas, A. & Antonietti, M. Toward tailorable porous organic polymer networks: a high-temperature dynamic polymerization scheme based on aromatic nitriles. *Macromolecules* **42**, 319–326 (2009).
- [23] Kuhn, P., Antonietti, M. & Thomas, A. Porous, covalent triazine-based frameworks prepared by ionothermal synthesis. *Angew. Chem. Int. Ed.* **47**, 3450–3453 (2008).
- [24] Herzing, A. A., Kiely, C. J., Carley, A. F., Landon, P. & Hutchings, G. J. Identification of active gold nanoclusters on iron oxide supports for CO oxidation. *Science* **321**, 1331–1335 (2008).
- [25] Sun, S., Zhang, G., Gauquelin, N., Chen, N., Zhou, J., Yang, S., Chen, W., Meng, X., Geng, D., Banis, M. N., Li, R., Ye, S., Knights, S., Botton, G. A., Sham, T.-K. & Sun, X. Single-atom catalysis using Pt/graphene achieved through atomic layer deposition. *Sci. Rep.* **3**, 1775 (2013).
- [26] Qiao, B., Wang, A., Yang, X., Allard, L. F., Jiang, Z., Cui, Y., Liu, J., Li, J. & Zhang, T. Single-atom catalysis of CO oxidation using Pt<sub>1</sub>/FeO<sub>x</sub>. *Nat. Chem.* **3**, 634–641 (2011).
- [27] Kuhn, P., Forget, A., Su, D., Thomas, A. & Antonietti, M. From microporous regular frameworks to mesoporous materials with ultrahigh surface area: dynamic reorganization of porous polymer networks. *J. Am. Chem. Soc.* **130**, 13333–13337 (2008).
- [28] Kuhn, P., Forget, A., Hartmann, J., Thomas, A. & Antonietti, M. Template-free tuning of nanopores in carbonaceous polymers through ionothermal synthesis. *Adv. Mater.* **21**, 897–901 (2009).
- [29] Wang, G., Sun, G., Wang, Q., Wang, S., Guo, J., Gao, Y. & Xin, Q. Improving the DMFC performance with Ketien Black EC 300J as the additive in the cathode catalyst layer. *J.*

*Power Sources* **180**, 176–180 (2008).

- [30] Tashima, D., Yoshitama, H., Otsubo, M., Maeno, S. & Nagasawa, Y. Evaluation of electric double layer capacitor using Ketjenblack as conductive nanofiller. *Electrochim. Acta* **56**, 8941–8946 (2011).
- [31] Cohen, J. L., Volpe, D. J. & Abruna, H. D. Electrochemical determination of activation energies for methanol oxidation on polycrystalline platinum in acidic and alkaline electrolytes. *Phys. Chem. Chem. Phys.* **9**, 49–77 (2007).
- [32] Kolics, A. & Wieckowski, A. Adsorption of bisulfate and sulfate anions on a Pt(111) electrode. *J. Phys. Chem. B* **105**, 2588–2595 (2001).
- [33] Hidai, S., Kobayashi, M., Niwa, H., Harada, Y., Oshima, M., Nakamori, Y. & Aoki, T. Platinum oxidation responsible for degradation of platinum-cobalt alloy cathode catalysts for polymer electrolyte fuel cells. *J. Power Sources* **215**, 233–239 (2012).
- [34] Wang, H., Wang, Y., Zhu, Z., Sapi, A., An, K., Kennedy, G., Michalak, W. D. & Somorjai, G. A. Influence of size-induced oxidation state of platinum nanoparticles on selectivity and activity in catalytic methanol oxidation in the gas phase. *Nano Lett.* **13**, 2976–2979 (2013).
- [35] Russell, A. E. & Rose, A. X-ray absorption spectroscopy of low temperature fuel cell catalysts. *Chem. Rev.* **104**, 4613–4635 (2004).
- [36] Toda, T., Igarashi, H., Uchida, H. & Watanabe, M. Enhancement of the electroreduction of oxygen on Pt alloys with Fe, Ni, and Co. *J. Electrochem. Soc.* **146**, 3750–3756 (1999).
- [37] Lim, D.-H. & Wilcox, J. DFT-based study on oxygen adsorption on defective graphene-supported Pt nanoparticles. *J. Phys. Chem. C* **115**, 22742–22747 (2011).
- [38] Nakamura, A., Tatsuno, Y., Yamamoto, M. & Otsuka, S. Oxygen-18 isotopic infrared study of dioxygen-transition metal complexes. *J. Am. Chem. Soc.* **93**, 6052–6058 (1971).
- [39] Li, T. & Balbuena, P. B. Computational studies of the interactions of oxygen with platinum clusters. *J. Phys. Chem. B* **105**, 9943–9952 (2001).
- [40] Gasteiger, H. A., Markovic, N., Ross, P. N. & Cairns, E. J. Electro-oxidation of small organic molecules on well-characterized Pt-Ru alloys. *Electrochim. Acta* **39**, 1825–1832

(1994).

- [41] Hernández-Fernández, P., Rojas, S., Ocón, P., Frutos, A., Figueora, J. M., Terreros, P., Peña, M. A. & Fierro, J. L. G. Relevance of the nature of bimetallic PtAu nanoparticles as electrocatalysts for the oxygen reduction reaction in the presence of methanol. *J. Power Sources* **177**, 9–16 (2008).
- [42] Kim, Y. T., Ohshima, K., Higashimine, K., Uruga, T., Tanaka, M., Suematsu, H. & Mitani, T. Fine size control of platinum on carbon nanotubes: From single atoms to clusters. *Angew. Chem. Int. Ed.* **45**, 407–411 (2006).
- [43] Nishanth, K. G., Sridhar, P., Pitchumani, S. & Shukla, A. K. A DMFC with methanol-tolerant-carbon-supported-Pt-Pd-alloy cathode. *J. Electrochem. Soc.* **158**, B871–B876 (2011).
- [44] Chen, Y. X., Miki, A., Ye, S., Sakai, H. & Osawa, M. Formate, an active intermediate for direct oxidation of methanol on Pt electrode. *J. Am. Chem. Soc.* **125**, 3680–3681 (2003).
- [45] Cuesta, A. At least three contiguous atoms are necessary for CO formation during methanol electrooxidation on platinum. *J. Am. Chem. Soc.* **128**, 13332–13333 (2006).
- [46] McNicol, B. D. Electrocatalytic problems associated with the development of direct methanol-air fuel cells. *J. Electroanal. Chem.* **118**, 71–87 (1981).
- [47] Lai, S. C. S., Lebedeva, N. P., Housmans, T. H. M. & Koper, M. T. M. Mechanisms of carbon monoxide and methanol oxidation at single-crystal electrodes. *Top. Catal.* **46**, 320–333 (2007).
- [48] Cuesta, A. Atomic ensemble effects in electrocatalysis: the site-knockout strategy. *ChemPhysChem* **12**, 2375–2385 (2011).
- [49] Kuzume, A., Mochiduki, Y., Tsuchida, T. & Ito, M. Methanol oxidation on a Pt(111)-OH/O surface. *Phys. Chem. Chem. Phys.* **10**, 2175–2179 (2008).



## Chapter 3.

# Oxygen-tolerant single Pt-atom catalysts supported on a covalent triazine framework for the hydrogen oxidation reaction

Reducing the use of platinum on anodes of polymer electrolyte fuel cells is critical for the widespread dissemination of these energy conversion systems. Although platinum usage can be minimized by the dispersion of isolated platinum atoms, no single platinum-atom catalysts that promote hydrogen oxidation at a rate required for practical fuel cells have been reported to date. In this chapter, the author demonstrates that a CTF loaded with single-atom Pt exhibited higher HOR and lower cathodic ORR electrocatalytic activity compared to commercially available Pt/C. These electrocatalytic properties contribute to protect PEFC cathodes from degradation in practical environments, particularly for their use in vehicles, which have frequent start-up/shut-down cycles.

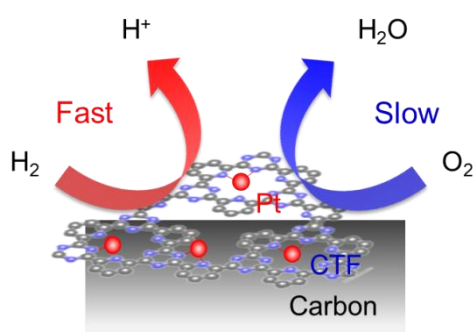


**Figure | Schematic illustration of the selective reaction between hydrogen oxidation reaction and oxygen reduction reaction on single Pt atom modified CTF.**

### 3.1. Introduction

Polymer electrolyte fuel cells (PEFC) that utilize hydrogen and oxygen as reactants have attracted considerable attention as environmentally friendly energy conversion systems, as they can be operated at relatively low temperature ( $< 100\text{ }^{\circ}\text{C}$ ) and generate only water as the reaction product [1-4]. Currently, platinum (Pt) or its alloys are typically used as the anode catalyst in PEFC systems [5, 6]. However, because Pt is rare and expensive, reducing the loading amount of Pt on the anode is desirable for cost reduction [7-12]. Another problem regarding Pt anode catalysts is that Pt is active not only for the hydrogen oxidation reaction (HOR), but also for the oxygen reduction reaction (ORR) [5,6,13,14]. During the start-up of PEFCs, air inevitably flows into the anode chamber and cathodic ORR proceeds on the Pt anode catalysts, leading to the degradation of the cathode. Thus, the ORR on Pt anode catalysts is recognized as a serious limitation of these systems, particularly for their use in vehicles, which have frequent start-up/shut-down cycles [15-18]. Due to the limitations associated with Pt, improvement of the anode catalyst is essential for the popularization of PEFC systems.

Single-atom Pt catalyst is a promising candidate to satisfy the requirements for PEFC anode catalysts. Because of the single-atom nature of the material, a lower loading amount of Pt is likely required, and in addition, unique reaction selectivity may be possible, as many types of reactions can only proceed on Pt ensemble sites [19-22]. Recently, the author reported that covalent triazine frameworks (CTFs) can serve as a platform for single-atom electrocatalyst [23]. Although CTFs are non-conductive, the author successfully developed a CTF-based electrocatalyst by hybridizing CTFs with conductive carbon particles (CTF/CP) [23]. As CTFs possess abundant nitrogen atoms with an electron lone pair, various metals can be loaded onto CTFs via coordination bonds with nitrogen. Using this approach, the author demonstrated that atomic-metal loaded CTFs exhibit unique reaction activity and selectivity [23-25].

In this chapter, the author demonstrates that a hybridized material composed of CTF and carbon nanoparticles loaded with single-atom Pt (hereafter termed Pt-CTF/CP) exhibit higher HOR and lower cathodic ORR electrocatalytic activity compared to commercially available Pt/C. These electrocatalytic properties suggest that Pt-CTF/CP may be suitable as a PEFC anode catalyst for practical applications.

## **3.2. Experimental details**

### **3.2.1. Catalyst synthesis**

To prepare CTF/CP, 1.363 g  $\text{ZnCl}_2$  (Wako), 0.0161 g 2,6-pyridinedicarbonitrile (Sigma Aldrich), and 0.129 g ketjen black (EC600JD, Lion) were mixed in a glove box. The mixture was placed in a Pyrex glass ampoule, which was then vacuum sealed and incubated at 400 °C for 21 h. The resulting powder was washed sequentially with 0.1 M HCl, water, tetrahydrofolate, and acetonitrile, and dried in vacuo. Platinum impregnation was performed by adding 100 mg of the resulting powder into 500 mL of an aqueous solution of 1 mM  $\text{K}_2[\text{PtCl}_4]$  (Wako), and the resulting mixture was ultrasonically stirred (USS-1, Nihon Seiki) at 30 °C for 1 h before being washed with water and acetone.

### **3.2.2. Electrochemical characterizations**

Electrocatalytic activity was evaluated using a rotating disk electrode (RDE) method. A catalyst slurry was prepared by ultrasonically dispersing 5.0 mg catalyst in 1.5 mL ethanol (>99.5%, Wako) and 100  $\mu\text{L}$  Nafion solution (5 wt% solution in a mixture of lower aliphatic alcohols and water; Sigma Aldrich). Two microliters of the resulting catalyst slurry was dropped onto a glassy carbon electrode (0.1256  $\text{cm}^2$ ), which was then used as a working electrode. The total catalyst loading was controlled to be 0.050  $\text{mg cm}^{-2}$ . A titanium coil and Ag/AgCl were used as counter and reference

electrodes, respectively. All potentials were converted to the reversible hydrogen electrode (RHE) reference scale. As reference catalysts for comparison, 20 wt% Pt/C (HiSPEC3000, Johnson Matthey) and 3.0 wt% Pt/C (Sigma Aldrich) were used. All measurements were conducted at 25 °C in an aqueous solution of 0.1 M HClO<sub>4</sub>. HOR activity was measured by linear sweep voltammetry (LSV) from 0 to 0.3 V at a scan rate of 1 mV s<sup>-1</sup> and a rotational rate of 2,500 rpm. The 0.1 M HClO<sub>4</sub> solution was saturated with 1 atm hydrogen for 30 min prior to the LSV measurements. For cyclic voltammetry (CV), the saturation gas was switched to 1 atm argon for 30 min before performing the measurements, which were conducted between 0.02 and 1 V at a scan rate of 10 mV s<sup>-1</sup> without rotation. The temporal changes in current density for HOR were measured at a constant potential of 0.1 V on carbon paper (TGP-H-090, Toray). The ORR activity was also measured by LSV between 0.2 and 1.15 V at a scan rate of 10 mV s<sup>-1</sup> and a rotational rate of 1,600 rpm. The solution was saturated with 1 atm oxygen for 30 min prior to performing the LSV measurements. The ring potential was set to 1.2 V and the ring current was corrected by the collection efficiency of 0.424.

### **3.2.3. Physical characterizations**

X-ray absorption fine structure (XAFS) measurements were conducted by a transmission method using the hard X-ray beam line BL01B01 of SPring-8, Japan and transmitted X-rays were detected using a double-crystal Si (111) monochromator. X-ray photoelectron spectra were measured using a X (Axis Ultra, Kratos Analytical Co.) with monochromatic Al K $\alpha$  X-rays of  $h\nu = 1486.6$  eV. Nitrogen adsorption-desorption isotherms at 77 K were determined by the BET method using an Autosorb-3 analyzer (Quantachrome).

### **3.2.4. Membrane electrode assembly (MEA) preparation**

Slurries of each anode catalyst were prepared by mixing 2.8 wt% Pt-CTF/CP or

20 wt% Pt/C with Aciplex (20 wt% dispersion, SS700C, Asahi Kasei) at a weight ratio of polymer to carbon support of 1.0. A cathode catalyst slurry was also prepared in the same manner using 47 wt% Pt/C (TEC10E50E, Tanaka Kikinzoku Kogyo) in place of the anode catalyst. The slurries were sprayed over microporous gas diffusion layers (GDLs; GDL24, SGL Carbon). Pt was loaded on the anodes at  $0.020 \pm 0.001$  and  $0.10 \pm 0.1 \text{ mg cm}^{-2}$  for 2.8 wt% Pt-CTF/CP and 20 wt% Pt/C, respectively, and Pt on the cathode was set at  $0.50 \pm 0.1 \text{ mg cm}^{-2}$ . A single cell (36-cm<sup>2</sup> active area) was assembled by sandwiching the electrolyte membrane (Nafion 211, DuPont) between the anode and cathode GDLs. The carbon separator plates have multiple-path serpentine flow-fields.

### **3.2.5. Fuel cell testing**

A fuel cell station (CHINO, Japan) was used to test the constructed MEAs. Pure H<sub>2</sub> and O<sub>2</sub> (>99.99% purity) were used for the anode and cathode, respectively, at fixed flow rates of 500 mL and 300 mL min<sup>-1</sup>, respectively. The cell temperature was fixed at 80 °C and humidity was controlled at RH 100%. The MEAs were initially stabilized in hydrogen-oxygen at 0.1 A cm<sup>-2</sup> at 80 °C for 1 h. Output voltages were collected after 20 s for each current density and the cells were maintained at 0.1 A cm<sup>-2</sup> for 5-min intervals for the measurement of each cycle, and 10 cycles were measured in total. Cell resistances were recorded as a function of the current density using an AC perturbation of 1 kHz.

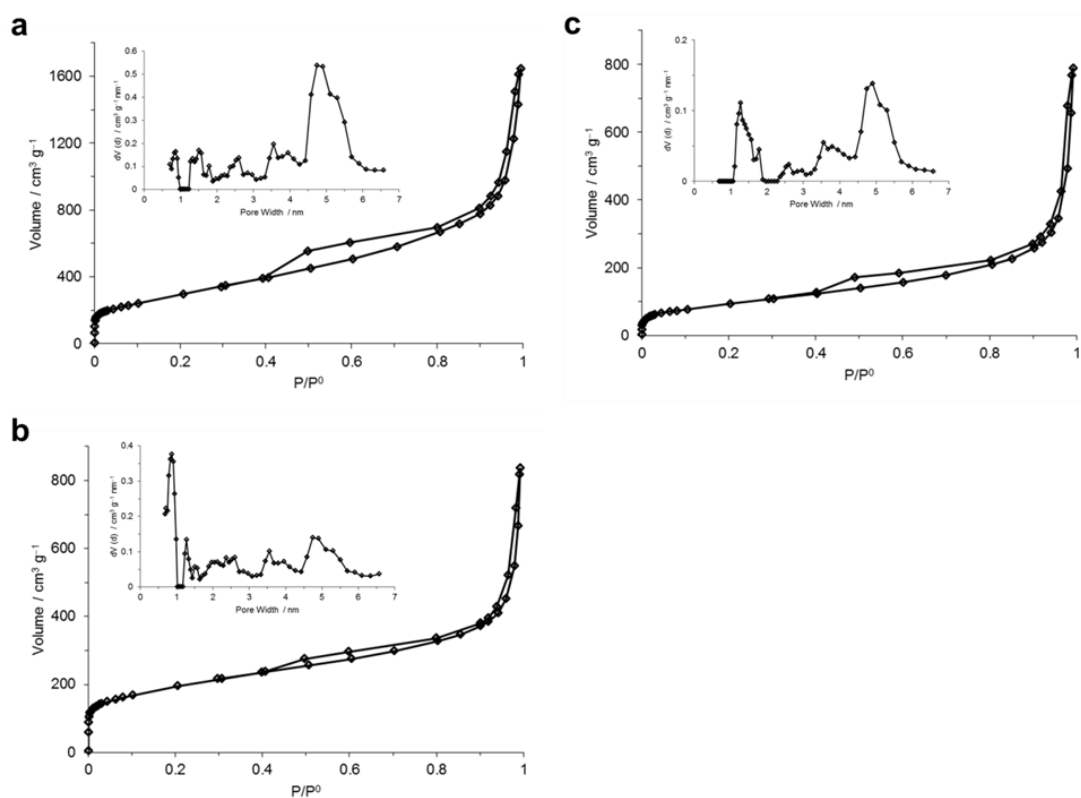
## **3.3. Results**

### **3.3.1. Physical characterization of Pt-CTF/CP**

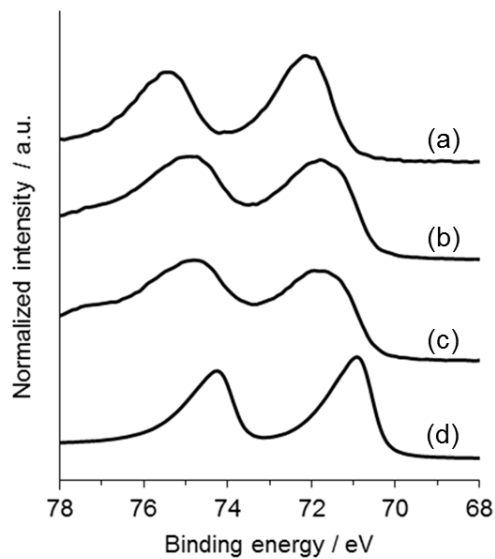
The author first conducted physical characterizations of Pt-CTF/CP, which was loaded with 2.8 wt% Pt (Fig. 3.1). Commercially available Pt cluster-loaded carbon particles (Pt/C) loaded with either 3.0 or 20 wt% Pt were used as comparative



Table 3.1   Physical characterizations of the catalysts.						
Catalyst	C content (at%)	N content (at%)	Pt content (at%)	Pt content (wt%)	BET surface area (m <sup>2</sup> /g)	Total pore volume (cm <sup>3</sup> /g)
Pt-CTF/CP	96	0.73	0.19	2.8	973	2.55
20 wt% Pt/C	92	—	1.4	19	673	1.29



**Fig. 3.2 | Nitrogen adsorption-desorption isotherms.** (a) 2.8 wt% Pt-CTF/CP, (b) 20 wt% Pt/C and (c) 3.0 wt% Pt/C. The insets show the pore size distribution calculated based on the nonlocal density functional theory (NL-DFT).



**Fig. 3.3 | Pt-4f XPS spectra.** (a) 2.8 wt% Pt-CTF/CP, (b) 20 wt% Pt/C, (c) 3.0 wt% Pt/C and (d) Pt metal.

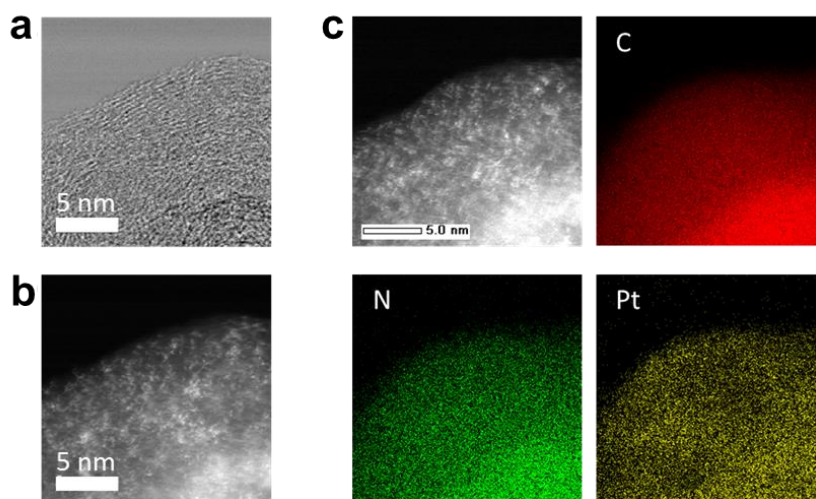


**Fig. 3.4 | Representative transmission electron microscopic images of Pt-CTF/CP.** (a) HR-TEM image of 2.8 wt% Pt-CTF/CP, (b) corresponding HAADF-STEM image, and (c) corresponding elemental maps for C, N and Pt atoms.

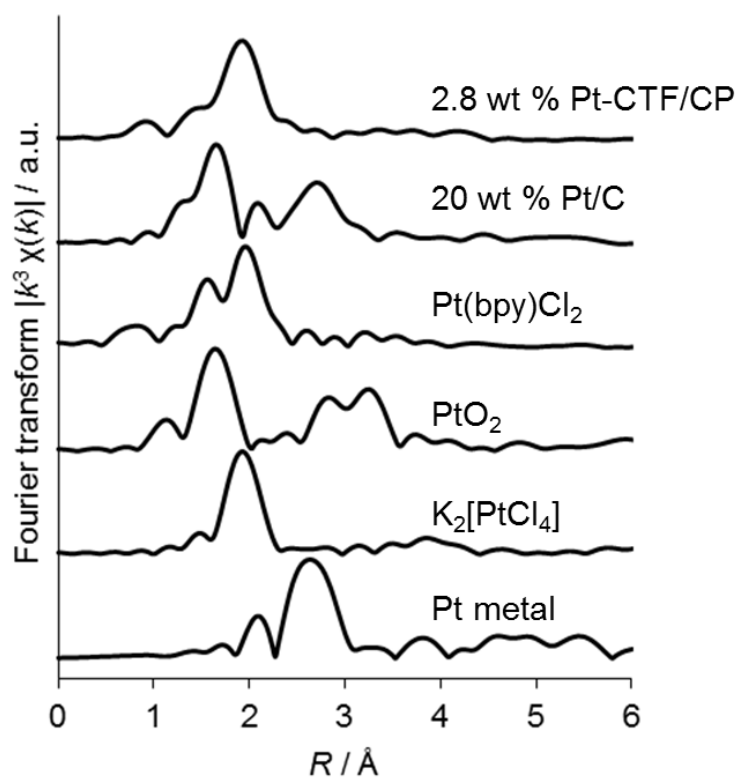


**Fig. 3.5 | EXAFS analysis.**  $k^3$ -weighted Fourier transform spectra of Pt  $L_3$ -edge EXAFS for as-prepared 2.8 wt% Pt-CTF/CP, 20 wt% Pt/C, and standard samples of Pt.

### 3.3.2. Electrocatalytic HOR activity

Pt-CTF/CP in an Ar-purged HClO<sub>4</sub> solution was examined by cyclic voltammogram (CV) (Fig. 3.6a, red curve). The CVs for 20 wt% and 3.0 wt% Pt/C catalysts were also determined as a reference (Fig 3.6a, blue and green curves, respectively). For the analysis, the amount of catalyst loaded onto the electrode substrates was adjusted to approximately 0.050 mg cm<sup>-2</sup> for all three samples. In the CVs, reversible peaks corresponding to formation and desorption of under-potentially-deposited hydrogen (upd-H) were observed for the Pt/C catalysts in the potential region of 0.02 ~ 0.30 V [26], but not for Pt-CTF/CP. As the formation of upd-H proceeds at Pt ensemble sites, such as step, three-fold hollow, and defect sites [27, 28], these results support the above findings that Pt exists in an atomically dispersed form on Pt-CTF/CP. In addition, no significant differences in the current density were observed between Pt-CTF/CP and the two Pt/C catalysts in the potential region of 0.30 ~ 0.45 V, where only charging and discharging of the electrical double layer occurs [29], indicating that the electrochemically active surface area did not differ markedly among the three samples.

The electrocatalytic activity of Pt-CTF/CP for HOR was next evaluated by conducting linear sweep voltammetry (LSV) in an HClO<sub>4</sub> solution saturated with 1 atm hydrogen (Fig. 3.6b, red curve). The current associated with HOR started to flow at 0 V (i.e., without an over-potential) and increased with a positive shift in the potential until reaching a peak at approximately 0.05 V. The time course of current density for Pt-CTF/CP on carbon paper at a constant potential of 0.1 V is shown in Fig. 3.6c (red curve). Carbon paper was used as the substrate to avoid the flaking of the catalyst layer that frequently occurred on the glassy carbon substrate. The electrochemical performance of Pt-CTF/CP was nearly identical as that of 20 wt% Pt/C (Fig. 3.6b, blue curve). However, 3.0 wt% Pt/C, which contained nearly the same loading amount of Pt as Pt-CTF/CP, exhibited a much lower HOR current than Pt-CTF/CP (Fig. 3.6b,

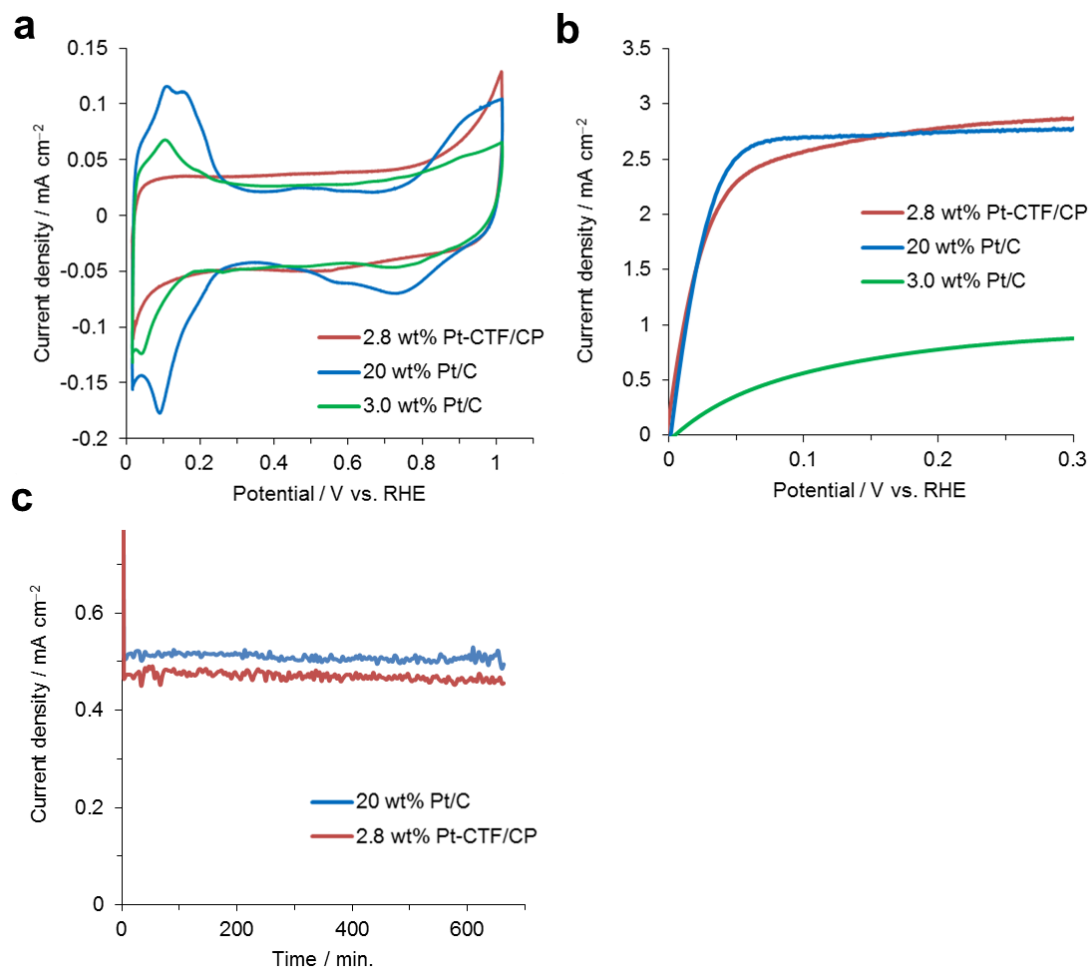


**Fig. 3.6 | Electrochemical characteristics of Pt-CTF/CP.** (a) Cyclic voltammograms recorded on RDE at a scan rate of 10 mV s<sup>-1</sup>. The electrolyte (0.1 M HClO<sub>4</sub>) was saturated with 1 atm argon. (b) Polarization curves for HOR recorded on RDE at a scan rate of 1 mV s<sup>-1</sup> and rotational rate of 2,500 rpm. The electrolyte (0.1 M HClO<sub>4</sub>) was saturated with 1 atm hydrogen. (c) Time course of the current density of the HOR current with 1 atm hydrogen recorded on carbon paper. Catalysts: 2.8 wt% Pt-CTF/CP (red), 20 wt% Pt/C (blue), and 3.0 wt% Pt/C (green). All of the measurements were conducted at 25 °C.

green curve). These results clearly indicated that the efficiency of Pt atom utilization is much higher for Pt-CTF/CP. It should be noted here that PEFCs are typically constructed with 20 ~ 50 wt% Pt/C as the anode catalyst [13,30-33]. Thus, the finding that 2.8 wt% Pt-CTF/CP exhibited similar performance to 20 wt% Pt/C is of high practical importance.

The HOR and hydrogen evolution reaction (HER) proceed on Pt via an identical reaction intermediate, and hence, are mutually reversible [34,35]. Therefore, Pt-CTF/CP is expected to exhibit superior electrocatalytic activity even for HER. To examine this speculation, LSVs for Pt-CTF/CP (red curve), 20 wt% Pt/C (blue curve), and 3.0 wt% Pt/C (green curve) obtained in the potential range of 0 to  $-0.3$  V, where HER proceeds, were measured (Fig. 3.7). Similar to the HOR activity, the electrocatalytic HER activity of Pt-CTF/CP was found to be approximately equal to that of 20 wt% Pt/C, as expected.

### **3.3.3. Electrocatalytic HOR activity of 0.29 wt% Pt-CTF/CP**

Pt-CTF/CP (2.8 wt% Pt) exhibited superior HOR activity to 3.0 wt% Pt/C and was shown to efficiently utilize the dispersed Pt atoms. Furthermore, the peaks for up-d-H formation and desorption were not detected in the CV even after the LSV (Fig. 3.6b) and chronoamperometric (Fig. 3.6c) analyses. Although these results suggest that single Pt atoms possess comparable HOR activity to Pt clusters, Pt atoms typically form clusters when loaded onto substrates [19-22]. To obtain more definitive evidence that single Pt atoms possess HOR activity, we prepared 0.29 wt% Pt-CTF/CP, in which the Pt loading amount was reduced by approximately 90%, to avoid the formation of Pt aggregates [19,22,36]. As shown in the LSV for 0.29 wt% Pt-CTF/CP (Fig. 3.8a), HOR current was detected from 0 V, similar to the 2.8 wt% Pt-CTF/CP and Pt/C catalysts. Importantly, no Pt aggregates were observed in the HR-TEM and HAADF-STEM images of 0.29 wt% Pt-CTF/CP (Figs. 3.9a and b, respectively), even after the LSV

experiments. These results clearly indicated that HOR proceeds on single Pt atoms in Pt-CTF/CP and requires almost no activation energy.

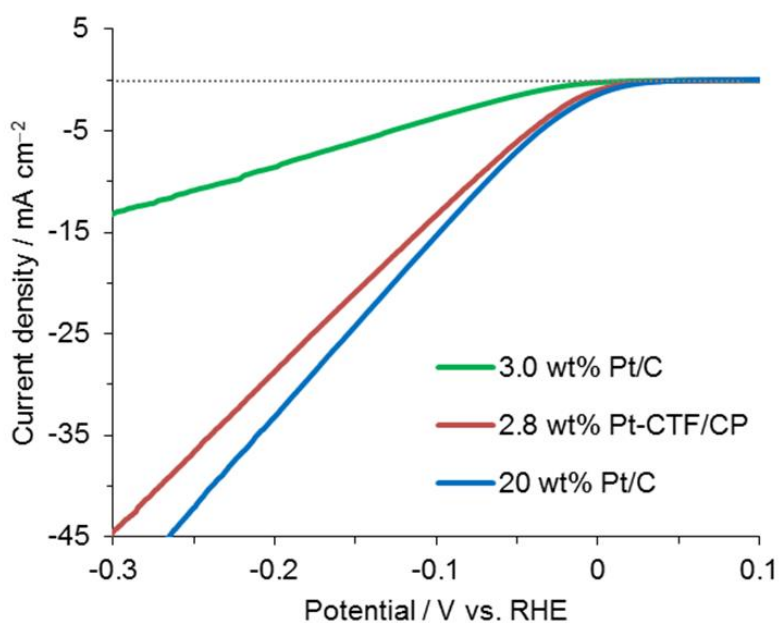


**Fig. 3.7 | Polarization curves for the hydrogen evolution reaction (HER).** All of the measurements were conducted on RDE with a sweep rate of  $10 \text{ mV s}^{-1}$  and rotational rate of 2,500 rpm in 0.1 M  $\text{HClO}_4$  at  $25 \text{ }^\circ\text{C}$ . The electrolyte was saturated with 1 atm argon. Catalysts: 2.8 wt% Pt-CTF/CP (red), 20 wt% Pt/C (blue), and 3.0 wt% Pt/C (green).

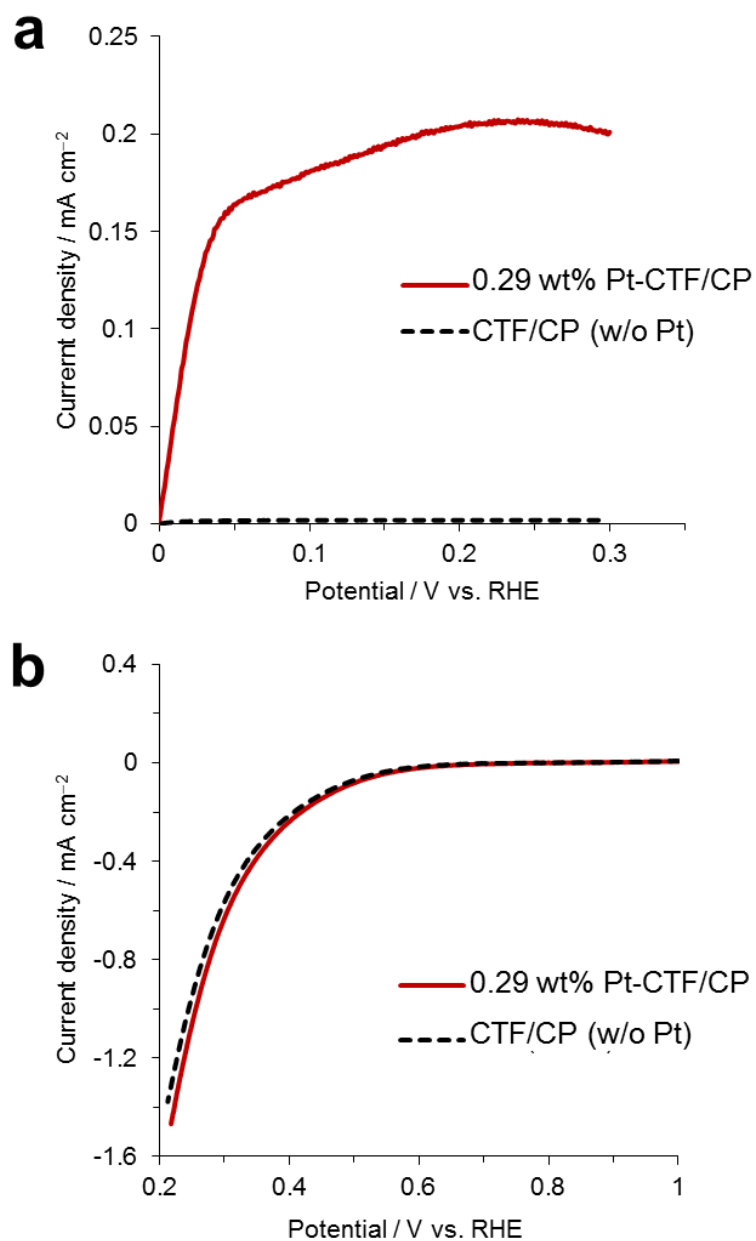


**Fig. 3.8 | Electrocatalytic activity of 0.29 wt% Pt-CTF/CP and CTF without Pt.** (a) Polarization curves for HOR at a scan rate of  $5 \text{ mV s}^{-1}$  and rotational rate of 2,500 rpm. The electrolyte ( $0.1 \text{ M HClO}_4$ ) was saturated with 1 atm hydrogen at  $25 \text{ }^\circ\text{C}$ . (b) Polarization curves for ORR at a scan rate of  $5 \text{ mV s}^{-1}$  and rotational rate of 1,600 rpm. The electrolyte ( $0.1 \text{ M HClO}_4$ ) was saturated with 1 atm oxygen at  $25 \text{ }^\circ\text{C}$ .

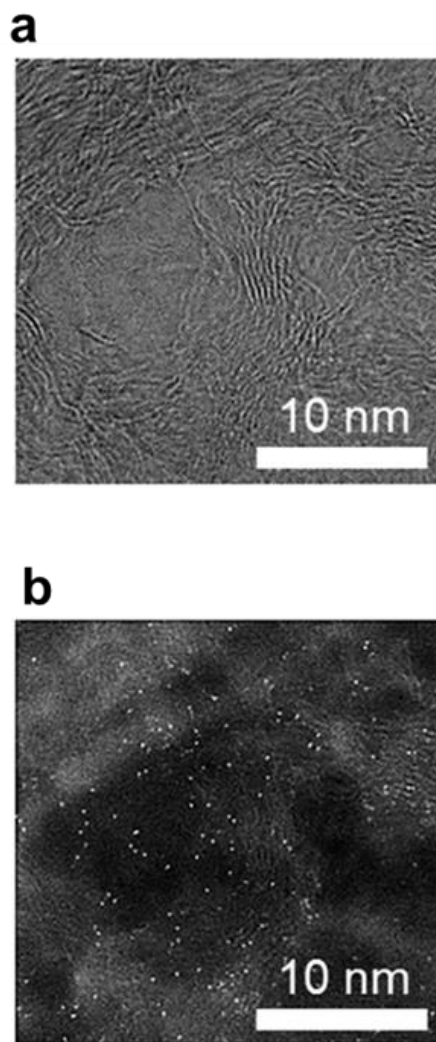


**Fig. 3.9 | Electron microscopic images of 0.29 wt% Pt-CTF. (b) HR-TEM image and (c) the corresponding HAADF-STEM image taken after the LSV measurement shown in Fig. 3.8a.**

### 3.3.4. Electrocatalytic ORR activity

The author next investigated the electrocatalytic ORR activity of 2.8 wt% Pt-CTF/CP using a rotating ring-disc electrode (RRDE) technique. Fig. 3.10b shows the LSVs obtained for the disc electrodes in oxygen-saturated HClO<sub>4</sub> solution. For 20 wt% Pt/C, ORR activity was first detectable at 1.06 V and was diffusion-limited at approximately 0.80 V (blue curve). In comparison to 20 wt% Pt/C, the electrocatalytic ORR activity of Pt-CTF/CP was markedly lower (Fig. 3.10b, red curve). Importantly, in the potential region more positive than +0.6 V ( $E > +0.6$  V), which is critical for the start-up/shut-down operation of PEFCs [16], the ORR current for Pt-CTF/CP was less than 23% of that generated by 20 wt% Pt/C.

Two different pathways for electrochemical ORR have been extensively characterized: a direct  $4e^-$  pathway and an indirect  $2e^-$  pathway, which generates hydrogen peroxide (H<sub>2</sub>O<sub>2</sub>) as the intermediate [37-39]. The relative ratio of these two ORR pathways can be estimated using the RRDE technique by poisoning the ring electrode at the potential (1.2 V) at which H<sub>2</sub>O<sub>2</sub> is electrochemically oxidized. Yang *et al.* reported that single-atom Pt (0.35 wt%) loaded on a titanium nitride substrate predominantly generates H<sub>2</sub>O<sub>2</sub> via the  $2e^-$  ORR pathway [22]. However, comparison of the anodic ring currents corresponding to Pt-CTF/CP (red curve) and Pt/C (blue curve; Fig. 3.10a) revealed that the concentration of H<sub>2</sub>O<sub>2</sub> generated by Pt-CTF/CP and 20 wt% Pt/C was similar at  $E > +0.6$  V. Although the ORR reaction mechanism for Pt-CTFCP cannot be conclusively determined from the RRDE data, the finding that the ring current did not significantly differ between the two catalysts at  $E > +0.6$  V is critical, as H<sub>2</sub>O<sub>2</sub> can degrade PEFC components, such as membranes and catalyst binders [40,41].

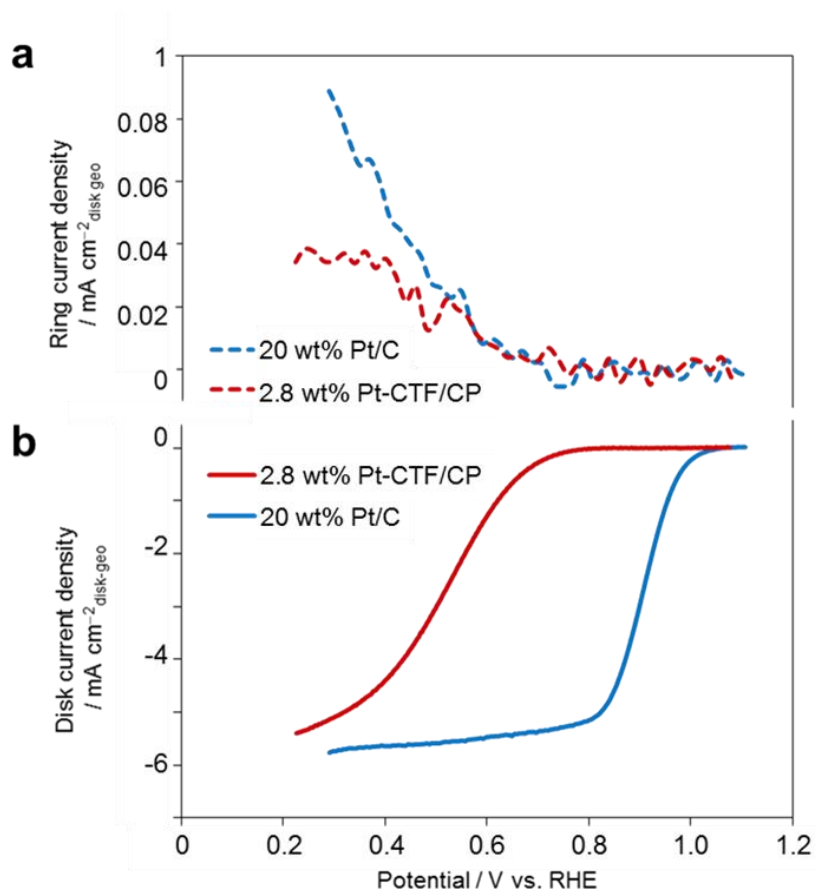


**Fig. 3.10 | Electrocatalytic ORR activities.** (a) H<sub>2</sub>O<sub>2</sub> oxidation currents recorded at 1.2 V vs. RHE on the ring electrode during the ORR on disc electrodes with the catalysts 20 wt% Pt/C (blue) and 2.8 wt% Pt-CTF/CP (red). The currents were corrected by the collection efficiency of 0.424. (b) Corresponding polarization curves for the ORR at a sweep rate of 10 mV s<sup>-1</sup> and a rotational rate of 1,600 rpm in 0.1 M HClO<sub>4</sub> at 25 °C.

### 3.3.5. Evaluation of Pt-CTF/CP as a PEFC anode catalyst

Finally, we evaluated the potential of Pt-CTF/CP to function as a PEFC anode catalyst. A membrane electrode assembly (MEA) was fabricated with 2.8 wt% Pt-CTF/CP ( $0.020 \pm 0.001 \text{ mg}_{\text{-Pt}} \text{ cm}^{-2}$ ) and 47 wt% Pt/C ( $0.50 \pm 0.01 \text{ mg}_{\text{-Pt}} \text{ cm}^{-2}$ ) as the anode and cathode catalysts, respectively, and the performance of a PEFC (PEFC<sub>Sam</sub>) equipped with the MEA was then evaluated (see the experimental details in the section). A PEFC (PEFC<sub>Ref</sub>) equipped with 20 wt% Pt/C ( $0.10 \pm 0.01 \text{ mg}_{\text{-Pt}} \text{ cm}^{-2}$ ) as the anode catalyst was also fabricated as a reference sample. Note that anodes and cathodes of MEAs are typically loaded with  $0.1 \sim 0.4 \text{ mg}_{\text{-Pt}} \text{ cm}^{-2}$  and  $0.3 \sim 0.5 \text{ mg}_{\text{-Pt}} \text{ cm}^{-2}$ , respectively [13,30-33]. Figs. 3.11a and b show the current density ( $j$ ) vs. voltage ( $V$ ) and  $j$  vs. power density relationships for PEFC<sub>Sam</sub> and PEFC<sub>Ref</sub>. The open circuit voltage of PEFC<sub>Sam</sub> (0.95 V) was 0.06 V smaller than that of PEFC<sub>Ref</sub>. In addition, the power density of PEFC<sub>Sam</sub> was also smaller than that of PEFC<sub>Ref</sub> when  $j < 0.8 \text{ A cm}^{-2}$ , but was larger when  $j > 0.8 \text{ A cm}^{-2}$ . Based on these values, the maximum power density of PEFC<sub>Sam</sub> was determined to be  $487 \text{ mW cm}^{-2}$  at  $1.2 \text{ A cm}^{-2}$ , a value that was nearly identical to that of PEFC<sub>Ref</sub> ( $462 \text{ mW cm}^{-2}$  at  $1.0 \text{ A cm}^{-2}$ ), which contained approximately 5 times more Pt anode catalyst. Taken together, these results demonstrate that Pt-CTF/CP has the potential to function as a cost-effective and efficient anode catalyst, as the amount of Pt required for catalytic activity is drastically reduced compared to conventional Pt/C catalysts.

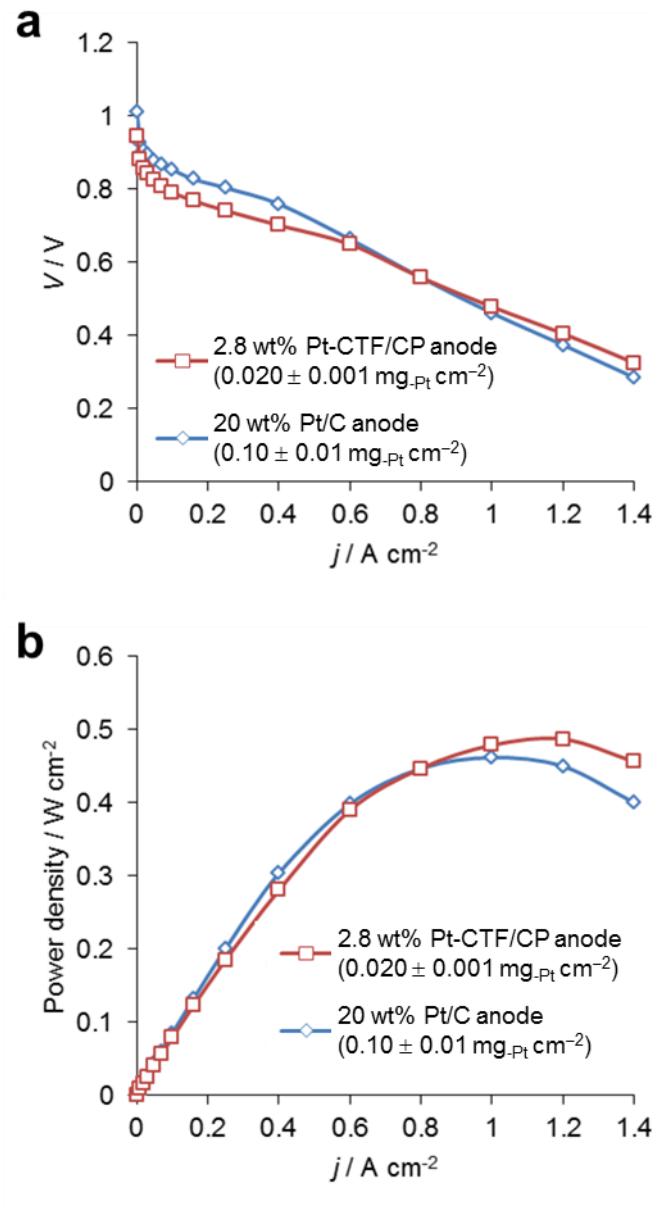


**Fig. 3.11 | Fuel cell performance of MEAs.** (a)  $j$ - $V$  performances, and (b)  $j$ -power density curves for MEAs prepared using 2.8 wt% Pt-CTF/CP (red curve) and 20 wt% Pt/C (blue curve) as the anode catalyst. The platinum loadings of both cathodes were  $0.50 \pm 0.01 \text{ mg}_{\text{Pt}} \text{ cm}^{-2}$ . The platinum loadings of the anodes prepared with 2.8 wt% Pt-CTF/CP and 20 wt% Pt/C were  $0.020 \pm 0.001$  and  $0.10 \pm 0.01 \text{ mg}_{\text{Pt}} \text{ cm}^{-2}$ , respectively. The data were collected at 80 °C and 100% RH using  $\text{H}_2/\text{O}_2$  as the reactants.

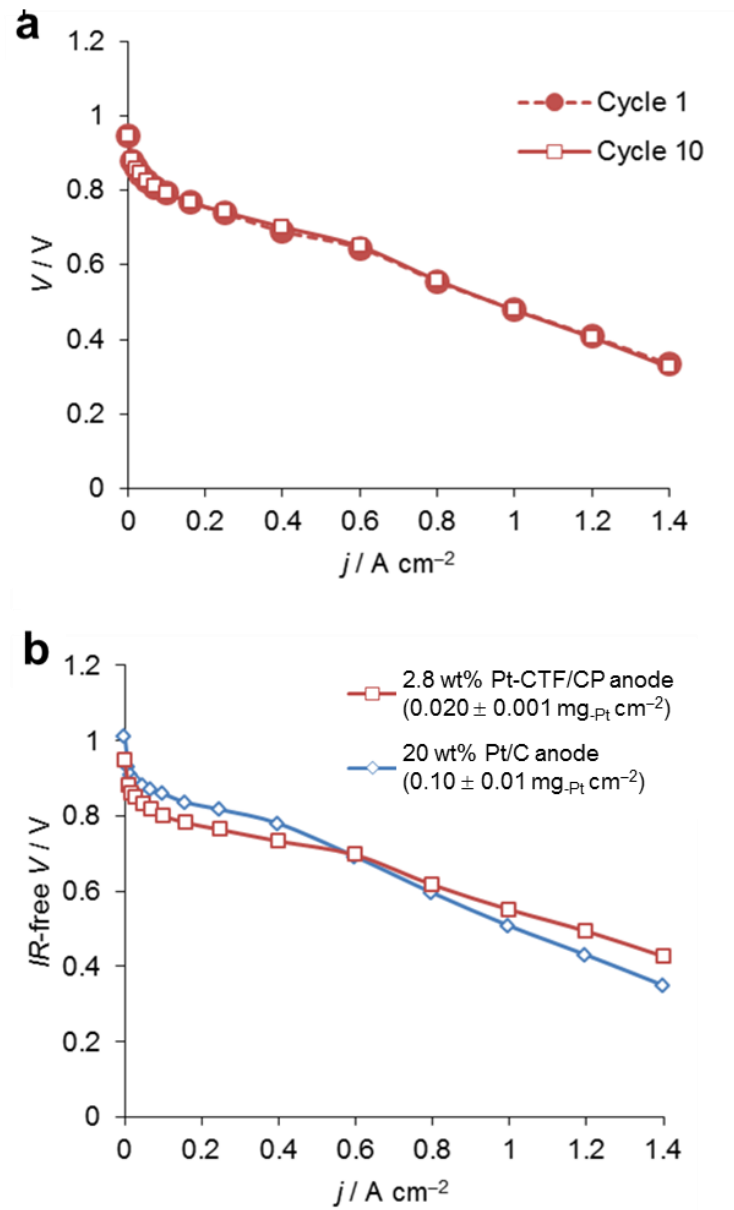


**Fig. 3.12** |  $j$ - $V$  curves of fuel cell. (a)  $j$ - $V$  performances of cycle 1 (circles) and cycle 10 (open squares) of the MEA prepared with a 2.8 wt% Pt-CTF/CP anode, and (b)  $j$ - $IR$  free  $V$  curves for the MEAs constructed using 2.8 wt% Pt-CTF/CP (red) and 20 wt% Pt/C (blue) anodes.

### 3.4. Discussion

The present analyses demonstrate that the ORR activity of Pt-CTF/CP is markedly lower than that of Pt/C and requires greater than 200 mV of over-potential to proceed (Fig. 3.10b). For the ORR pathway to occur by the side-on or end-on adsorption of oxygen molecules on Pt atoms, higher activation energy is needed compared to the bridge-type adsorption of oxygen [42-44]. As the ORR can only proceed on single-Pt atoms via the former mechanism, it is reasonable that Pt-CTF/CP exhibited lower ORR activity than Pt/C. Thus, the single atom nature of Pt-CTF/CP was clearly responsible for the reduction of the electrocatalytic ORR activity.

In addition to having lower ORR activity, Pt-CTF/CP exhibited superior electrocatalytic HOR activity to Pt/C (Fig. 3.6b). The number of electrochemically active Pt atoms on Pt/C can be calculated from the electrical charge for the adsorption of upd-H in the CV, and was estimated to be  $3.7 \times 10^{15} \text{ cm}^{-2}$ . On the other hand, the total number of Pt atoms on 2.8 wt% Pt-CTF/CP can be evaluated to be  $4.3 \times 10^{15} \text{ cm}^{-2}$  (see Note 3.1 for details of the estimation). Because a proportion of the Pt atoms on Pt-CTF/CP were likely not exposed to the electrolyte and were therefore electrochemically inactive, the HOR activity per Pt atom on Pt-CTF/CP was concluded to be equal to or more than that on Pt/C. The HOR can proceed by two different mechanisms on Pt: the Heyrovsky-Volmer mechanism via the end-on adsorption of hydrogen molecules and the Tafel-Volmer mechanism via bridge-type adsorption [34]. The dissociative adsorption of hydrogen molecules via bridge-type adsorption, which is the rate-determining step for HOR, is reportedly able to occur on single Pt atoms [45-47]. As comparable HOR activities were observed here between Pt-CTF/CP and commercial 20 wt% Pt/C, we speculate that both mechanisms are able to occur on single Pt atoms.

Bulk-Pt electrodes modified with a self-assembled patterned monolayer of calix[4]arene molecules were shown to have oxygen tolerance [16]. The adsorbed

calix[4]arene molecules selectively blocked the ORR, whereas HOR was able proceed without suppression. The selectivity for these reactions was determined by the number of available Pt sites, with HOR requiring significantly fewer sites compared to ORR. In the present work, reaction selectivity was achieved by loading CTF with single atoms of Pt, thereby decreasing the ORR activity via the suppression of one of the ORR reaction pathways without interfering with the HOR pathways. Using this novel strategy, the author successfully obtained an oxygen-tolerant Pt anode catalyst that was loaded with a significantly reduced amount of Pt compared to conventional Pt anode catalysts and which may have practical application in PEFCs.

Although single-atom Pt exhibits catalytic activity for various reactions [19-22,48,49], constructing electrodes with a high density of atomically dispersed Pt remains challenging, as Pt atoms easily form aggregates via surface diffusion. For example, although single Pt atoms supported on  $\text{FeO}_x$  ( $\text{Pt}_1/\text{FeO}_x$ ) exhibited catalytic activity for CO oxidation, the loading amount of Pt was limited to  $< 0.2$  wt%, and Pt formed aggregates when the loading amount exceeded 2.5 wt% [19]. Yang *et al.* also reported that single Pt atoms on titanium nitride functioned as a selective electrocatalyst for the indirect  $2e^-$  ORR pathway [22], but the loading amount of Pt was only approximately 0.35 wt%. Here, we successfully synthesized Pt-CTF/CP loaded with 2.8 wt% of Pt. Importantly, CV peaks for upd-H could not be observed, even after performing various electrochemical measurements, indicating that Pt aggregation was highly suppressed. In Pt-CTF/CP, Pt atoms are strongly anchored on the CTF substrate via coordination bonds with nitrogen, which are abundantly present in the pores of CTF. These structural features are the possible reason why more Pt could be loaded onto CTF without forming aggregates compared to other existing single-atom Pt catalysts.

**Note 3.1 | Estimation method for the number of electrochemically active Pt atoms.**

The number of electrochemically active Pt atoms in 20 wt% Pt/C was calculated from the electrical charge for the adsorption of upd-H (Fig. 3.6a, blue curve). The electrical charge was determined using the baseline current at 0.35 V as the current caused by the double layer. The number of electrochemically active Pt atoms ( $N_s$ ) was calculated based on the following formula:

$$N_s = QN_A/F$$

where  $Q$  is the electrical charge for the adsorption of upd-H,  $N_A$  is Avogadro's constant, and  $F$  is the Faraday constant.

### 3.5. Conclusions

In this chapter, the author demonstrated that 2.8 wt% Pt-CTF/CP had electrocatalytic HOR activity that was comparable to commercial 20 wt% Pt/C. Notably, Pt-CTF/CP also exhibited high oxygen tolerance, which was attributable to the dispersion of single Pt atoms throughout the CTF substrate and is of high practical importance for protecting PEFC cathodes from degradation during start-up/shut-down cycles. As various types of covalent organic frameworks other than CTF are available, and because metals other than Pt can also be doped into such frameworks, the author anticipates that synthesis strategy reported here can be used to construct novel electrocatalytic materials with both high activity and selectivity.

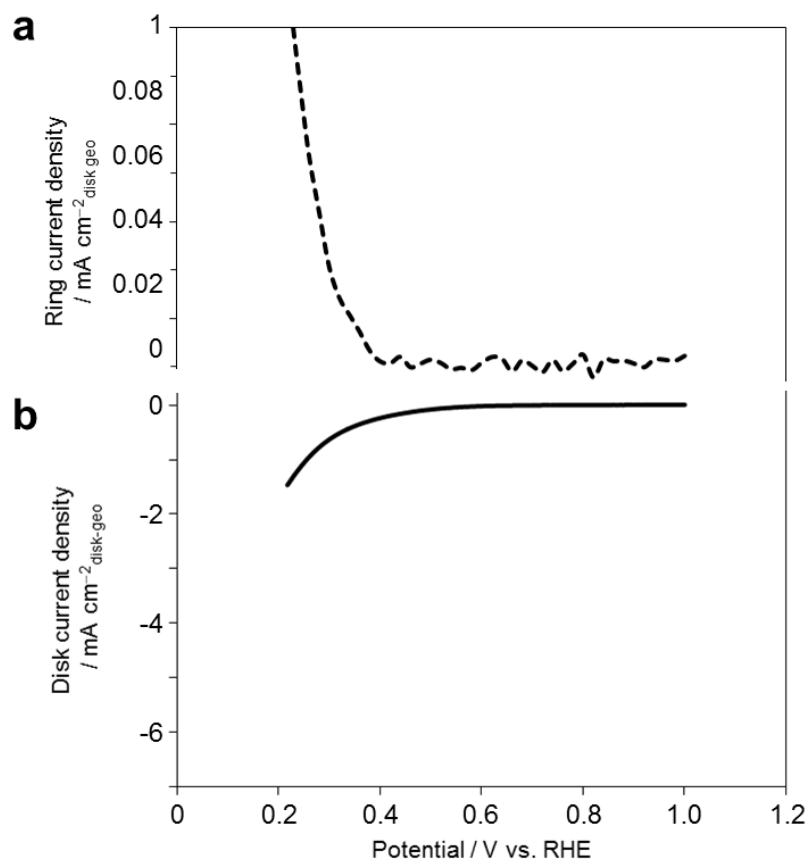


**Fig. 3.13 | RRDE measurements of 0.29 wt% Pt-CTF/CP for ORR.** (a) H<sub>2</sub>O<sub>2</sub> oxidation current recorded at 1.2V vs. RHE on the ring electrode during the ORR on the disc electrode. (b) Corresponding polarization curve for the ORR at the sweep rate of 10 mV s<sup>-1</sup> and the rotation rate of 1,600 rpm in 0.1 M HClO<sub>4</sub> at 25 °C.

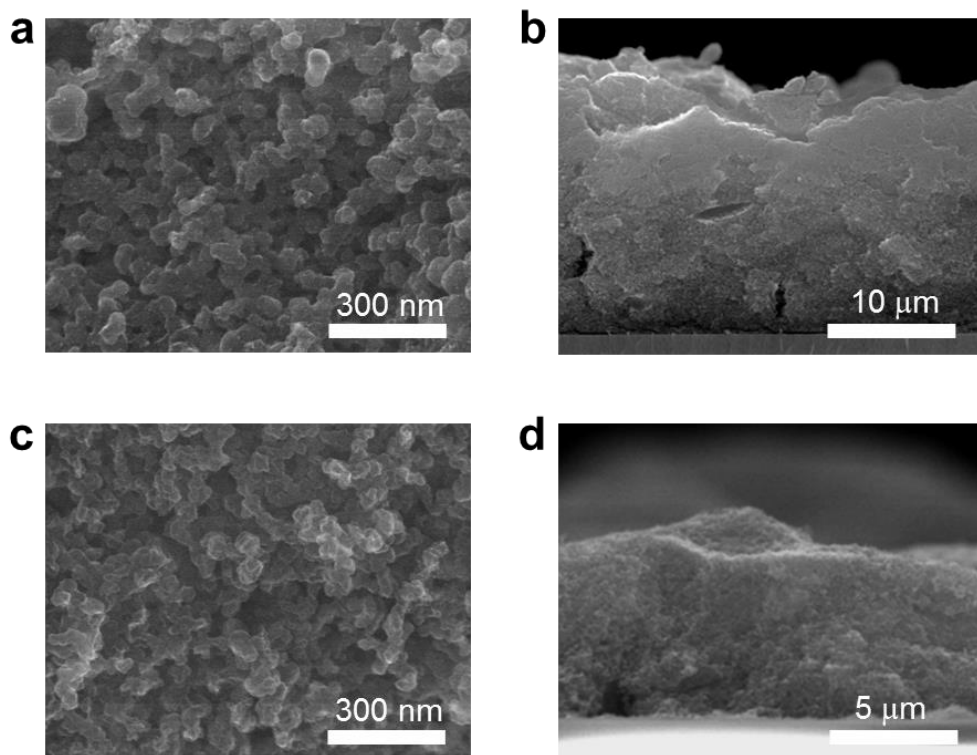


**Fig. 3.14 | Cross-sectional scanning electron microscope (SEM) images of the anode catalyst layers. (a), (b) 2.8 wt% Pt-CTF/CP, and (c), (d) 20 wt% Pt/C.**

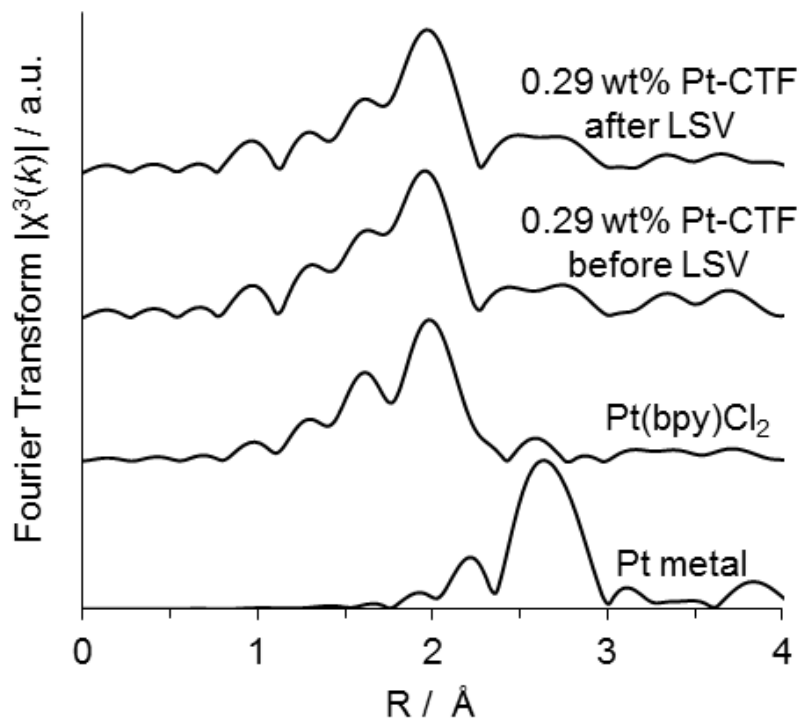


**Fig. 3.15** | Fourier transformations of  $k^3$ -weighted Pt  $L_3$ -edge EXAFS oscillations taken after the LSV measurement shown in Figure 3.8a. Pt(bpy)Cl<sub>2</sub>: (2,2'-bipyridine)dichloroplatinum(II).

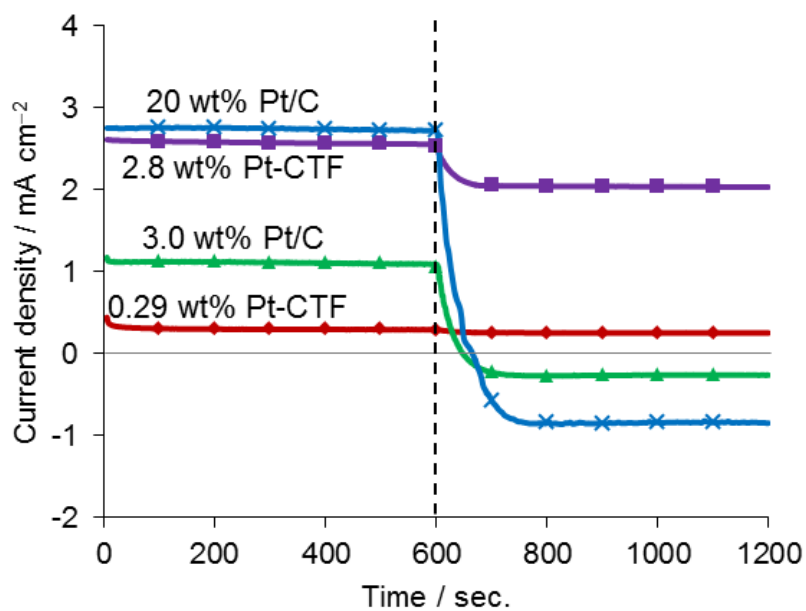


**Fig. 3.16 | Chronoamperometric curves obtained in 0.1 M HClO<sub>4</sub> at +0.6 V vs. RHE.**

(red) 0.29 wt% Pt-CTF/CP, (purple) 2.8 wt% Pt-CTF/CP, (green) 3.0 wt% Pt/C, and (blue) 20 wt% Pt/C. Rotational rate: 2,500 rpm. The input gas was altered at 600 s (dotted line) from pure H<sub>2</sub> to the mixed gas of H<sub>2</sub> and O<sub>2</sub> (H<sub>2</sub>:O<sub>2</sub> = 1:1).

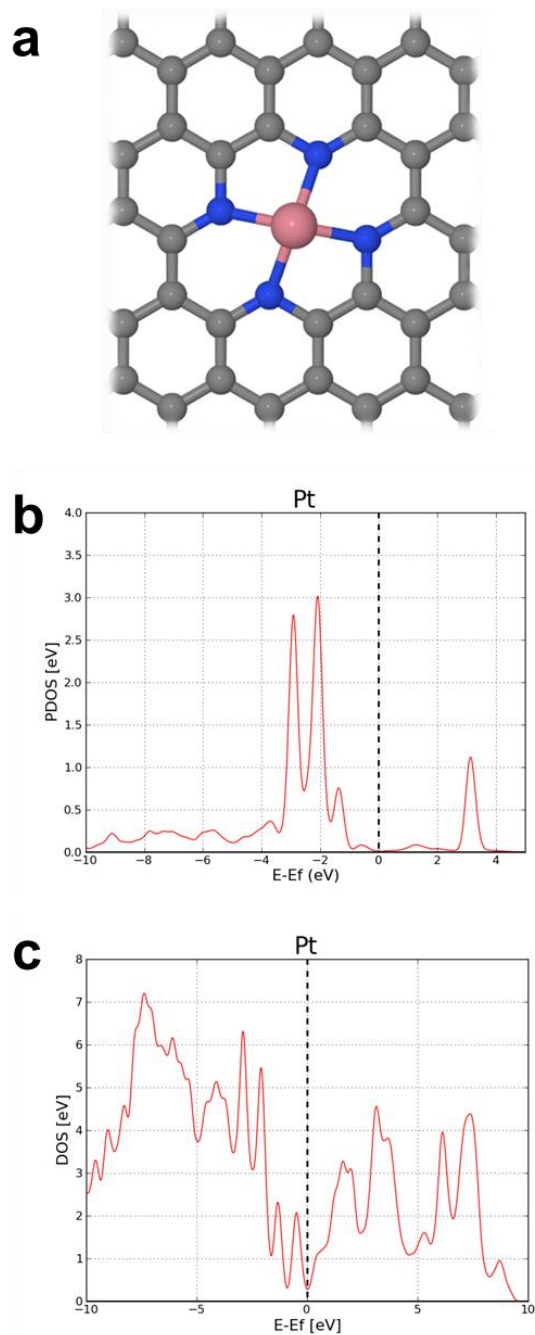


**Fig. 3.17 | The density of states (DOS) projected onto the *d*-orbitals of Pt.** (a) The structure of porphyrin-like graphene used for the calculation, (b) projected DOS onto the *d*-orbitals of the Pt atom in the porphyrin ring shown in Fig. 3. 17a, and (c) total DOS of bulk Pt metal. Reproduced with permission for Ref. 50. Copyright © 2013 American Chemical Society.

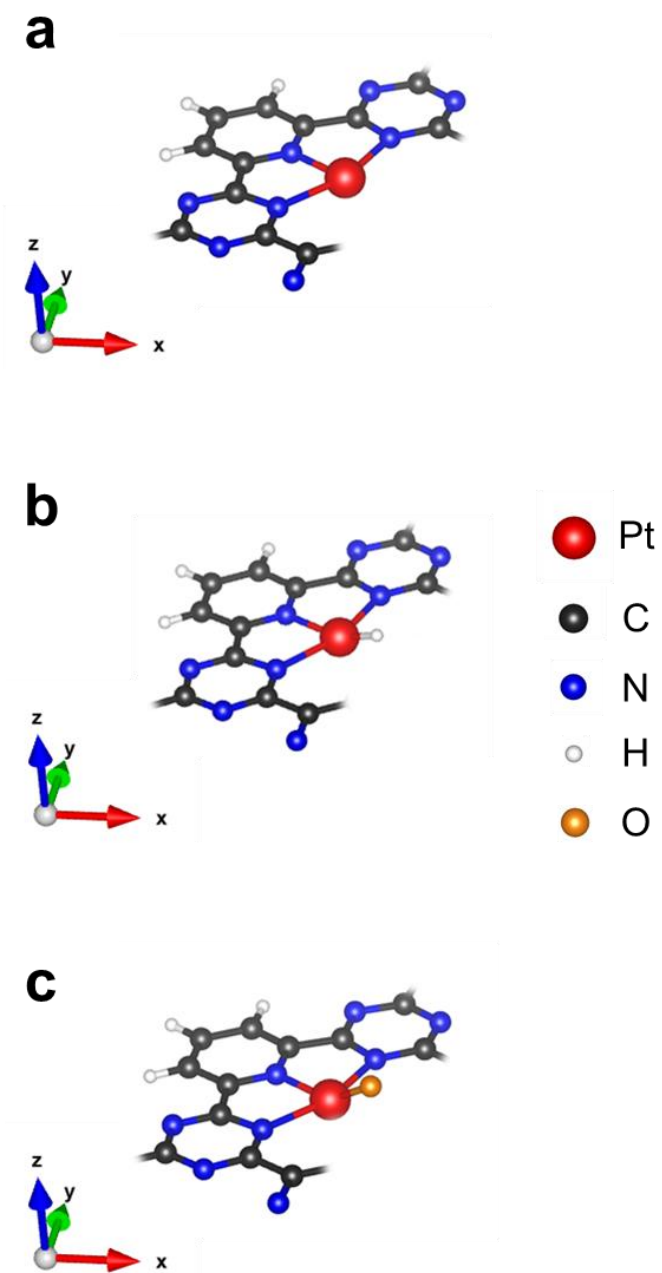


**Fig. 3.18 | Estimated structure of Pt-CTF and its reaction intermediate calculated by density functional theory. (a) Pt-CTF, (b) hydrogen adsorbed intermediate for HOR/HER, and (c) oxygen adsorbed intermediate for ORR. The calculation was carried out by Open MX.**

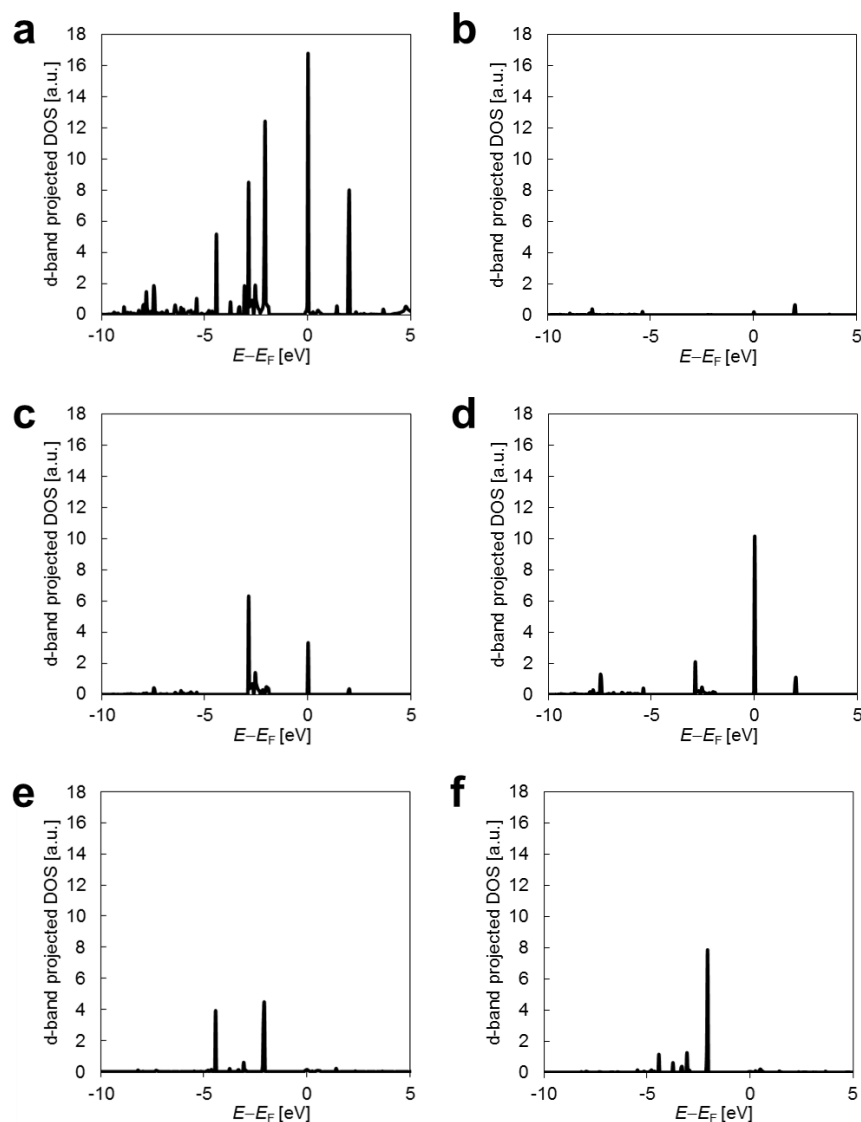


**Fig. 3.19 | Projected DOS (PDOS) onto the Pt atoms of Pt-CTF shown in Fig. 3.18a.** (a) Total DOS of Pt atoms in Pt-CTF, (b) PDOS onto  $d_{z^2}$ , (c)  $d_{x^2-y^2}$ , (d)  $d_{xy}$ , (e)  $d_{xz}$ , and (f)  $d_{yz}$ . The orientation of axis is based on Fig. 3.18a. The calculation was carried out by Open MX. Total DOS shown in Fig. 3.19a is similar to the Pt atom on porphyrin-like graphene (Fig. 3.17b). However, the reactants such as hydrogen and oxygen are able to contact with Pt atom only through z-axis on Pt coordinated porphyrin-like graphene, while they are able to contact through x-axis where electron density is high in Pt-CTF/CP, indicating that Pt-CTF/CP has higher catalytic activity than Pt coordinated porphyrin-like graphene.

## References

- [1] Chan, K.-Y., Ding, J., Ren, J., Cheng, S. & Tsang, K. Y. Supported mixed metal nanoparticles as electrocatalysts in low temperature fuel cells. *J. Mater. Chem.* **14**, 505-516 (2004).
- [2] Baxster, J., Bian, Z., Chen, G., Danielson, D., Dresselhaus, M. S., Fedorov, A. G., Fisher, T. S., Jones, C. W., Maginn, E., Kortshagen, U., Manthriam, A., Nozik, A., Rolison, D. R., Sands, T., Shi, L., Sholl, D. & Wu, Y. Nanoscale design to enable the revolution in renewable energy. *Energy Environ. Sci.* **2**, 559-588 (2009).
- [3] Du, S. & Pollet, B. G. Catalyst loading for Pt-nanowire thin film electrodes in PEFCs. *Int. J. Hydrogen Energy* **37**, 17892-17898 (2012).
- [4] Fugane, K., Mori, T., Ou, D. R., Yan, P., Ye, F., Yoshikawa, H. & Drennan, J. Improvement of Cathode Performance on Pt-CeO<sub>x</sub> by Optimization of Electrochemical Pretreatment Condition for PEFC Application. *Langmuir* **28**, 16692–16700 (2012).
- [5] Saida, T., Sekizawa, O., Ishiguro, N., Hoshino, M., Uesugi, K., Uruga, T., Ohkoshi, S., Yokoyama, T. & Tada, M. 4D Visualization of a Cathode Catalyst Layer in a Polymer Electrolyte Fuel Cell by 3D Laminography–XAFS. *Angew. Chem. Int. Ed.* **51**, 10311-10314 (2012).
- [6] Takeguchi, T., Yamanaka, T., Asakura, K., Muhamad, E. N., Uosaki, K. & Ueda, W. Evidence of Nonelectrochemical Shift Reaction on a CO-Tolerant High-Entropy State Pt–Ru Anode Catalyst for Reliable and Efficient Residential Fuel Cell Systems. *J. Am. Chem. Soc.* **134**, 14508–14512 (2012).
- [7] Silva, F. T., Dalmazzo, V. A., Becker, M. R., Souza, M. O., Souza, M. O. & Martini, E. M. A. Effect of Ni proportion on the performance of proton exchange membrane fuel cells using PtNi/C electrocatalysts. *Ionics* **20**, 381–388 (2014).
- [8] Rao, Ch. V. & Viswanathan, B. Monodispersed Platinum Nanoparticle Supported Carbon Electrodes for Hydrogen Oxidation and Oxygen Reduction in Proton Exchange Membrane

- Fuel Cells. *J. Phys. Chem. C* **114**, 8661–8667 (2010).
- [9] Strmcnik, D., Uchimura, M., Wang, C., Subbaraman, R., Danilovic, N., Vliet, D., Paulikas, A. P., Stamenkovic, V. R. & Markovic, N. M. Improving the hydrogen oxidation reaction rate by promotion of hydroxyl adsorption. *Nat. Chem.* **5**, 300-306 (2013).
- [10] Wang, X., Ahluwalia, R. K. & Steinbach, A. J. Kinetics of Hydrogen Oxidation and Hydrogen Evolution Reactions on Nanostructured Thin-Film Platinum Alloy Catalyst. *J. Electrochem. Soc.* **160**, F251-F261 (2013).
- [11] Durst, J., Simon, C., Hasché, F. & Gasteiger, H. A. Hydrogen Oxidation and Evolution Reaction Kinetics on Carbon Supported Pt, Ir, Rh, and Pd Electrocatalysts in Acidic Media. *J. Electrochem. Soc.* **162**, F190-F203 (2015).
- [12] Billy, E., Maillard, F., Morin, A., Guetaz, L., Emieuxa, F., Thurier, C., Doppelt, P., Donet, S. & Mailley, S. Impact of ultra-low Pt loadings on the performance of anode/cathode in a proton-exchange membrane fuel cell. *J. Power Sources* **195**, 2737–2746 (2010).
- [13] Gasteiger, H. A., Kocha, S. S., Sompalli, B. & Wanger, F. T. Activity benchmarks and requirements for Pt, Pt-alloy, and non-Pt oxygen reduction catalysts for PEMFCs. *Appl. Catal., B* **56**, 9–35 (2005).
- [14] Suryamas, A. B., Anikumar, G. M., Sago, S., Ogi, T. & Okuyama, K. Electrospun Pt/SnO<sub>2</sub> nanofibers as an excellent electrocatalysts for hydrogen oxidation reaction with ORR-blocking characteristic. *Catal. Commun.* **33**, 11-14 (2013).
- [15] Reiser, C. A., Bregoli, L., Patterson, T. W., Yi, J. S., Yang, J. D., Perry, M. L. & Jarvi, T. D. A Reverse-Current Decay Mechanism for Fuel Cells. *Electrochem. Solid-State Lett.* **8**, A273-A276 (2005).
- [16] Genorio, B., Strmcnik, D., Subbaraman, R., Tripkovic, D., Karapetrov, G., Stamenkovic, V. R., Pejovnik, S. & Marković, N. M. Selective catalysts for the hydrogen oxidation and oxygen reduction reactions by patterning of platinum with calix[4]arene molecules. *Nat. Mater.* **9**, 998-1003 (2010).
- [17] Genorio, B., Subbaraman, R., Strmcnik, D., Tripkovic, D., Stamenkovic, V. R. & Marković,

- N. M. Tailoring the Selectivity and Stability of Chemically Modified Platinum Nanocatalysts To Design Highly Durable Anodes for PEM Fuel Cells. *Angew. Chem. Int. Ed.* **50**, 5468–5472 (2011).
- [18] Kaspar, R. B., Wittkopf, J. A., Woodroof, M. D., Armstrong, M. J. & Yan, Y. Reverse-Current Decay in Hydroxide Exchange Membrane Fuel Cells. *J. Electrochem. Soc.*, **163**, F377-F383 (2016).
- [19] Qiao, B., Wang, A., Yang, X., Allard, L. F., Jiang, Z., Cui, Y., Liu, J., Li, J. & Zhang, T. Single-atom catalysis of CO oxidation using Pt<sub>1</sub>/FeO<sub>x</sub>. *Nat. Chem.* **3**, 634–641 (2011).
- [20] Wei, H., Liu, X., Wang, A., Zhang, L., Qiao, B., Yang, X., Huang, Y., Miao, S., Liu, J. & Zhang, T. FeO<sub>x</sub>-supported platinum single-atom and pseudo-single-atom catalysts for chemoselective hydrogenation of functionalized nitroarenes. *Nat. Commun.* **5**, 5634 (2014).
- [21] Lin, J., Qiao, B., Li, N., Li, L., Sun, X., Liu, J., Wang, X. & Zhang, T. Little do more: a highly effective Pt<sub>1</sub>/FeO<sub>x</sub> single-atom catalyst for the reduction of NO by H<sub>2</sub>. *Chem. Commun.* **51**, 7911-7914 (2015).
- [22] Yang, S., Kim, J., Tak, Y. J., Soon, A. & Lee, H. Single-Atom Catalyst of Platinum Supported on Titanium Nitride for Selective Electrochemical Reactions. *Angew. Chem. Int. Ed.* **55**, 2058–2062 (2016).
- [23] Kamiya, K., Kamai, R., Hashimoto, K. & Nakanishi, S. Platinum-modified covalent triazine frameworks hybridized with carbon nanoparticles as methanol-tolerant oxygen reduction electrocatalysts. *Nat. Commun.* **5**, 5040 (2014).
- [24] Iwase, K., Yoshioka, T., Nakanishi, S., Hashimoto, K. & Kamiya, K. Copper-Modified Covalent Triazine Frameworks as Non-Noble-Metal Electrocatalysts for Oxygen Reduction. *Angew. Chem. Int. Ed.* **54**, 11068–11072 (2015).
- [25] Yoshioka, T., Iwase, K., Nakanishi, S., Hashimoto, K. & Kamiya, K. Electrocatalytic Reduction of Nitrate to Nitrous Oxide by a Copper-Modified Covalent Triazine Framework. *J. Phys. Chem. C*, in press.
- [26] Llopis, J. F. & Colom, F. in *Encyclopedia of Electrochemistry of the Elements*, Vol, VI,

- Bard, A. J., Editors, p.169, Marcel Dekker, New York (1976).
- [27] Ogasawara, H. & Ito, M. Hydrogen adsorption on Pt(100), Pt(110), Pt(111) and Pt(1111) electrode surfaces studied by *in situ* infrared reflection absorption spectroscopy. *Chem. Phys. Lett.* **211**, 213-218 (1994).
- [28] Marković, N. M., Grgur, B. M. & Ross, P. N. Temperature-Dependent Hydrogen Electrochemistry on Platinum Low-Index Single-Crystal Surfaces in Acid Solutions. *J. Phys. Chem. B*, **101**, 5405–5413 (1997).
- [29] Kinoshita, K., Lundquist, J. & Stonehart, P. Hydrogen adsorption on high surface area platinum crystallites. *J. Catal.*, **31**, 325-334 (1973).
- [30] Gasteiger, H. A., Panels, J. E. & Yan, S. G. Dependence of PEM fuel cell performance on catalyst loading. *J. Power Sources* **127**, 162–171 (2004).
- [31] Pozio, A., Silva, R. F., Francesco, M. Giorgi, L. Nafion degradation in PEFCs from end plate iron contamination. *Electrochim. Acta* **48**, 1543-1549 (2003).
- [32] Cho, Y.-H., Lim J. W., Kang, Y. S., Cho, Y.-H., Kim, O.-H., Kwon, N.-H., Kwon, O. J., Yoon, W.-S., Choe, H. & Sung, Y.-E. The dependence of performance degradation of membrane electrode assembly on platinum loading in polymer electrolyte membrane fuel cell. *Int. J. Hydrogen Energ.* **37**, 2490-2497 (2012).
- [33] Litster, S. & McLean, G. PEM fuel cell electrodes. *J. Power Sources* **130**, 61-76 (2004).
- [34] Skúlason, E., Tripkovic, V., Björketun, M. E., Gudmundsdóttir, S., Karlberg, G., Rossmeisl, J., Bligaard, T., Jónsson, H. & Nørskov, J. K. Modeling the Electrochemical Hydrogen Oxidation and Evolution Reactions on the Basis of Density Functional Theory Calculations. *J. Phys. Chem. C* **114**, 18182–18197 (2010).
- [35] Tripkovic, V., Vanin, M., Karamad, M., Björketun, M. E., Jacobsen, K. W., Thygesen, K. S. & Rossmeisl, J. Electrochemical CO<sub>2</sub> and CO Reduction on Metal-Functionalized Porphyrin-like Graphene. *J. Phys. Chem. C* **117**, 9187–9195 (2013).
- [36] Yang, X.-F., Wang, A., Qiao, B., Li, J., Liu, J. & Zhang, T. Single-Atom Catalysts: A New Frontier in Heterogeneous Catalysis. *Acc. Chem. Res.* **46**, 1740-1748 (2013).

- [37] Wroblowa, H. S., Pan, Y. C & Razumney, G.. Electroreduction of oxygen: A new mechanistic criterion. *J. Electroanal. Chem.* **69**, 195–201 (1976).
- [38] Appleby, A. J. & Savy, M. Kinetics of oxygen reduction reactions involving catalytic decomposition of hydrogen peroxide: Application to porous and rotating ring-disk electrodes. *J. Electroanal. Chem.* **92**, 15–30 (1978).
- [39] Huang, J. C., Sen, R. K. & Yeager, E. Oxygen Reduction on Platinum in 85% Orthophosphoric Acid. *J. Electrochem. Soc.* **126**, 786–792 (1979).
- [40] Kinumoto, T. Inaba, M., Nakayama, Y., Ogata, K., Umebayashi, R., Tasaka, A., Iriyama, Y., Abe, T. & Ogumi, Z. Durability of perfluorinated ionomer membrane against hydrogen peroxide. *J. Power Sources* **158**, 1222-1228 (2006).
- [41] Qiao, J., Saito, M., Hayamizu, K. & Okada, T. Degradation of Perfluorinated Ionomer Membranes for PEM Fuel Cells during Processing with H<sub>2</sub>O<sub>2</sub>. *J. Electrochem. Soc.* **153**, A967-A974 (2006).
- [42] Adžić, R. R. & Wang, J. X. Configuration and Site of O<sub>2</sub> Adsorption on the Pt(111) Electrode Surface. *J. Phys. Chem. B* **102**, 8988-8993 (1998).
- [43] Li, T. & Balbuena, P. B. Computational Studies of the Interactions of Oxygen with Platinum Clusters. *J. Phys. Chem. B* **105**, 9943-9952 (2001).
- [44] Ou, L. & Chen, S. Comparative Study of Oxygen Reduction Reaction Mechanisms on the Pd(111) and Pt(111) Surfaces in Acid Medium by DFT. *J. Phys. Chem. C* **117**, 1342–1349 (2013).
- [45] Dyllal, K. G. Relativistic effects on the bonding and properties of the hydrides of platinum. *J. Chem. Phys.* **98**, 9678-9686 (1993).
- [46] Minaev, B. & Ågren, H. Spin uncoupling in molecular hydrogen activation by platinum clusters. *J. Mol. Catal. A: Chem.* **149**, 179-195 (1999).
- [47] Huda, M. N. & Kleinman, L. Hydrogen adsorption and dissociation on small platinum clusters: An electronic structure density functional study. *Phy. Rev. B* **74**, 195407 (2006).
- [48] Li, X., Bi, W., Zhang, L., Tao, S., Chu, W., Zhang, Q., Luo, Y., Wu, C., & Xie, Y.

Single-Atom Pt as Co-Catalyst for Enhanced Photocatalytic H<sub>2</sub> Evolution. *Adv. Mater.* **28**, 2427–2431 (2016).

[49] Dvořák, F., Camellone, M. F., Tovt, A., Tran, N.-D., Negreiros, F. R., Vorokhta, M., Skála, T., Matolínová, I., Mysliveček, J., Matolín, V. & Fabris, S. Creating single-atom Pt-ceria catalysts by surface step decoration. *Nat. Commun.* **7**, 10801 (2016).

[50] Tripkovic, V., Vanin, M., Karamad, M., Björketun, M. E., Jacobsen, K. W., Thygesen, K. S. & Rossmeisl, J. Electrochemical CO<sub>2</sub> and CO Reduction on Metal-Functionalized Porphyrin-like Graphene. *J. Phys. Chem. C* **117**, 9187–9195 (2013).



## Chapter 4.

### Selective electrochemical reduction of nitrogen oxides by covalent triazine frameworks modified with single Pt atoms

As mentioned in the previous chapter, single Pt atoms carried on CTF exhibited unique properties of inability to form under-potentially-deposited hydrogen (upd-H). The hydrogen-free Pt sites are thought to be attractive as selective electrocatalysts, as the electrochemical reactions which required the adsorbed hydrogen atoms should be inhibited. In this chapter, the author investigated the electrocatalytic properties of single Pt atoms carried on CTF for the reduction reactions of nitrate and nitrite, and then put our focus on clarifying the role of adsorbed hydrogen for the reactions.

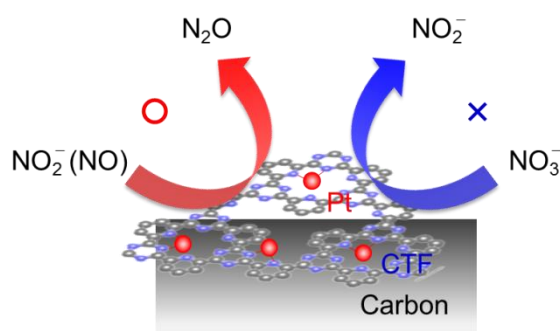


Figure | Schematic illustration of the selective reaction between nitrate and nitrogen monoxide derived from nitrite on single Pt atom modified CTF.

## 4.1. Introduction

Platinum (Pt) is definitely the best catalyst for various useful reactions, such as electrocatalytic reactions of fuel cells [1-3] and exhaust gas purification [4-6]. Recently, Pt single-atom catalysts (Pt-SACs) have attracted considerable attention not only because they can maximize the efficiency of Pt atom utilization but also because they offer great potential for achieving high activity and unique selectivity. For example, Qiao *et al.*, synthesized Pt-SACs supported on FeO<sub>x</sub>, which functioned as an efficient catalyst for carbon monoxide oxidation [7]. Yang *et al.* reported that a Pt-SACs on titanium nitride selectively reduced oxygen to hydrogen peroxide [8]. However, Pt atoms of these Pt-SACs easily aggregate with the increase in Pt content to approximately 1 wt% [7-10].

Covalent triazine frameworks (CTFs) have 1,3,5-triazine units as linkers, represent microporous conjugated polymers. As CTFs possess abundant nitrogen (N) atoms with electron lone pair for metal coordination, CTFs are expected to stabilize Pt single atoms through coordination with the N atoms. As mentioned in previous chapter, the author has indeed synthesized single-Pt atoms modified CTF hybridized with conductive carbon nanoparticles (Pt-CTF/CP) as an electrocatalyst [11]. The resulting Pt-CTF/CP was inactive towards methanol oxidation (see Chapter 2), and selectively catalyzed hydrogen oxidation even in the presence of dissolved oxygen (see Chapter 3) [12]. These unique properties were attributed to the atomic dispersion of the Pt atoms. In terms of selectivity, Pt-CTF/CP is very interesting material showing significantly different electrocatalytic properties from the Pt metal electrode. Although the knowledge on reactivity and selectivity is still very limited, considering its mononuclear structure, it is expected that Pt-CTF/CP exhibit particularly different reactivity from the bulk surface in reactions which involve co-adsorption intermediate structure.

In this chapter, the author investigated the electrocatalytic properties of Pt-CTF/CP for the reduction reactions of nitrate and nitrite, and then put our focus on clarifying the role of adsorbed hydrogen for the reactions.

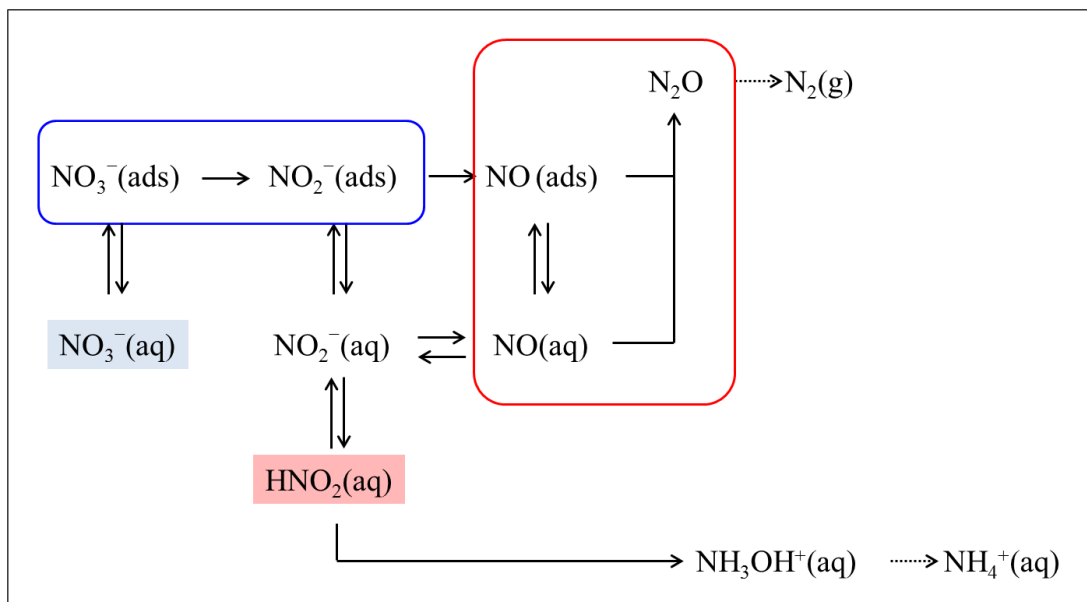


**Fig. 4.1 | The major nitrogen oxide reduction reaction pathway on the Pt metal electrode in acidic solutions ( $pK_a < 3.4$ ).** The nitrate reduction reaction [Eq(1)] is emphasized by blue line, and the nitrite reduction reaction [Eq(3)] is emphasized by red line.

## 4.2. Experimental details

### 4.2.1. Catalyst synthesis

Pt-CTF/CP was prepared in the same manner as described in Chapter 2 [11]. In brief, a mixture of ZnCl<sub>2</sub> (1.36 g, Wako), 2,6-dicyanopyridine (129 mg, Sigma-Aldrich) and Ketjen Black EC600JD (129 mg, Lion Corp.) was heat treated in a vacuum-sealed glass tube at 400 °C for 21 h. The resulting powder was washed with 0.1 M HCl, water, tetrahydrofolate and acetonitrile, and then modified with Pt atoms by stirring in 160 mM K<sub>2</sub>[PtCl<sub>4</sub>] (Wako) solution at 60 °C for 4 h. The sample named Pt-CTF/CP (agg.) was prepared by heating of Pt-CTF/CP at 450 °C for 2 h under hydrogen atmosphere in a quartz tube, as a comparative material having aggregated Pt atoms on CTF. The catalysts were compared with commercially available 20 wt% Pt/C (HiSPEC3000, Johnson Matthey).

### 4.2.2. Electrochemical measurements

All electrochemical measurements were conducted in three-electrode systems at room temperature using rotating disk electrodes (RDE) in 0.1 M HClO<sub>4</sub> aqueous solution. Working electrodes were prepared by dispersing each catalyst in 120 μL ethanol and 47.5 μL Nafion solution (5 wt% solution; Aldrich), and then the resulting catalyst inks were dropped onto a glassy carbon electrode. The loading amounts of the catalysts were unified by the weight of the carbon support, and the carbon supports were controlled to be 0.40 mg cm<sup>-2</sup>. A Pt wire and Ag/AgCl (sat. KCl) were used as the counter and reference electrodes, respectively. All potentials were converted into a reversible hydrogen electrode (RHE).

## 4.3. Results

### 4.3.1. Characterizations

The author previously demonstrated using extended X-ray absorption fine structure (EXAFS) spectra and high-angle annular dark-field scanning transmission electron microscopy (HAADF-STEM) that Pt atoms in Pt-CTF/CP are individually isolated [11]. Fig. 4.2 shows the current density ( $j$ ) versus potential ( $U$ ) curves of CP (Ketjen Black), CTF/CP, Pt-CTF/CP, Pt-CTF/CP (agg.) and Pt/C in 0.1 M Ar-saturated HClO<sub>4</sub>. On Pt atoms in Pt-CTF/CP, a pair of peaks assignable to the adsorption/desorption of under-potentially-deposited hydrogen (upd-H) on Pt atom was not observed (Fig.4.2, red curve) [12]. Considering that the formation of upd-H proceeds on Pt ensemble sites, such as step, three-fold hollow and defect sites [13], the absence of adsorption–desorption peaks of upd-H is due to the isolation of Pt atoms in Pt-CTF/CP.

Table 4.1   XPS-elemental analysis and estimated numbers of Pt atoms.						
Catalyst	C content (at%)	N content (at%)	Pt content (at%)	Pt content (wt%)	Total Pt atoms <sup>†</sup> (cm <sup>-2</sup> )	Surface Pt atoms <sup>‡</sup> (cm <sup>-2</sup> )
Pt-CTF/CP	91	5.6	1.0	12	$1.8 \times 10^{17}$	N/A
Pt-CTF/CP (agg.)	92	5.4	0.69	8.3	$1.2 \times 10^{17}$	$3.6 \times 10^{16}$
20 wt% Pt/C	92	—	1.4	20	$3.0 \times 10^{17}$	$4.5 \times 10^{16}$

<sup>†</sup> Total Pt atoms are calculated from the XPS results.

<sup>‡</sup> Surface Pt atoms are calculated from the electric charge for the adsorption of the upd-H in CV (Fig. 4.1). The electrical charges are determined using the baseline current at 0.40 V as the current caused by the double layer.

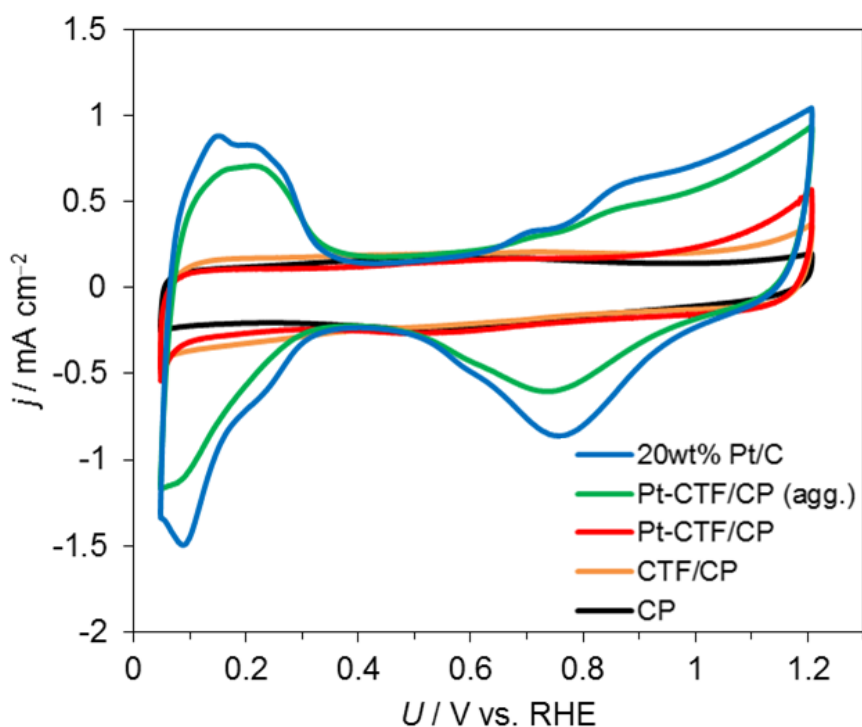


**Fig. 4.2 | Cyclic voltammograms of the catalysts and its support deposited on glassy carbon electrode.** Electrolyte (0.1 M  $\text{HCO}_4^-$ ) was purged by Ar. Scan rate:  $10 \text{ mV s}^{-1}$ .

When hypothesized that all of Pt atoms of Pt-CTF/CP were isolated and electrochemically active, the total number of Pt atoms on 12 wt% Pt-CTF/CP can be evaluated to be  $1.8 \times 10^{17} \text{ cm}^{-2}$ . In contrast, the number of electrochemically active Pt atoms on Pt/C and Pt-CTF/CP (agg.), which were calculated from the electric charge for the adsorption of the upd-H in CV, were estimated to be  $4.5 \times 10^{16} \text{ cm}^{-2}$  and  $3.6 \times 10^{16} \text{ cm}^{-2}$ , respectively (Table 4.1). Although some of Pt atoms on Pt-CTF/CP might not be exposed to the electrolyte and are electrochemically inactive, the amount of active Pt atom on Pt-CTF/CP would be comparable to that on Pt/C.

### 4.3.2. Electrochemical characteristics for nitrate reduction

The nitrate reduction activity of Pt-CTF/CP was compared to those of Pt-CTF/CP (agg.) and 20 wt% Pt/C by measuring  $j$  vs.  $U$  relationships in 0.1 M HClO<sub>4</sub> aqueous solution with the addition of nitrate (Fig. 4.3). The Pt-CTF/CP generated almost no current even at high nitrate concentrations, whereas the nitrate reduction current was clearly observed from about 0.4 V for the Pt/C and Pt-CTF/CP (agg.) electrodes. Considering that the number of the active Pt atoms does not differ significantly among Pt-CTF/CP, Pt/C and Pt-CTF/CP (agg.), these results indicated that Pt single atoms were inactive for the nitrate reduction reaction.

The first step of nitrate reduction reaction is known to form nitrite (Eq(1)) [14-17].



As nitrate adsorption on Pt sites is essential to facilitate the reaction [18], the author next examines the nitrate adsorption on Pt-CTF/CP by measuring the oxygen reduction reaction (ORR) activities in the presence of nitrate. The polarization curves for ORR in the presence of each concentration of NaNO<sub>3</sub> are shown in Fig. 4.4. The ORR onset potential was about 0.86 V, which was consistent with the result in previous chapter (Chapter 2, Fig. 2.5, green curve). Although the onset value (0.86 V) did not depend on the nitrate concentration, the decrease in the diffusion limiting current was observed in higher nitrate concentration (> 0.1 M). This is presumably because the adsorption of O<sub>2</sub> on single atom Pt in Pt-CTF/CP was inhibited by the adsorbed NO<sub>3</sub><sup>-</sup>. Actually, Groot *et al* reported that the reaction order of nitrate reduction on Pt metal became negative at high concentrations (> 0.1 M) because the excess amount of adsorbed nitrate inhibited the adsorption of a second species necessary for the reaction [15]. Namely, although nitrate can adsorb on the Pt sites of Pt-CTF/CP, the catalyst showed no nitrate reduction reaction activity.

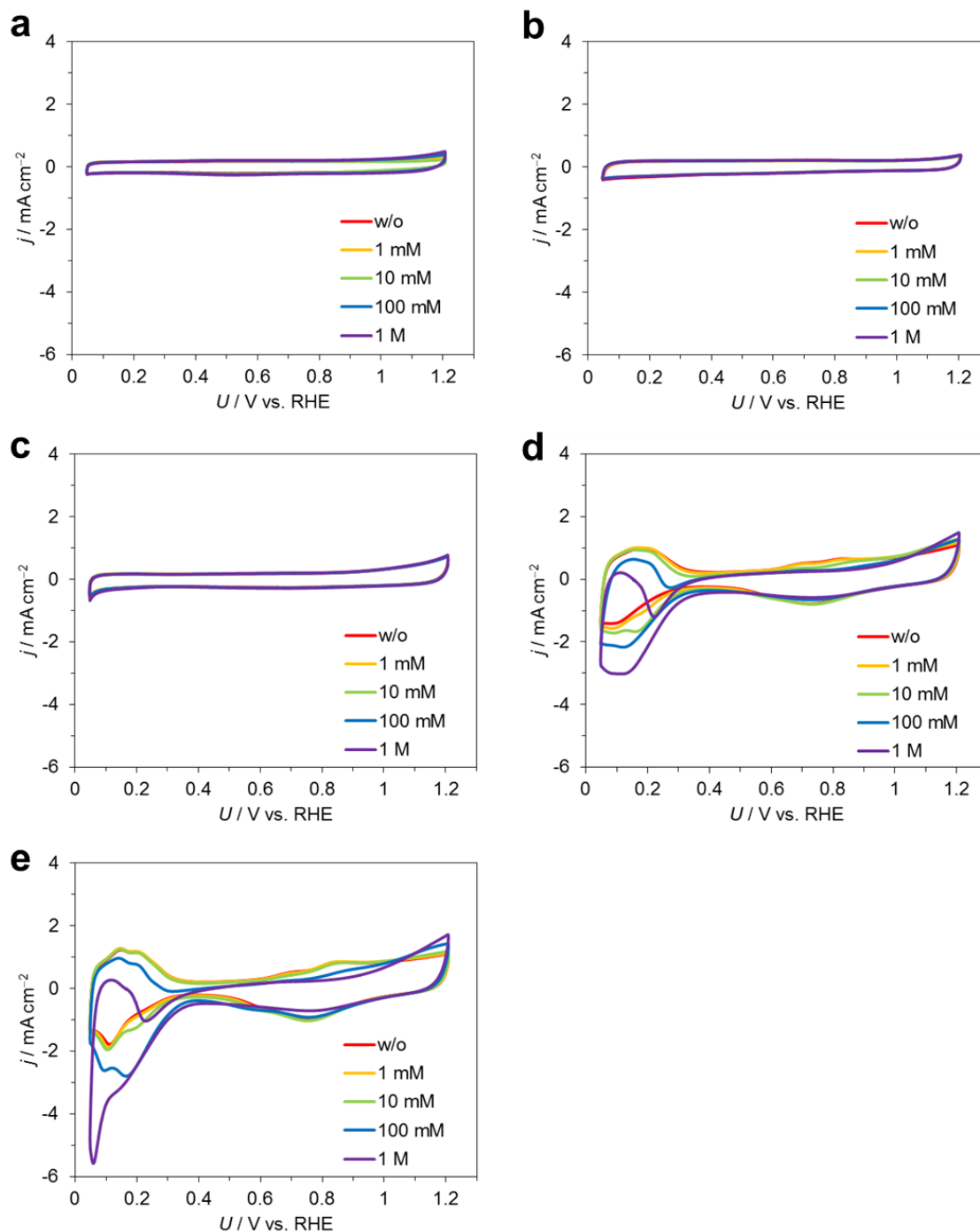


**Fig. 4.3 | Nitrate reduction activity of catalysts and its support.** (a) CP, (b) CTF/CP, (c) Pt-CTF/CP, (d) Pt-CTF/CP (agg.) and (e) Pt/C in Ar-saturated 0.1 M HClO<sub>4</sub> containing each concentrations of NaNO<sub>3</sub>. Rotation rate: 1,500 rpm. Scan rate: 10 mV<sup>-1</sup>.

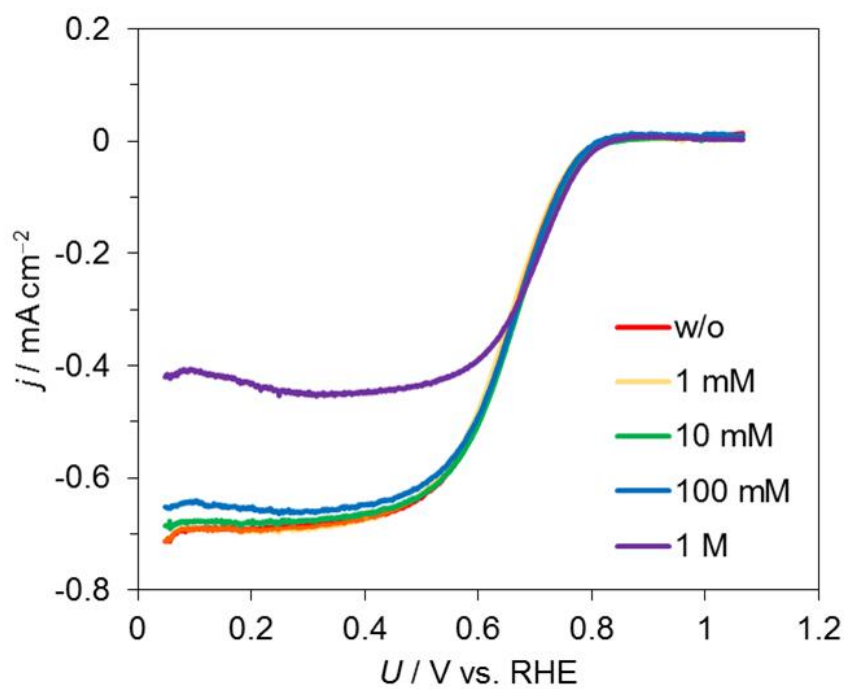
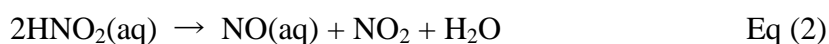


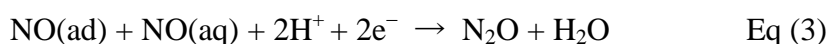
**Fig. 4.4 | Polarization curves for ORR in the presence of each concentration of  $\text{NaNO}_3$ .**

### 4.3.3. Electrochemical characteristics for nitrite reduction

Fig. 4.5 shows the Faradaic current density vs.  $U$  curves of nitrite reduction reaction in 0.1 M HClO<sub>4</sub>. Although small reduction currents were observed on CP and CTF/CP from 0.6 V, the cathodic current density was clearly enhanced by Pt-CTF/CP, Pt-CTF/CP (agg.) and Pt/C, indicating that both metallic Pt and single Pt atoms accelerated the nitrite reduction reaction. In order to consider the nitrite reduction reaction in detail, we need to be aware of the nitrous acid decomposition in acidic solutions. The value of  $pK_a$  for HNO<sub>2</sub> is about 3.2, and thus, HNO<sub>2</sub> definitely dominates over NO<sub>2</sub><sup>-</sup> in highly acidic solutions (< pH 2). The HNO<sub>2</sub> is known to be decomposed into NO and NO<sub>2</sub> by the following equilibrium.



The NO generated by this equilibrium is an important electrochemically active species for the nitrite reduction. Duca *et al.* reported that the Pt metal electrode catalyze the NO dimerization and subsequent N<sub>2</sub>O formation in the potential range of 0.25–0.6 V (Eq(3)), while NH<sub>2</sub>OH gradually became dominate at lower potential (< 0.25 V) [19].



In the  $j$  vs.  $U$  curve for our Pt-CTF/CP (Figure 4.5c), the change in slope was clearly observed at 0.25 V, which coincides with the results of Pt-CTF/CP (agg.) and Pt/C. Considering these results and literatures, our Pt-CTF/CP likely reduced nitrite in a similar manner to Pt metal electrodes.

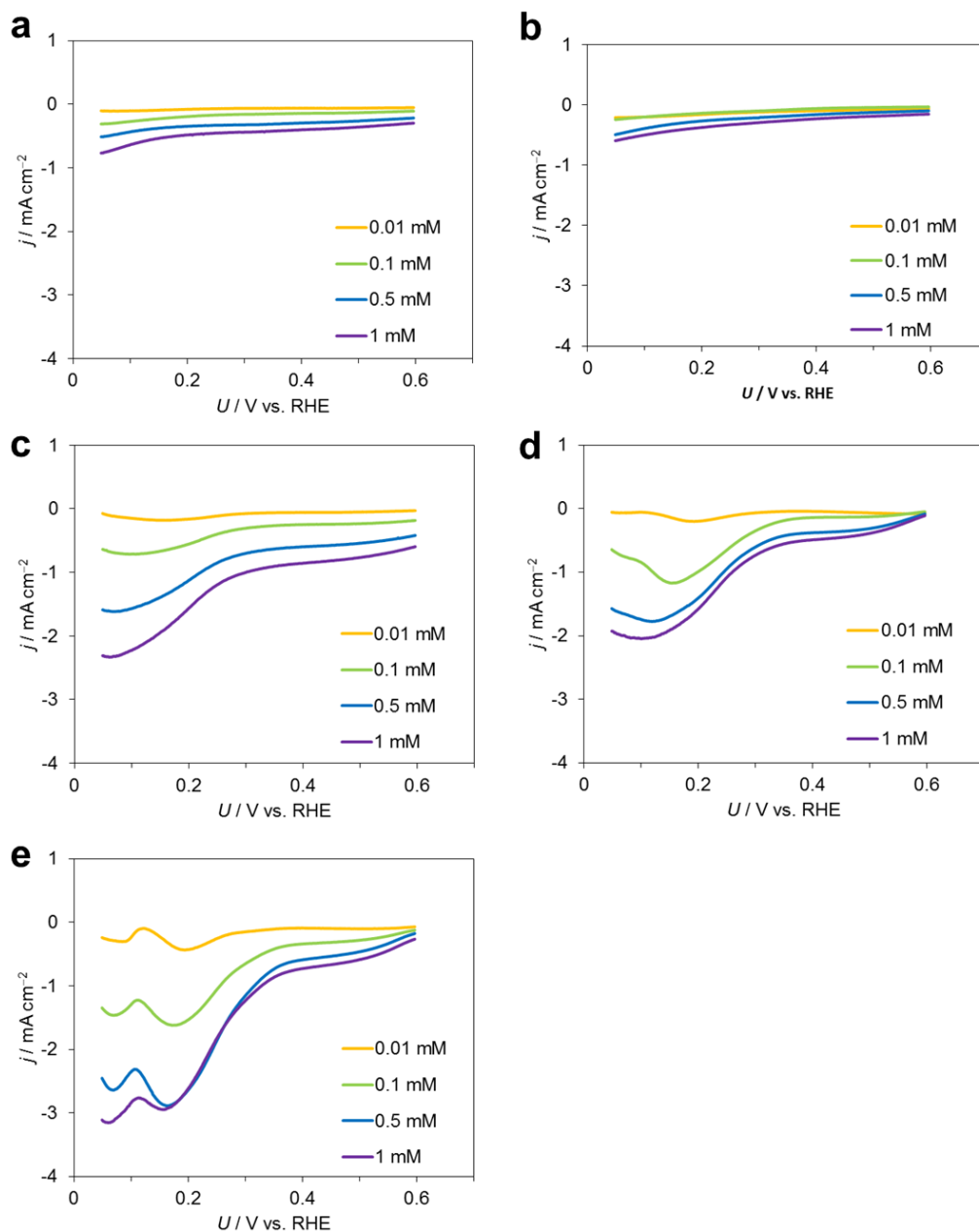


**Fig. 4.5 | Faradaic current density vs.  $U$  curves of nitrite reduction reaction.** (a) CP, (b) CTF/CP, (c) Pt-CTF/CP, (d) Pt-CTF/CP (agg.) and (e) Pt/C in Ar-saturated 0.1 M HClO<sub>4</sub> containing each concentrations of NaNO<sub>2</sub>. Rotation rate: 1,500 rpm. Scan rate: 10 mV<sup>-1</sup>. Faradaic currents were calculated by subtracting the current observed when the CVs were performed in electrolyte solutions in the absence of nitrite from the current observed when the CV was then performed in electrolyte solutions with nitrite.

#### 4.4. Discussion

Before discuss the mechanisms of nitrate and nitrite reduction reactions on Pt-CTF/CP, it is appropriate to summarize that on Pt metal electrode. For nitrate reduction reaction, as mentioned above, Groot *et al.* observed the inverse correlation between the NRR current and the nitrate concentration at high concentrations ( $> 0.1$  M) [15]. Based on this result, they assumed that nitrate adsorbates blocked the surface for the adsorption of hydrogen or water. Therefore, the second adsorbate (hydrogen or water) were considered to be essential for the nitrate reduction reaction. Taguchi *et al.* also showed that simultaneous present of adsorbed hydrogen and of adsorbed nitrate enhanced the rate of nitrate reduction reaction on the Pt electrodes [16,20]. In addition, in the case of our result of Pt/C, the nitrate reduction occurred from 0.4 to 0.05 V, which corresponds to upd-H potential region. Considering these literatures and our result, nitrate is thought to be reduced on the Pt surface by the reaction of the adsorbed nitrate and the upd-H (Langmuir-Hinshelwood mechanism). In the case of the nitrite reduction reaction, the electrochemical active species in acidic solutions is the NO molecule which is produced by Eq (2), and  $N_2O$  is known to be the majority product of the NO reduction above 0.25 V. Claybone *et al.* demonstrated by the DFT calculation that the following pathway of the NO reduction reaction was energetically favorable: solvated NO reacted with surface-bound NO to form an adsorbed  $(NO)_2$ -dimer, and then the dimer abstracted a proton from water [21]. Thus, adsorbed hydrogen might not be required for the nitrite (NO) reduction reaction on the Pt surface, at least in higher potential region ( $> 0.25$  V).

Here, let me move on to discuss the reaction mechanism of Pt-CTF/CP to gain insight into the electrocatalytic properties of Pt single atom catalysts. Reversible peaks corresponding to formation and desorption of upd-H were absent, meaning that the single Pt site is free from adsorbed hydrogen above 0.05 V. Thus, although the ORR results suggested that a certain portion of nitrate bound on Pt sites, Pt-CTF/CP exhibited

almost no activity for nitrate reduction due to the lack of the adsorbed proton which is required for the Langmuir-Hinshelwood process. In contrast, the nitrite (NO) reduction reaction was facilitated by Pt-CTF/CP because only solvated proton is involved in the NO dimerization (Eq (3)). The electrocatalytic activities of Pt-CTF/CP for nitrate and nitrite reduction reactions investigated in this study were in good agreement with the involvement of adsorbed hydrogen in reaction mechanism that has been proposed on Pt metal so far (Eq (1) and (3)).

Moreover, in the same way as upd-H, electrochemical formations of the adsorbed oxygen species are also supposed to show different tendency on Pt single atoms of Pt-CTF/CP from Pt metal because atomic oxygen prefers to adsorb at hollow site of Pt metal surface [22]. Although the oxidative current corresponds to the formation of the Pt-oxide can be seen on Pt metal higher than 0.8 V (Fig. 4.2, blue curve) [23], the current value was significantly small on Pt-CTF/CP in the same potential region (Fig. 4.2, red curve). This indicates that the number of adsorbed oxygen species on Pt-CTF/CP is prominently smaller than that on Pt/C. Therefore, Pt single sites of Pt-CTF/CP are expected to have selectivity not only to the reaction systems involving adsorbed hydrogen but also to the reaction systems involving adsorbed oxygen.

## 4.5. Conclusions

In this chapter, the author demonstrated that the reduction reaction activities of nitrogen oxides on Pt single sites of Pt-CTF/CP. The nitrate reduction reaction was inactive on Pt-CTF/CP; in contrast with the reduction reaction of NO decomposed from nitrite was active. This selectivity was revealed to be derived from the inability of the formation of upd-H on Pt sites of Pt-CTF/CP. These hydrogen-free Pt sites are thought to be attractive as selective electrocatalysts, as the electrochemical reactions which required the adsorbed hydrogen atoms should be inhibited. Further, it can be said that Pt single sites are useful to clarify the involvement of adsorption species in the reaction mechanisms.

## References

- [1] Saida, T., Sekizawa, O., Ishiguro, N., Hoshino, M., Uesugi, K., Uruga, T., Ohkoshi, S., Yokoyama, T. & Tada, M. 4D Visualization of a Cathode Catalyst Layer in a Polymer Electrolyte Fuel Cell by 3D Laminography–XAFS. *Angew. Chem. Int. Ed.* **51**, 10311-10314 (2012).
- [2] Gasteiger, H. A., Kocha, S. S., Sompalli, B. & Wanger, F. T. Activity benchmarks and requirements for Pt, Pt-alloy, and non-Pt oxygen reduction catalysts for PEMFCs. *Appl. Catal., B* **56**, 9–35 (2005).
- [3] Suryamas, A. B., Anikumar, G. M., Sago, S., Ogi, T. & Okuyama, K. Electrospun Pt/SnO<sub>2</sub> nanofibers as an excellent electrocatalysts for hydrogen oxidation reaction with ORR-blocking characteristic. *Catal. Commun.* **33**, 11-14 (2013).
- [4] Hauff, K., Tuttlies, U., Eigenberger, G. & Nieken, U. A global description of DOC kinetics for catalysts with different platinum loadings and aging status. *Appl. Catal., B* **100**, 10–18 (2010).
- [5] Yamamoto, K., Nakamura, M., Yane, H. & Yamashita, H. Simulation on catalytic reaction in diesel particulate filter. *Catal. Today* **153**, 118-124 (2010).
- [6] Morales-Torres, S., Maldonado-Hódar, F. J., Pérez-Cadenas, A. F. & Carrasco-Marín, F. Design of low-temperature Pt-carbon combustion catalysts for VOC's treatments. *J. Hazard. Mater.* **183**, 814-822 (2010).
- [7] Qiao, B., Wang, A., Yang, X., Allard, L. F., Jiang, Z., Cui, Y., Liu, J., Li, J. & Zhang, T. Single-atom catalysis of CO oxidation using Pt<sub>1</sub>/FeO<sub>x</sub>. *Nat. Chem.* **3**, 634–641 (2011).
- [8] Yang, S., Kim, J., Tak, Y. J., Soon, A. & Lee, H. Single-Atom Catalyst of Platinum Supported on Titanium Nitride for Selective Electrochemical Reactions. *Angew. Chem. Int. Ed.* **55**, 2058 –2062 (2016).
- [9] Wei, H., Liu, X., Wang, A., Zhang, L., Qiao, B., Yang, X., Huang, Y., Miao, S., Liu, J. & Zhang, T. FeO<sub>x</sub>-supported platinum single-atom and pseudo-single-atom catalysts for

- chemoselective hydrogenation of functionalized nitroarenes. *Nat. Commun.* **5**, 5634 (2014).
- [10] Shi, Y., Zhao, C., Wei, H., Guo, J., Liang, S., Wang, A., Zhang, T., Liu, J. & Ma, T. Single-Atom Catalysis in Mesoporous Photovoltaics: The Principle of Utility Maximization. *Adv. Mater.* **26**, 8147–8153 (2014).
- [11] Kamiya, K., Kamai, R., Hashimoto, K. & Nakanishi, S. Platinum-modified covalent triazine frameworks hybridized with carbon nanoparticles as methanol-tolerant oxygen reduction electrocatalysts. *Nat. Commun.* **5**, 5040 (2014).
- [12] R. Kamai, K. Kamiya, K. Hashimoto & S. Nakanishi, in preparation.
- [13] Ogasawara, H. & Ito, M. Hydrogen adsorption on Pt(100), Pt(110), Pt(111) and Pt(1111) electrode surfaces studied by *in situ* infrared reflection absorption spectroscopy. *Chem. Phys. Lett.* **211**, 213-218 (1994).
- [14] Dima, G. E., De Voys, A. C. A. & Koper, M.T.M. Electrocatalytic reduction of nitrate at low concentration on coinage and transition-metal electrodes in acid solutions. *J. Electroanal. Chem.* **554-555**, 15-23 (2003).
- [15] De Groot, M. T. & Koper, M. T. M. The influence of nitrate concentration and acidity on the electrocatalytic reduction of nitrate on platinum. *J. Electroanal. Chem.* **562**, 81-94 (2004).
- [16] Taguchi, S. & Feliu, J. M. Kinetic study of nitrate reduction on Pt(1 1 0) electrode in perchloric acid solution. *Electrochim. Acta* **53**, 3626-3634 (2008).
- [17] Rima, F. R., Nakata, K., Shimazu, K. & Osawa, M. Surface-Enhanced Infrared Absorption Spectroscopic Studies of Adsorbed Nitrate, Nitric Oxide, and Related Compounds. 3. Formation and Reduction of Adsorbed Nitrite at a Platinum Electrode. *J. Phys. Chem. C* **114**, 6011-6018 (2010).
- [18] Yang, J., Calle-Vallejo, F., Duca, M. & Koper, M. T. M. Electrocatalytic Reduction of Nitrate on a Pt Electrode Modified by p-Block Metal Adatoms in Acid Solution. *ChemCatChem* **5**, 1773-1783 (2013).
- [19] Duca, M., Kavvadia, V., Rodriguez, P., Lai, S. C. S., Hoogenboom, T. & Koper, M. T. M.

- New insights into the mechanism of nitrite reduction on a platinum electrode. *J. Electroanal. Chem.* **649**, 59-68 (2010).
- [20] Taguchi, S. & Feliu, J. M. Electrochemical reduction of nitrate on Pt(S)[n(111)×(111)] electrodes in perchloric acid solution. *Electrochim. Acta* **52**, 6023-6033 (2007).
- [21] Clayborne, A., Chun, H.-J., Rankin, R. B. & Greeley, J. Elucidation of Pathways for NO Electroreduction on Pt(111) from First Principles. *Angew. Chem. Int. Ed.* **54**, 8255-8258 (2015).
- [22] Imai, H., Izumi, K., Matsumoto, M., Kubo, Y., Kato, K. & Imai, Y. In Situ and Real-Time Monitoring of Oxide Growth in a Few Monolayers at Surfaces of Platinum Nanoparticles in Aqueous Media. *J. Am. Chem. Soc.* **131**, 6293-6300 (2009).
- [23] Jerkiewicz, G., Vatankhah, G., Lessard, J., Soriaga, M. P. & Park, Y.-S. Surface-oxide growth at platinum electrodes in aqueous H<sub>2</sub>SO<sub>4</sub>: Reexamination of its mechanism through combined cyclic-voltammetry, electrochemical quartz-crystal nanobalance, and Auger electron spectroscopy measurements. *Electrochim. Acta* **49**, 1451–1459 (2004).



# Chapter 5.

## Conclusions and Perspectives

### 5.1. Conclusions

Heterogeneous catalyst having a single metal atom active center is expected to show specific catalytic activity different from a bulk metal surface. Such specificity is attractive from a point of view of the electron transfer catalysts which are the key material for electrical—chemical energy conversion. Although single metal atoms are expected to show interesting properties, in general, they are easy to aggregate because of their high surface energy. Therefore, development of the electrocatalyst which stably supports practical concentrations of single metal atoms, especially Pt: the most widely utilized catalyst material, is strongly desired. As a support material for single metal atoms, covalent triazine framework (CTF) is attractive because it has a regular porous structure including high density of nitrogen with lone pair which can be a coordination environment of single metal atoms. However, there is a problem that the electrical conductivity of CTF itself is extremely low for directly use as an electrocatalyst.

Based on this background, in this study, the author developed a novel CTF-based electrocatalyst modified with single Pt atoms (Pt-CTF/CP) through overcoming its low electrical conductivity by hybridizing CTF with conductive carbon nanoparticles. Then, the author focused on the reaction selectivity on Pt single site of Pt-CTF/CP. As a result, the author constructed useful selective reaction systems by using single Pt atom modified Pt-CTF/CP electrocatalyst on which selectivities were derived from its single atom nature.

In chapter 1, the background of this thesis was introduced; especially the single atom catalysis on electrochemistry was overviewed. The author mentioned the specific

features of single atom electrocatalysts, and the expectations for them to realize reaction selectivity.

In chapter 2, firstly, the author successfully developed a novel electrocatalyst which has practical concentration of single Pt atoms by carrying Pt atoms on hybridized material of CTF and conductive carbon nanoparticles. The resulting material (Pt-CTF/CP) did not show the aggregated Pt particle, although it possessed high density of atomically dispersed Pt particles. Then, the author demonstrated that Pt-CTF/CP functions as an electrocatalyst by confirming its catalytic behavior for the oxygen reduction reaction (ORR). Besides, the author revealed that Pt-CTF/CP is inactive to the methanol oxidation reaction, and it selectively catalyzes ORR even in the presence of 1 M methanol. This selectivity is useful as a cathode catalyst of direct methanol fuel cells.

In chapter 3, the author demonstrated that single Pt sites of Pt-CTF/CP can catalyze hydrogen oxidation reaction (HOR) effectively with almost zero overpotential. Notably, the atomically dispersed 2.8 wt% Pt-modified CTF showed comparable catalytic activity for HOR to the commercially available carbon-supported 20 wt% Pt catalyst. In addition, 2.8 wt% Pt-CTF/CP showed a much lower catalytic activity towards ORR less than 1/4 at 0.6 V versus RHE. Thus, the author revealed that single Pt sites of 2.8 wt% Pt-CTF/CP selectively catalyze hydrogen oxidation, even in the presence of dissolved oxygen. This property is important because oxygen tolerance of an anode catalyst of polymer electrolyte fuel cells (PEFCs) has a potential to overcome the problem of cathode degradation during start/stop cycles of PEFCs.

In chapter 4, selective catalytic activity on the single Pt site of Pt-CTF/CP for nitrogen oxide reduction reactions were demonstrated. Although the adsorbed hydrogen atoms are required only for nitrate reduction, the formation of under-potentially-deposited hydrogen (upd-H) on single Pt atoms of Pt-CTF/CP was inhibited because upd-H only forms on the Pt ensemble site such as step, three fold hollow and defect sites. From this feature, Pt-CTF/CP was revealed to be inactive towards nitrate

reduction reaction. In contrast, the reduction reaction of NO decomposed from nitrite was active on the single Pt site of Pt-CTF/CP because it only involves dissolved hydrated proton. Thus, the author revealed that the lack of upd-H on Pt sites of Pt-CTF/CP likely resulted in this unique selectivity for nitrogen oxide reduction reactions. Therefore, the hydrogen-free Pt sites are thought to be attractive as selective electrocatalysts, as the electrochemical reactions which requires adsorbed hydrogen atoms should be inhibited.

The present study is the first example to demonstrate experimentally the selective electrochemical reaction on the single Pt site. Through the whole of this study, the author constructed a new concept for the selective reactions on the electrocatalysts which have a single metal atom active center. On bulk metal surfaces, in general, both of the following electrochemical catalytic reactions (i) and (ii) non-selectively proceed if the proper potential is applied to the reaction system.

- (i) The reactions which proceeds via the adsorbed structure to multiple metal atom site, typical to the reactions following Langmuir-Hinshelwood mechanism (Fig. 5.1a).
- (ii) The reactions which proceeds via the adsorbed structure only to a single metal atom site, typical to the reactions following Eley-Rideal mechanism (Fig. 5.1b).

In contrast, on the single metal site, the reactions (i) are inhibited because of its structural factor while the reactions (ii) favorably proceed. Thus, in the reaction system both (i) and (ii) are present together, (ii) would be selectively catalyzed on a single metal atom. As long as the author knows, this concept for the selective reaction on the electrocatalyst had never been clarified to date. Therefore, the present study provided a new guideline for constructing a useful reaction system.

At last, the final purpose of this study is to realize environmental-friendly electrical–chemical energy conversion systems through the electrocatalyst. As shown in the present study, acquisition of highly reaction-selective electrocatalyst to the aimed reaction contributes greatly to the improvement of energy conversion efficiency and device durability. Also, the high reaction selectivity is useful characteristics for many situations, for example, the production of useful substances, the treatment of hazardous materials, and so on. In addition, the electrocatalyst with a single metal atom active center has a possibility to improve metal utilization efficiency. Such effective use of metal is expected to contribute to the cost reduction of a device which uses a precious metal, such as PEFCs loaded with Pt. Therefore, the development of the electrocatalysts with a single metal atom active center has a great possibility to realize environmental-friendly society by enabling efficient and cost effective electrical–chemical energy conversion.

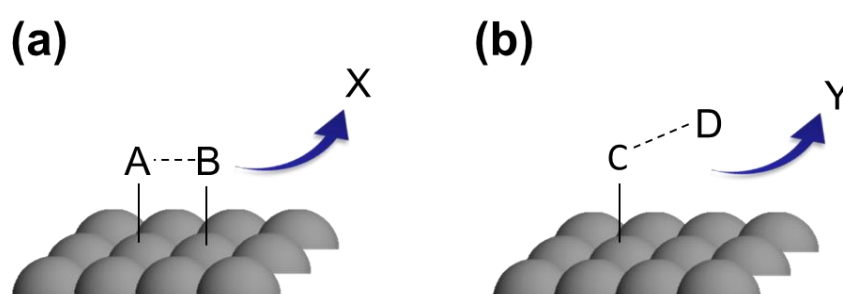


**Fig. 5.1 | Schematic illustration of reaction mechanisms on the metal surface. (a)**

Adsorption structure onto multiple metal atom site and (b) adsorption structure only onto single metal atom site.

## 5.2. Future perspectives

In the present study, the author developed the highly reaction-selective electrocatalysts based on covalent triazine frameworks (CTFs) modified with single Pt atoms. The catalyst synthesized in this study is expected to be extended to a variety of reaction systems because it is possible to easily tune the properties of the catalyst. Firstly, the pore diameter of the catalytic active site is possible to easily adjust by choosing the structure of the monomer used in the polymerization process. Even only CTFs, a variety of structures have been reported so far as shown in Figs. 5.2 a-c [1-3]. The polymerization conditions of CTFs shown in Figs. 5.2a-c are basically the same; those CTFs can be easy to apply to the catalyst demonstrated in the present study. Secondly, the electron density of the metal can be controlled by changing the coordination environment by introducing the heteroatoms or functional group. CTFs having such hetero atoms had also been reported as shown in Figs. 5.2c and d [4,5]. In addition to the CTFs, covalent organic frameworks (COFs) which have coordination environment of the metal atoms are also able to apply. For example, Feng *et al.* reported the synthesis method of COF containing porphyrin ring, and revealed that the porphyrin sites are possible to carry Zn atoms (Fig. 5.3a) [6]. Neti *et al.* demonstrated another COF containing both porphyrin ring and phthalocyanine ring (Fig. 5.3b) [7]. Other type of COFs which contains nitrogen with lone pair are also applicable [8,9]. Thirdly, the kind of a metal atom carried on COFs is easily selected by changing the metal salt used in the impregnation process [10-13]. Thus, it is expected to find a variety of catalytic behaviors on the COF-based electrocatalyst by adjusting a structure of COF and deposit a metal atom appropriate to the purpose. In the future, the developments of application of these COF-based electrocatalysts to a various electrochemical systems are greatly expected.

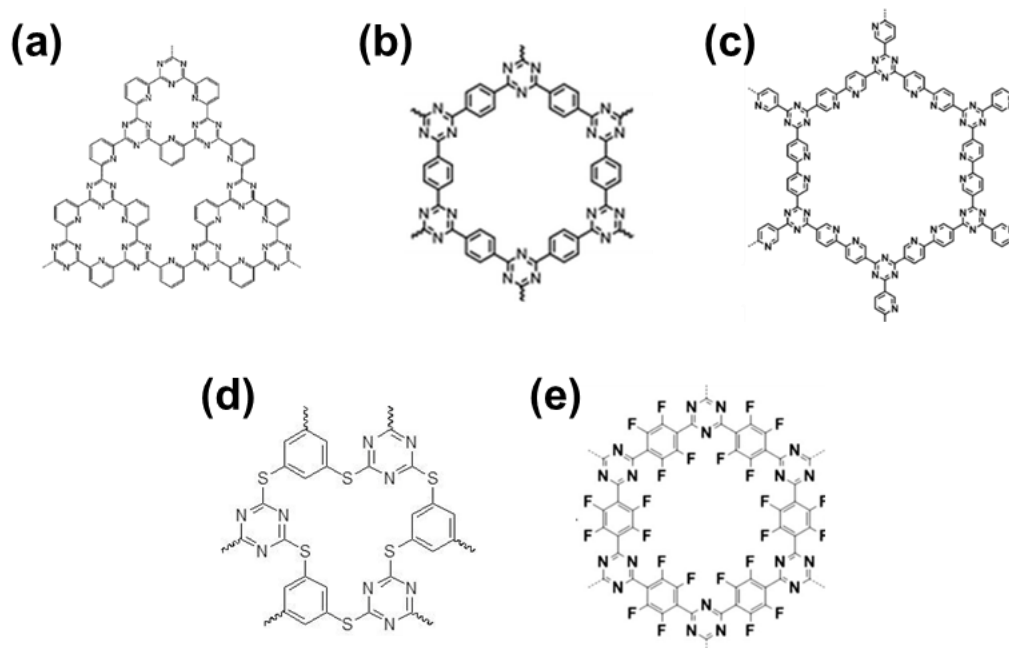


**Fig. 5.2 | Various types of the structure of CTFs.** CTFs are polymerized from (a) 2,6-dicyanopyridine, reproduced with permission for Ref. 1. © 2009 Wiley-VCH Verlag GmbH & Co. KGaA, Weinheim, (b) 1,4-dicyanobenzene, reproduced with permission for Ref. 2. © 2008 Wiley-VCH Verlag GmbH & Co. KGaA, Weinheim, (c) 5,5'-dicyanobipyridine, reproduced with permission for Ref. 3. © The Royal Society of Chemistry 2012, (d) 1,3,5-benzenetrithiol and cyanuric chloride, reproduced with permission for Ref. 4. © 2013 Wiley-VCH Verlag GmbH & Co. KGaA, Weinheim, and (e) tetrafluoroterephthalonitrile, reproduced with permission for Ref. 3. © The Royal Society of Chemistry 2013.

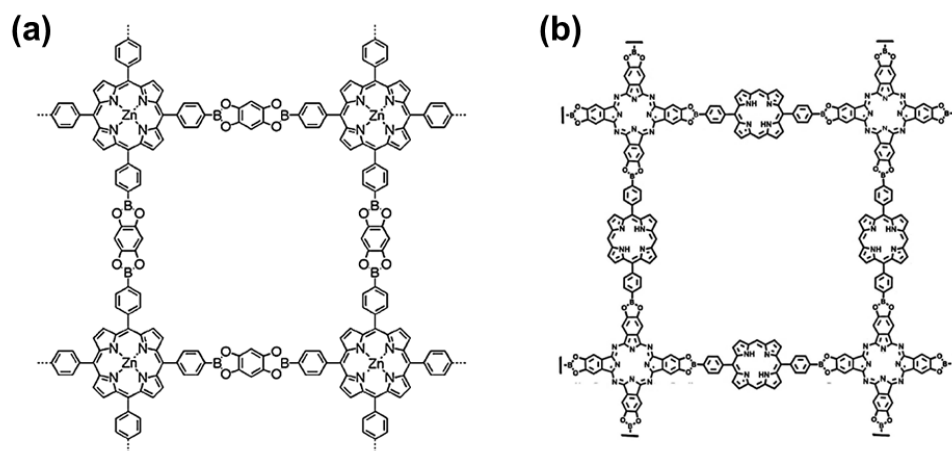


**Fig. 5.3 | Structure of COFs containing porphyrin and phthalocyanine rings.** (a) Reproduced with permission for Ref. 6. © The Royal Society of Chemistry 2011, (b) Reproduced with permission for Ref. 7. © The Royal Society of Chemistry 2013.

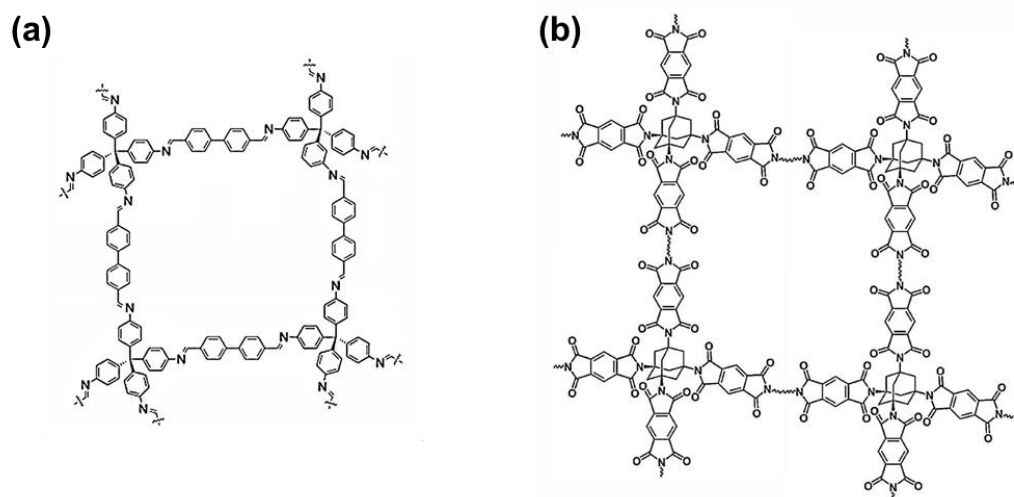


**Fig. 5.4 | Structure of 3-dimensional COFs containing nitrogen.** (a) Reproduced with permission for Ref. 8. Copyright © 2013 American Chemical Society, (b) Reproduced with permission for Ref. 9. Copyright © 2015 American Chemical Society.

## References

- [1] Palkovits, R., Antonietti, A., Kuhn, P., Thomas, A. & Schüth, F. Solid Catalysts for the Selective Low-Temperature Oxidation of Methane to Methanol. *Angew. Chem. Int. Ed.* **48**, 6909–6912 (2009).
- [2] Kuhn, P., Antonietti, M. & Thomas, A. Porous, Covalent Triazine-Based Frameworks Prepared by Ionothermal Synthesis. *Angew. Chem. Int. Ed.* **47**, 3450–3453 (2008).
- [3] Hug, S., Tauchert, M. E., Li, S., Pachmayr, U. E. & Lotsch, B. V. A functional triazine framework based on N-heterocyclic building blocks. *J. Mater. Chem.* **22**, 13956–13964 (2012).
- [4] Patel, H. A., Karadas, F., Byun, J., Park, J., Deniz, E., Canlier, A., Jung, Y., Atilhan, M. & Yavuz, C. T. Highly Stable Nanoporous Sulfur-Bridged Covalent Organic Polymers for Carbon Dioxide Removal. *Adv. Funct. Mater.* **23**, 2270–2276 (2013).
- [5] Zhao, Y., Yao, K. X., Teng, B., Zhang, T. & Han, Y. A perfluorinated covalent triazine-based framework for highly selective and water-tolerant CO<sub>2</sub> capture. *Energy Environ. Sci.* **6**, 3684–3692 (2013).
- [6] Feng, X., Chen, L., Dong, Y. & Jiang, D. Porphyrin-based two-dimensional covalent organic frameworks: synchronized synthetic control of macroscopic structures and pore parameters. *Chem. Commun.* **47**, 1979–1981 (2011).
- [7] Neti, V. S. P. K., Wu, X., Deng, S. & Echegoyen, L. Synthesis of a phthalocyanine and porphyrin 2D covalent organic framework. *CrystEngComm* **15**, 6892–6895 (2013).
- [8] Zhang, Y.-B., Su, J., Furukawa, H., Yun, Y., Gándara, F., Duong, A., Zou, X. & Yaghi, O. M. Single-Crystal Structure of a Covalent Organic Framework. *J. Am. Chem. Soc.* **135**, 16336–16339 (2013).
- [9] Fang, Q., Wang, J., Gu, S., Kaspar, R. B., Zhuang, Z., Zheng, J., Guo, H., Qiu, S. & Yan, Y. 3D Porous Crystalline Polyimide Covalent Organic Frameworks for Drug Delivery. *J. Am. Chem. Soc.* **137**, 8352–8355 (2015).

- [10] Ham, Y., Maeda, K., Cha, D., Takahabe, K. & Domen, K. Synthesis and Photocatalytic Activity of Poly(triazine imide). *Chem.-Asian J.* **8**, 218-224 (2013).
- [11] Iwase, K., Yoshioka, T. Nakanishi, S., Hashimoto, K. & Kamiya, K. Copper-Modified Covalent Triazine Frameworks as Non-Noble-Metal Electrocatalysts for Oxygen Reduction. *Angew. Chem. Int. Ed.* **54**, 11068 –11072 (2015).
- [12] Artz, J., Mallmann, S. & Palkovits, R. Selective Aerobic Oxidation of HMF to 2,5-Diformylfuran on Covalent Triazine Frameworks-Supported Ru Catalysts. *ChemSusChem* **8**, 672-679 (2015).
- [13] Bavykina, A. V., Goesten, M. G., Kapteijn, F., Makkee, M. & Gascon, J. Efficient production of hydrogen from formic acid using a Covalent Triazine Framework supported molecular catalyst. *ChemSusChem* **8**, 809 – 812 (2015).



## List of publications

(1) “Platinum-modified covalent triazine frameworks hybridized with carbon nanoparticles as methanol-tolerant oxygen reduction electrocatalysts”

K. Kamiya, **R. Kamai**, K. Hashimoto, S. Nakanishi, *Nature Communications* **5**, 5040 (2014).

(2) “Oxygen-tolerant single Pt-atom catalysts supported on a covalent triazine framework for the hydrogen oxidation reaction”

**R. Kamai**, K. Kamiya, K. Hashimoto, S. Nakanishi, *Angewandte Chemie International Edition*, in revision.

(3) “Selective electrochemical reduction of nitrogen oxides by covalent triazine frameworks modified with single Pt atoms”

**R. Kamai**, S. Nakanishi, K. Hashimoto, K. Kamiya, submitted to *Journal of Electroanalytical Chemistry*.

## The papers not included in the present thesis

(4) “Electrochemical Synthesis of  $\text{CuIn}(\text{Se},\text{S})_2$  Layer for Thin-Film Solar Cell with a Superstrate Configuration”

S. Ikeda, **R. Kamai**, T. Yagi, M. Matsumura, *Journal of The Electrochemical Society* **157**, B99-B103 (2010).

(5) “A superstrate solar cell based on  $\text{In}_2(\text{Se},\text{S})_3$  and  $\text{CuIn}(\text{Se},\text{S})_2$  thin films fabricated by electrodeposition combined with annealing”

S. Ikeda, **R. Kamai**, S. M. Lee, T. Yagi, T. Harada, M. Matsumura, *Solar Energy Materials & Solar Cells* **95**, 1446–1451 (2011).

(6) “Effect of Heat Treatment on Activity of Fe/N/C Catalyst Prepared by Hemin for Oxygen Reduction Reaction”

G. Tei, **R. Kamai**, H. Gyoten, T. Hayashi, M. Aizawa, *ECS Transactions* **61**, 31-37 (2014).

(7) “Reaction Kinetics of Active Centers in Fe/N/C Oxygen Reduction Reaction Catalyst”

G. Tei, **R. Kamai**, A. Sakai, S. Yotsuhashi, T. Hayashi, M. Aizawa, submitted to *ChemElectroChem*.

## **Acknowledgement**

The present study in this thesis had been accomplished under the supervision of Professor Dr. Kazuhito Hashimoto in his laboratory at The University of Tokyo from October 2013 to March 2016, and under the direction of Professor Dr. Shuji Nakanishi in his laboratory at Osaka University from April 2016 to September 2016. First of all, the author would like to express profound gratitude to Professor Dr. Kazuhito Hashimoto for many fruitful discussions, continuous guidance and encouragement. The author also expresses deep appreciation to Professor Dr. Shuji Nakanishi for his important suggestions and insightful discussions throughout the course of this study.

Grateful acknowledgements are also expressed to Professor Dr. Hiroshi Ishikita for his supervision at The University of Tokyo from April 2016 to September 2016.

The author is deeply grateful to Assistant Professor Dr. Kazuhide Kamiya for his many invaluable suggestions and many practically useful advices.

The author also deeply appreciates to Assistant Professor Dr. Akihiro Okamoto, Professor Dr. Keisuke Tajima, Professor Dr. Kayano Sunada and Dr. Takashi Harada for their salutary suggestions and helps.

Many thanks are given to Dr. Koichi Takahama, Mr. Toshiharu Sako, Mr. Shin Matusgi, Dr. Kenji Tsubaki, Mr. Mitsuo Yaguchi, Mr. Kenji Kusano, Mr. Takashi Sekiguchi, Mr. Hiroaki Usui, Mr. Michihiko Tani, Mr. Naoki Yoshikawa, Mr. Yuya Suzuki and Mr. Kota Kurahata in Panasonic Corporation for their continuous support and encouragement.

Finally, the author would like to thank his wife, children and parents for their warm encouragement and continuous assistant.